seit 1558

Friedrich-Schiller-Universität Jena
Physikalisch-Astronomische Fakultät
Theoretisch-Physikalisches Institut

Renormalization group flows of a (2+1)-dimensional chiral fermion system with collective degrees of freedom

Masterarbeit

vorgelegt von Julia Borchardt,
geboren am 19.02.1990 in Jena

23. September 2013, Jena

Erstgutachter:
Prof. Dr. rer. nat. habil. Holger Gies
Theoretisch-Physikalisches Institut
Friedrich-Schiller-Universität Jena

Zweitgutachter:
Dr. rer. nat. Lukas Janssen
Department Of Physics
Simon Fraser University Burnaby

Contents

1. Introduction

During the last decades, the renormalization group (RG) method has been celebrating considerable success and hence has become an important tool not only in quantum field theory (QFT) and statistical physics, but also in condensed matter physics. While getting rid off the problem of infinities induced by quantum fluctuations which occur on all scales, renormalization in general relates physical parameters to observable quantities. Calculations using renormalization methods provide impressive agreement with experimental measurements, for example referring to the anomalous magnetic moment of the electron in quantum electrodynamics [1].

The first reference to the RG dates back to a short publication [2] from Ernest Stückelberg and André Petermann in 1951, which was followed by another paper [3] in 1953. However, some important pre-works had been already contributed by Bethe, Feynman, Schwinger and Dyson, who found in the late 1940s that all infinities can be swallowed by multiplicative renormalizations. Stückelberg and Petermann's notes were first noticed by Nicolai Bogoliubov and Dmitry Shirkov, who gave a more complete and transparent picture of the RG method and established an algorithm in terms of differential group equations and beta functions. In two short notes, they connected both works of Stückelberg and Petermann and of Gell-Mann and Low, who had written a fundamental paper [4] in 1954. Translating these notes from Russian to English [5, 6] and devoting one chapter of a monograph to the RG [7] gave impetus to the RG method to become an indispensable tool in QFT. However, as already mentioned its range of applicability is not limited to QFT: Moreover, the method is also used in quantum statistics for investigating and analyzing phase transitions. Kenneth Wilson has contributed important works [8] in the beginning of the 1970s for which he was honored with the Nobel Prize in 1982. His works can be traced back to Leo Kadanoff's idea of "blocking" [9] and describe its application to critical phenomena in the vicinity of continuum phase transitions going beyond mean field approximations.[1]

Until today, phase transitions remained a fascinating but challenging topic in modern physics. For a profound understanding, one needs to employ non-perturbative techniques such as large N_f expansion [11–19] where N_f is the flavor number of the fermions in a fermionic theory, lattice Monte Carlo simulations [14, 20, 21] often using *staggered* fermions [22, 23] or exact RG equations [24, 25]. In this work, we employ the functional renormalization group (FRG) method providing RG flow equations derived from the Wetterich equation [26] to examine strongly interacting field theories. Within this description, thermodynamic quantities and correlation functions, which behave as power laws characterized by universal, critical exponents close to continuous phase transitions [27], can be determined.

To be more precise in what follows, we consider a (2+1)-dimensional relativistic fermion system in a partially bosonized form, which serves as an effective theory for graphene. Therefore, we devote a few words to this interesting material that became very famous during the last years. However, first serious investigations of graphene date back to the 1940s, when Philip Wallace examined its band structure. He showed the unusual semimetalic behavior [28], although his observations were embedded in a study about graphite [29]. It took almost sixty years until graphene was first isolated [30], an achievement for which Konstantin Novoselov and Andre Geim were awarded the Nobel Prize in 2010. Graphene exhibits a wide range of unique properties, for reviews see among others [29, 31]. One of the most interesting properties is the extraordinary

[1] For a more complete summary about the history of the RG method written by Shirkov, see [1, 10].

dispersion relation of the electrons, which is almost linear at the Dirac points. Therefore, the electrons can be described as massless, chiral Dirac fermions [29] at a low energy level. If spontaneous symmetry breaking occurs, the fermions acquire a mass resulting in a non-vanishing valence-conduction band gap. However, due to this dispersion relation, graphene offers the possibility to observe QED phenomena, but at comparatively small speeds [32–34], as well as quantum relativistic phenomena in general, such as the Klein paradox [33, 35] or Zitterbewegung [36–38].

In fact, there are several effective theories describing graphene, for example the three dimensional Thirring model exhibiting a chiral $\mathrm{U}(2N_\mathrm{f})$ symmetry [39], where $\mathrm{U}(n)$ is the group of unitary $n \times n$ matrices. However, within lattice Monte Carlo studies, the $\mathrm{U}(2N_\mathrm{f})$ symmetry is often realized only in part, for example in terms of an $\mathrm{U}(N_\mathrm{f}) \otimes \mathrm{U}(N_\mathrm{f})$ symmetry [40] for staggered fermions which is hoped to approach the $\mathrm{U}(2N_\mathrm{f})$ symmetry approaching the continuum limit. In different lattice studies, an ultra violet (UV) fixed point exhibiting a second order phase transition was observed [40–45]. In order to confirm these results by means of the RG, in this work we consider a chiral $\mathrm{U}(N_\mathrm{f}) \otimes \mathrm{U}(N_\mathrm{f})$ symmetric theory with a certain four-fermion interaction channel which we believe gives rise to the observed phase transition with the symmetry breaking pattern $\mathrm{U}(N_\mathrm{f}) \otimes \mathrm{U}(N_\mathrm{f}) \to \mathrm{U}(N_\mathrm{f})$.

After these introductory words, we give a short overview of the basics of functional QFT and RG in chapter 2. In this context, we clarify the mathematical definition and physical meaning of fixed points and come back to phase transitions, introducing critical exponents and scaling as well as hyperscaling relations. In chapter 3, we establish the microscopic theory of our fermionic system implementing the chiral $\mathrm{U}(N_\mathrm{f}) \otimes \mathrm{U}(N_\mathrm{f})$ symmetry. After partial bosonization, which enables us to study occurring phase transitions in detail, we construct a suitable truncation of the effective average action. Besides the investigation of the different kinds of symmetry breaking patterns, we compute the flow equations of the model's parameters where we implement the special $\mathrm{U}(N_\mathrm{f}) \otimes \mathrm{U}(N_\mathrm{f}) \to \mathrm{U}(N_\mathrm{f})$ symmetry breaking pattern. It is worth mentioning that our system is similar to the effective quark-meson model of quantum chromodynamics (QCD), which is treated in [46] for four dimensions and gives rise to the same beta functions.

The goal of this work is to analyze the fixed point structure of the chiral $\mathrm{U}(N_\mathrm{f}) \otimes \mathrm{U}(N_\mathrm{f})$ symmetric model and to search for phase transitions in their vicinity. Chapter 4 is devoted to the former. We search for fixed points in both the symmetric and the symmetry broken regime. To this end, we first employ the large N_f limit to get an impression of the equations' dynamics and then examine the finite N_f case. Especially for the symmetry broken regime, it is instructive to consider the pure bosonic case as well. During these investigations, we introduce some criteria to isolate physically reliable solutions from unreliable ones. In chapter 5, we obtain a more extensive picture of the fixed points by means of a flow analysis. Additionally, we compute critical exponents and compare them with those obtained by use of scaling and hyperscaling relations. Furthermore, we discuss the occurrence of phase transitions. There we concentrate on the order of the identified phase transitions and the question of universality. Against our intention in the previous chapters, we have to extend our examinations to phase transitions of first order. Finally, in chapter 6, we summarize and discuss our results.

2. Basics

Quantum field theory is fully described by its *n-point correlation functions*. However, if computed by perturbative methods, correlation functions usually contain divergencies we may eliminate by a renormalization prescription. In the following sections, we give a short introduction into the basic ideas of the FRG. Afterwards, we clarify why the RG method is such a powerful tool referring to fixed points and its application to critical phenomena. A more detailed treatment of the following topics may be found in [47–50].

2.1. Basics of quantum field theory

In order to present the main ideas of the FRG method, we first start with a short introduction into the basics of QFT. For this purpose, we point out that we consider all functions and quantities in Euclidean coordinates with d dimensions which we obtain from a Wick rotation in Minkowski space, see [49]. Therefore, we assume that we can recover all Minkowski-valued quantities by analytic continuation. From the generating functional

$$Z[J] \equiv \mathrm{e}^{W[J]} := \int_\Lambda \mathcal{D}\phi \, \mathrm{e}^{-S[\phi]+\int J\phi}, \tag{2.1}$$

where $\int J\phi = \int \mathrm{d}^d x J(x)\phi(x)$, we may derive all n-point functions

$$\langle \phi(x_1)\dots\phi(x_n)\rangle = \frac{1}{Z[0]} \left(\frac{\delta^n Z[J]}{\delta J(x_1)\dots\delta J(x_n)} \right)\Bigg|_{J=0}. \tag{2.2}$$

The functional $S[\phi]$ denotes the classical action. The field ϕ stands for a real scalar field, but paying attention to some modifications, one may easily transfer the following discussion to other kinds of fields, for example fermionic ones [50]. We emphasize that the functional integral over field configurations is regularized by a UV cutoff Λ. Computing the Legendre transform of the generating functional $W[J]$ of the connected n-point functions, we obtain the effective action

$$\Gamma[\varphi] := \sup_J \Big(J\varphi - W[J] \Big). \tag{2.3}$$

From the effective action, one may generate the one-particle irreducible (1PI) correlators. Therefore, it stores quantum information in a more efficient way than $Z[J]$ or $W[J]$. The quantities φ and J are conjugated variables for which we can show

$$\varphi(x) = \frac{W[J]}{\delta J(x)} = \langle \phi(x)\rangle_J, \tag{2.4}$$

$$J(x) = \frac{\delta\Gamma[\varphi]}{\delta\varphi(x)}. \tag{2.5}$$

Equation (2.4) is derived from the supremum condition and illustrates that φ may be understood as the expectation value of the field ϕ with a non-vanishing source J. The quantum equation of motion (2.5) is obtained by exploiting (2.3) and inserting (2.4). From both equations, we get the important identity

$$\int \mathrm{d}^d z \frac{\delta^2\Gamma[\varphi]}{\delta\varphi(x)\delta\varphi(z)} \frac{\delta^2 W[J]}{\delta J(z)\delta J(y)} = \delta(x-y). \tag{2.6}$$

After having introduced the generating functional Γ, it is an important question how to compute the effective action. The definition (2.3) gives rise to

$$\mathrm{e}^{-\Gamma[\varphi]} = \int_\Lambda \mathcal{D}\phi \exp\left(- S[\varphi + \phi] + \int \frac{\delta\Gamma[\varphi]}{\delta\varphi}\phi \right), \tag{2.7}$$

which is a non-linear first order functional integro-differential equation [47]. Solutions of such an equation are hard to derive. In addition to the vertex expansion, leading to the Dyson-Schwinger equations, the FRG provides a suitable method to compute Γ. This will be the topic in the following section.

2.2. The renormalization group flow equation

The fundamental, underlying idea of the FRG is the description of the change of physics from scale to scale. The inclusion of quantum fluctuations generally causes divergencies which are hard to get rid off. However, following Wilson's idea, fluctuations are now successively integrated out from scale to scale. Hence, instead of considering quantum effects over the wide range of momentum space at once, only infinitesimal momentum shells are picked up. In comparison to perturbative methods, such a prescription results in a reordering of fluctuations. Doing so step by step, we naturally flow from a given microscopic theory to the full quantum theory.

In general, there are different renormalization schemes. The parameters of a given theory depend on the choice of this scheme. Observables measured in experiments, of course, should be scheme invariant. However, because of the choice of a certain truncation, they usually suffer from an artificial dependency. Applying the "Idea of optimization" [51], one intends to remove this error as far as possible. However, in practice it is a highly non-trivial task to give an estimate for this error.

The FRG transformations are parametrized by a momentum scale k. The initial parameters can be fixed at a chosen UV cutoff Λ. The evolution of those parameters is provided by the Wetterich equation, which we will derive in the following.

With regard to the effective action Γ, we introduce the more general effective average action Γ_k. The momentum scale k denotes the infrared (IR) cutoff. The quantity Γ_k shall be designed in such a way that it includes all quantum effects in the range between k and Λ. On the one hand, for $k \to 0$ we request $\Gamma_k \to \Gamma$, on the other hand, we demand $\Gamma_k \to S$ for $k \to \Lambda$.

For the derivation of an equation for Γ_k, we choose an analogous way with regard to the section above. We start with a more general IR regulated functional

$$Z_k[J] \equiv \mathrm{e}^{W_k[J]} := \int_\Lambda \mathcal{D}\phi\, \mathrm{e}^{-S[\phi] - \Delta S_k[\phi] + \int J\phi}, \tag{2.8}$$

with

$$\Delta S_k[\phi] = \frac{1}{2}\int \frac{\mathrm{d}^d p}{(2\pi)^d}\phi(-p)R_k(p)\phi(p). \tag{2.9}$$

This regulator term gives rise to the main difference to our consideration above. From its form, it can be interpreted as a momentum and scale dependent mass term of the scalar fields. The regulator function R_k is a central piece of the RG method. It cannot be chosen arbitrarily. Moreover, for ensuring that $\Gamma_k \xrightarrow{k\to 0} \Gamma$, we require

$$\lim_{k^2/p^2 \to 0} R_k(p) = 0 \tag{2.10}$$

and for $\Gamma_k \xrightarrow{k\to\Lambda} S+$ const.

$$\lim_{k\to\Lambda\to\infty} R_k(p) \to \infty. \tag{2.11}$$

Finally, for implementing the IR regularization, we further demand

$$\lim_{p^2/k^2 \to 0} R_k(p) > 0. \tag{2.12}$$

According to (2.3), we define the effective average action Γ_k to be

$$\Gamma_k[\varphi] = \sup_J \Big(J\varphi - W_k[J] \Big) - \Delta S_k[\varphi]. \tag{2.13}$$

We emphasize that we consider scale independent fields φ, however, the source J yielding the supremum will depend on k. As the slight modification ΔS_k only depends on φ, we may again interpret the field φ as the expection value of the scalar field ϕ in presence of a non-vanishing source. The quantum equation of motion changes due to the regulator contribution

$$J(x) = \frac{\delta\Gamma_k[\varphi]}{\delta\varphi(x)} + \int \frac{\mathrm{d}^d p}{(2\pi)^d} \mathrm{e}^{ipx} R_k(p)\varphi(p). \tag{2.14}$$

Both again leads to the identity (2.6) which recieves only a minor modification

$$\int \mathrm{d}^d z (\Gamma_k^{(2)}[\varphi] + R_k)(x,z) G_k(z-y) = \delta(x-y), \tag{2.15}$$

where

$$\frac{\delta\varphi(x)}{\delta J(y)} = \frac{\delta^2 W_k[J]}{\delta J(y)\delta J(x)} =: G_k(x-y) \tag{2.16}$$

can be shown to be the full, connected propagator at the scale k. Here, we have denoted the second functional derivative by

$$\Gamma_k^{(2)}[\varphi] := \frac{\delta^2\Gamma_k[\varphi]}{\delta\varphi\delta\varphi}. \tag{2.17}$$

Finally, we derive the Wetterich equation [26]

$$\partial_t \Gamma_k[\varphi] = \frac{1}{2}\mathrm{STr}\Big[\partial_t R_k \big(\Gamma_k^{(2)}[\varphi] + R_k\big)^{-1}\Big] =: \frac{1}{2}\mathrm{STr}\Big[\tilde{\partial}_t \ln\big(\Gamma_k^{(2)}[\varphi] + R_k\big)\Big] \tag{2.18}$$

where $\partial_t := k\partial_k$ and $t := \ln(k/\Lambda)$ is the so-called RG "time". The operator $\tilde{\partial}_t$ only acts on the k-dependency of the regulator function R_k, see appendix B. The super trace produces an additional minus sign for fermionic fields ψ and $\bar{\psi}$. In the mixed fermionic and bosonic case, the second functional derivative has to be performed in the way

$$\begin{gathered}\Gamma_k^{(2)} = \frac{\overrightarrow{\delta}}{\delta\Phi^{\mathrm{T}}}\Gamma_k \frac{\overleftarrow{\delta}}{\delta\Phi} \quad \text{with} \\ \Phi \equiv \Phi(p) := \begin{pmatrix} \psi(p) \\ \bar{\psi}^{\mathrm{T}}(-p) \\ \varphi(p) \end{pmatrix} \quad \text{and} \quad \Phi^{\mathrm{T}} \equiv \Phi^{\mathrm{T}}(-p) := \big(\psi^{\mathrm{T}}(-p), \bar{\psi}(p), \varphi(-p)\big)\end{gathered} \tag{2.19}$$

In contrast to (2.7), the Wetterich equation is a functional differential equation for Γ_k, but without having to perform a functional integral. We point out that the super trace suggests a one loop structure of the equation (2.18). The exactness of this equation, however, can be seen from the occurrence of the full propagator, $G_k = \big(\Gamma_k^{(2)}[\varphi] + R_k\big)^{-1}$ in operator notation. Possible sources of divergencies are removed by the IR regulating effect of R_k in the denominator, and the UV regularization by $\partial_t R_k$ in the numerator. Additionally, $\partial_t R_k$ implements the Wilsonian idea due to its peaked structure. Solutions of (2.18) are trajectories in the theory space of all action functionals preserving the demanded symmetry globally. The starting and the end point are given by S and Γ being independent of the specific choice of the regulator function. However, the shape of the trajectories in between is a non-universal quantity and may change for different renormalization schemes.

In most cases, the Wetterich equation cannot be solved exactly. As already mentioned above, in terms of a certain truncation, one may obtain an approximate solution. We will work at next-to-leading order in a systematic derivative expansion for constructing a suitable truncation of our theory. By derivative expansion, we understand an operator expansion, especially referring to derivative operators, which are ordered in terms of increasing canonical mass dimension [27]. For the interaction potential, this procedure can also be applied, leading to an increasing number of contributing fields. The kinetic and interaction terms are parametrized by the wave function renormalization and by coupling constants, respectively, which are assumed to be scale dependent. For the dimensionless, renormalized coupling constants g_i, we derive from (2.18) the flow equations

$$\beta_{g_i} := \partial_t g_i \tag{2.20}$$

which are called beta functions.

2.3. Critical behavior and renormalization group scaling

The FRG is a powerful tool for the search for fixed points of the theory. Fixed points arise as zeros of the beta functions

$$\beta_{g_i}(\boldsymbol{g}_*) = 0 \qquad \forall \beta_{g_i}. \tag{2.21}$$

Thus, starting at such a point in theory space we will always stay at this point during the RG evolution. Therefore, the model becomes independent of the artificial UV cutoff Λ if its RG trajectory runs into a fixed point for $k \to \Lambda \to \infty$. If the UV cutoff Λ is not removable in such a way, one considers trajectories passing very close to a fixed point to ensure that the values of the measured observables are much smaller than Λ. It is worth emphasizing that the values of the coupling constants themselves are not universal at fixed points. However, one may find, in addition to their existence, universal quantities. Important ones are the critical exponents which can be derived from the stability matrix B_{ij} linearizing the flow around the fixed point

$$\beta_{g_i} = B_{ij}(g_j - g_{j*}) + \mathcal{O}\left((g - g_*)^2\right). \tag{2.22}$$

Note that Einstein's summation convention is employed. It turns out that close to fixed points the flow can be then easily computed

$$g_i = g_{i*} + \sum_j c_j (\vec{v}_j)_i \left(\frac{k_0}{k}\right)^{\theta_j}, \tag{2.23}$$

where the so-called critical exponents θ_j are the negative eigenvalues and $\vec{v}_j$ the corresponding eigenvectors of B_{ij}. The integration constants c_j fix the initial values at $k = k_0$. It is obvious that depending on the sign of θ_i, the qualitative behavior of the flow significantly changes. For $\theta_j > 0$, the direction $\vec{v}_j$ is called relevant since it is IR repulsive. Therefore, with an initial deviation in the direction $\vec{v}_j$, we will move far away from the fixed point during the flow. On the contrary, directions with critical exponents $\theta_j < 0$ are irrelevant because despite small perturbations in the direction $\vec{v}_j$, the flow always leads us back to the fixed point. Finally, directions with $\theta_j = 0$ are called marginal.

The critical exponents θ_i can be related to exponents describing the quantitative behavior of continous phase transitions, which may be found in the vicinity of the fixed points, and fulfill scaling and hyperscaling relations then. To show this, we consider a fixed point with only one relevant direction $\vec{v}_1$ which is a relevant case for phase transitions of second order. This example will be applicable in a certain manner to our findings in chapter 5.

For concreteness we consider a simple bosonic effective average action of Ginzburg-Landau-Wilson type[2] with N scalar fields φ^a

$$\Gamma_k[\varphi] = \int \mathrm{d}^d x \left[\frac{Z_k}{2} (\partial_\mu \varphi^a)(\partial_\mu \varphi^a) + \frac{\bar{\lambda}_k}{8} (\varphi^a \varphi^a - \varphi^a_{0k} \varphi^a_{0k})^2 \right], \tag{2.24}$$

where the index a counts the N flavors and μ the d space-time dimensions. Note that Z_k denotes the wave function renormalization. This model exhibits an $\mathrm{O}(N)$ symmetry

$$\varphi^a \mapsto O^{ab} \varphi^b \qquad \text{with} \qquad O \in \mathrm{O}(N), \tag{2.25}$$

which can be spontaneously broken for $d > 2$. Actually, the model in the given truncation is only adequate for the regime of symmetry breaking. In the symmetric regime we would additionally introduce a bosonic mass term $\propto \varphi^a \varphi^a$. In the disordered phase the vacuum expection value (VEV) $\varphi_{0k} = \langle \phi \rangle = 0$ for $k \to 0$. On the contrary, the VEV as the minimum of the effective potential $U = \Gamma|_{\varphi = \text{const.}} / \Omega_d$ with Ω_d denoting the space-time volume, is non-zero in the ordered phase. We fix the minimizing field configuration to be $\varphi^a_{0k} = \sigma_{0k} \delta^{a1}$. Thus, the VEV can be taken as an order parameter. The corresponding fixed point, dominating the flow at the phase transition, is the well known and much investigated Wilson-Fisher fixed point [52], which exists in $2 < d < 4$ dimensions. According to the *Goldstone* theorem [53, 54], the breakdown of a global continuous symmetry results in massless bosons, the so-called Nambu-Goldstone bosons or Goldstone bosons. In short, the number of these bosons corresponds to the number of broken symmetry generators. As we observe a residual $\mathrm{O}(N-1)$ symmetry, we only count one massive mode, but $N-1$ massless Goldstone bosons.

We go on with the 2-point correlation function $G_k(x; \vec{v}_1, \ldots)$ corresponding to the full, connected propagator we have already introduced above. At the critical point, the long range behavior of the correlator can be described by the critical exponent η_* in the way

$$G_k(x; 0, \ldots) \propto \frac{1}{|x|^{d-2+\eta_*}}, \tag{2.26}$$

for $|x| \to \infty$. On the other hand, if we perform an RG step from Λ to $k = \Lambda/b$, we obtain

$$G_{k=\Lambda/b}(p; \vec{v}_1, \ldots) = Z_k^{-1} b^2 G_\Lambda(bp; b^{\theta_1} \vec{v}_1, \ldots) \tag{2.27}$$

in momentum space following the scaling hypothesis [55–57]. As the ratio b may be chosen arbitrarily, we decide to fix it $b = \Lambda/p$ which turns out to be advantageous for the next step. Additionally, we define the scale dependent anomalous dimension at the fixed point $\eta_* = -\partial_t \ln Z_k$ from which $Z_k = b^{\eta_*}$ for wave function renormalization follows. If we put everything into (2.27), we finally get

$$G_k(p; 0, \ldots) \propto \frac{1}{p^{2-\eta_*}} \tag{2.28}$$

which, transforming into space-time coordinates, shows the equality of the critical exponent η_* and the anomalous dimension. The exponents ν and γ are related to the correlation length ξ and susceptibility χ respectively

$$\xi = \bar{m}_{\mathrm{R}}^{-1} \propto |\delta g_\Lambda|^{-\nu}, \tag{2.29}$$
$$\chi = \bar{m}^{-2} \propto |\delta g_\Lambda|^{-\gamma}, \tag{2.30}$$

[2] The following line of argument follows [27].

where δg_Λ denotes the distance at $k = \Lambda$ from the fixed point or phase transition. We have introduced the renormalized mass which is $\bar{m}_\mathrm{R}^2(k=0) = \lim_{k\to 0} \bar{\lambda}_k \sigma_{0k}^2 / Z_k$ in the ordered regime and the unrenormalized mass $\bar{m}^2(k=0) = \lim_{k\to 0} Z_k \bar{m}_\mathrm{R}^2(k)$ which is the bare mass coupling of the term $\propto \varphi^a \varphi^a$ in the symmetric regime. Choosing $b^{\theta_1} = |\vec{v}_1|$, we may derive from (2.27) the scaling relation

$$\nu = \frac{1}{\theta_1}, \tag{2.31}$$

and the hyperscaling relation

$$\gamma = \nu(2 - \eta_*). \tag{2.32}$$

Finally, one also finds a critical exponent β for the order parameter

$$\langle \phi \rangle = \sigma_0 \propto (\delta g_\Lambda)^\beta, \tag{2.33}$$

which is to be calculated in the ordered phase. Exploiting (2.27) and the scaling assumption for the singular part of the effective potential

$$U_{S,k=\Lambda/b}(\vec{v}_1, \ldots) = b^{-d} U_{S,\Lambda}(b^{\theta_1} \vec{v}_1, \ldots) \tag{2.34}$$

we derive the second hyperscaling relation

$$\beta = \frac{1}{2}(d - 2 + \eta_*). \tag{2.35}$$

It is worth emphasizing that all these exponents refer to bosonic quantities. This gives a first hint of the necessity of a partially bosonized theory for quantitatively studying phase transitions in detail.

3. Renormalization group analysis of the chiral fermion model

We investigate a Gross-Neveu like model exhibiting a chiral $\mathrm{U}(N_\mathrm{f}) \otimes \mathrm{U}(N_\mathrm{f})$ symmetry where N_f is the flavor number of the massless fermions in $d = 2+1$ Euclidean dimensions. By partial bosonization and a special truncation of the bosonic potential, we are able to examine a certain symmetry breaking pattern in detail. The microscopic action will include, apart from the pure bosonic potential, a Yukawa-type term mediating the fermion-boson interactions and providing a finite fermion mass in the regime of broken symmetry. Analyzing the mass spectra, we will also have a closer look at other kinds of symmetry breaking patterns besides our special one.

Later on we will investigate the scale dependency of the couplings. Therefore, we compute the flow equations in the symmetric and symmetry broken regime.

3.1. Classical and effective action

The classical action defines a model at the UV scale Λ disregarding any fluctuations. In order to take quantum effects into account, we need to introduce the effective action. For the effective average action, we employ a certain truncation which provides scale-dependent couplings.

3.1.1. Classical action

Before we discuss the microscopic action, we briefly comment on the representation of the Dirac algebra which is used in this work. For the dimension of the matrices, fulfilling the Dirac algebra,

$$\{\gamma_\mu, \gamma_\nu\} = 2\delta_{\mu\nu}\mathbb{1}_4, \qquad \mu, \nu = 1, 2, 3, \tag{3.1}$$

we choose $d_\gamma = 4$. The quantity $\delta_{\mu\nu}$ stands for the Euclidean metric. We could employ 2×2 matrices as well, but the reducible representation is a natural and convenient choice to parametrize the fermionic degrees of freedom of layered systems considered in the condensed matter context. A possible reducible representation of the Dirac algebra is given by the 4×4 matrices

$$\gamma_1 = \sigma_3 \otimes \sigma_1, \qquad \gamma_2 = \sigma_3 \otimes \sigma_2, \qquad \gamma_3 = \sigma_3 \otimes \sigma_3 \tag{3.2}$$

with $\{\sigma_i\}_{i=1,2,3}$ denoting the standard 2×2 Pauli matrices. The matrix γ_3 correponds to the time component in the Minkowski case, in a similar way x_3 can be understood as the Euclidean time coordinate. Therefore, $\psi^\dagger = -\mathrm{i}\bar{\psi}\gamma_3$ is a reasonable definition for a conjugate spinor for the Euclidean case which preserves the Osterwalder-Schrader positivity of the action.

Besides γ_1, γ_2 and γ_3, one finds two additional matrices

$$\gamma_4 = -\sigma_1 \otimes \sigma_0, \qquad \gamma_5 = \sigma_2 \otimes \sigma_0 \qquad \text{with} \qquad \gamma_4^2 = \gamma_5^2 = \mathbb{1}_4, \tag{3.3}$$

where $\sigma_0 = \mathbb{1}_2$, which anticommute with all gamma matrices and each other since the representation is reducible. It is easy to see that $\gamma_i^\dagger = \gamma_i$ for $i = 1, \ldots, 5$. Because of equivalence, this holds for all other possible representations. Using all the gamma matrices, we can form a complete basis

$$\{\gamma_A\}_{A=1,\ldots,16} = \{\mathbb{1}_4, \gamma_\mu, \gamma_4, \gamma_{\mu\nu}, \mathrm{i}\gamma_\mu\gamma_4, \mathrm{i}\gamma_\mu\gamma_5, \gamma_{45}, \gamma_5\} \tag{3.4}$$

of the 4×4 Dirac algebra where $\gamma_{\mu\nu} := \mathrm{i}[\gamma_\mu, \gamma_\nu]/2$ for $\mu < \nu$ ($\mu, \nu = 1, 2, 3$) and $\gamma_{45} := \mathrm{i}\gamma_4\gamma_5$. We introduce a chiral projector

$$P_{\mathrm{L/R}} := \frac{1}{2}(\mathbb{1}_4 \pm \gamma_{45}) \tag{3.5}$$

satisfying the projector property $P_{\mathrm{L/R}}^2 = P_{\mathrm{L/R}}$. Additionally, the two projectors are orthogonal to each other, thus $P_{\mathrm{L}}P_{\mathrm{R}} = 0$ and $P_{\mathrm{R}} + P_{\mathrm{L}} = \mathbb{1}_4$. It is worth mentioning that the definition of the chiral projectors we have chosen is not the only possible one which embodies the notion of chirality [27]. We could also employ $P_{\mathrm{L/R}}^{(4)} := \frac{1}{2}(\mathbb{1}_4 \pm \gamma_4)$ or $P_{\mathrm{L/R}}^{(5)} := \frac{1}{2}(\mathbb{1}_4 \pm \gamma_5)$.

Applying P_{R} and P_{L} to the four component spinors, they become decomposed into left- and right-handed Weyl spinors

$$\psi_{\mathrm{L/R}} = P_{\mathrm{L/R}}\psi, \qquad \bar{\psi}_{\mathrm{L/R}} = \bar{\psi}P_{\mathrm{L/R}}. \tag{3.6}$$

The $\mathrm{U}(N_{\mathrm{f}}) \otimes \mathrm{U}(N_{\mathrm{f}})$ symmetry transformation changes the Weyl spinors in a non-trivial way

$$\psi^a_{\mathrm{L/R}} \mapsto U^{ab}_{\mathrm{L/R}}\psi^b_{\mathrm{L/R}} \qquad \bar{\psi}^a_{\mathrm{L/R}} \mapsto \bar{\psi}^b_{\mathrm{L/R}}(U^\dagger_{\mathrm{L/R}})^{ba} \tag{3.7}$$

where $U_{\mathrm{L/R}}$ are unitary $N_{\mathrm{f}} \times N_{\mathrm{f}}$ matrices. A special choice is $U^{ab}_{\mathrm{L/R}} = \mathrm{e}^{\pm\mathrm{i}\alpha}\delta^{ab}$, representing the vectorial $\mathrm{U}^{45}(1)$ transformation. The symmetry group may be rewritten

$$\mathrm{U}(N_{\mathrm{f}}) \otimes \mathrm{U}(N_{\mathrm{f}}) \cong \mathrm{SU}(N_{\mathrm{f}}) \otimes \mathrm{SU}(N_{\mathrm{f}}) \otimes \mathrm{U}(1) \otimes \mathrm{U}(1) \tag{3.8}$$

which gives a deeper insight into the kind of symmetry. Demanding chiral symmetry preservation, there are several appropriate four-fermion interaction terms the action may consist of. For details we refer to [58]. In this work, we consider a model where the low-energy physics is driven by the particular fermionic channel parametrized by the action

$$S[\psi, \bar{\psi}] = \int \mathrm{d}^d x \left\{ \mathrm{i}\bar{\psi}^a \partial\!\!\!/ \psi^a - \frac{\bar{g}}{4N_{\mathrm{f}}} \left[(\bar{\psi}^a\gamma_4\psi^b)^2 + (\bar{\psi}^a\gamma_5\psi^b)^2 \right] \right\}, \tag{3.9}$$

where $\bar{g}$ is the bare coupling of $(\bar{\psi}^a\gamma_i\psi^b)^2 := (\bar{\psi}^a\gamma_i\psi^b)(\bar{\psi}^b\gamma_i\psi^a)$. The interaction may be rewritten in terms of Weyl spinors

$$(\bar{\psi}^a\gamma_4\psi^b)^2 + (\bar{\psi}^a\gamma_5\psi^b)^2 = 4(\bar{\psi}^a_{\mathrm{L}}\gamma_4\psi^b_{\mathrm{R}})(\bar{\psi}^b_{\mathrm{R}}\gamma_4\psi^a_{\mathrm{L}}) = 4(\bar{\psi}^a_{\mathrm{L}}\gamma_5\psi^b_{\mathrm{R}})(\bar{\psi}^b_{\mathrm{R}}\gamma_5\psi^a_{\mathrm{L}}). \tag{3.10}$$

In this notation the chiral symmetry becomes obvious.

3.1.2. Partially bosonized effective action

The chiral symmetry in our model may be broken spontaneously. To investigate this phenomenon, we need to introduce partial bosonization which is performed by the *Hubbard-Stratonovich* transformation. The multiplication of the generating functional

$$Z \propto \int \mathcal{D}\psi\mathcal{D}\bar{\psi}\ \mathrm{e}^{-S[\psi,\bar{\psi}]} \tag{3.11}$$

with

$$\mathcal{N} \int \mathcal{D}\varphi\ \mathrm{e}^{-\int \mathrm{d}^d x \{\bar{m}^2(\varphi^\dagger)^{ab}\varphi^{ba}\}} = 1, \tag{3.12}$$

where $\mathcal{N}$ is a normalization factor, leads to the action

$$S[\psi, \bar{\psi}, \varphi, \varphi^\dagger] = \int \mathrm{d}^d x \left\{ \mathrm{i}\bar{\psi}^a \partial\!\!\!/ \psi^a - \frac{\bar{g}}{N_{\mathrm{f}}}(\bar{\psi}^a_{\mathrm{L}}\gamma_5\psi^b_{\mathrm{R}})(\bar{\psi}^b_{\mathrm{R}}\gamma_5\psi^a_{\mathrm{L}}) + \bar{m}^2(\varphi^\dagger)^{ab}\varphi^{ba} \right\} \tag{3.13}$$

with an additional mass term provided by the constant $\bar{m}^2$ of the auxiliary scalar fields φ and $\varphi^\dagger$. This term has to be compatible with the symmetry of course. We employ the substitution

$$\begin{aligned}\varphi^{ba} &\to \varphi^{ba} + \mathrm{i}\frac{\bar{h}}{\bar{m}^2}(\bar{\psi}^a_{\mathrm{R}}\gamma_5\psi^b_{\mathrm{L}}),\\ (\varphi^\dagger)^{ab} &\to (\varphi^\dagger)^{ab} - \mathrm{i}\frac{\bar{h}}{\bar{m}^2}(\bar{\psi}^b_{\mathrm{L}}\gamma_5\psi^a_{\mathrm{R}}),\end{aligned} \tag{3.14}$$

where we have introduced the auxiliary coupling $\bar{h}$ which can be chosen arbitrarily. If we require

$$\frac{\bar{g}}{N_{\mathrm{f}}} \equiv \frac{\bar{h}^2}{\bar{m}^2} \tag{3.15}$$

we obtain the partially bosonized action

$$S[\psi,\bar{\psi},\varphi,\varphi^\dagger] = \int \mathrm{d}^d x \left\{ \mathrm{i}\bar{\psi}^a\partial\!\!\!/\psi^a + \mathrm{i}\bar{h}\left[\bar{\psi}^a_{\mathrm{R}}(\varphi^\dagger)^{ab}\gamma_5\psi^b_{\mathrm{L}} - \bar{\psi}^b_{\mathrm{L}}\varphi^{ba}\gamma_5\psi^a_{\mathrm{R}}\right] + U(\varphi^\dagger,\varphi)\right\}, \tag{3.16}$$

where the four-fermion interaction term is replaced by a Yukawa-type interaction. Besides the mass term, we consider a more general bosonic potential which is already introduced here. By use of the equations of motion of the scalar fields and only taking the mass term of the bosonic potential into account, we may trace back the bosonized action to the pure fermionic one (3.9).

In general, quantum fluctuations may generate an infinite number of interaction terms during the flow. This renders the choice of a suitable truncation of the effective average action Γ_k quite delicate. Hence, it is a highly non-trivial question whether a certain truncation describes the main properties of a theory sufficiently. The truncation given by

$$\begin{aligned}\Gamma_k[\psi,\bar{\psi},\varphi,\varphi^\dagger] = \int \mathrm{d}^d x \Big\{ &\mathrm{i}Z_{\psi,k}\bar{\psi}^a\partial\!\!\!/\psi^a + Z_{\varphi,k}\partial_\mu(\varphi^\dagger)^{ab}\partial_\mu\varphi^{ba}\\ &+\mathrm{i}\bar{h}_k\left[\bar{\psi}^a_{\mathrm{R}}(\varphi^\dagger)^{ab}\gamma_5\psi^b_{\mathrm{L}} - \bar{\psi}^b_{\mathrm{L}}\varphi^{ba}\gamma_5\psi^a_{\mathrm{R}}\right] + U_k(\varphi,\varphi^\dagger)\Big\}\end{aligned} \tag{3.17}$$

follows from the next-to-leading order in a systematic derivative expansion and appears to be quite natural. We assume the wave function renormalizations $Z_{\psi,k}$ and $Z_{\varphi,k}$ of the standard kinetic terms to be field independent. Note the introduced scale dependency of the wave function renormalizations, coupling constant $\bar{h}_k$ and potential U_k. We stress that we did not distinguished between the bosonic fields and their expectation value in this section, but the relation (2.4) given in the chapter 2 holds.

From the potential, we know the contribution of the bosonic mass term. Moreover, it may contain terms corresponding to higher than four-fermion interactions. We further search for other bosonic contributions compatible with the chiral $\mathrm{U}(N_{\mathrm{f}}) \otimes \mathrm{U}(N_{\mathrm{f}})$ symmetry. The scalar fields transform in the way

$$\begin{aligned}\varphi^{ab} &\mapsto U^{ac}_{\mathrm{L}}\varphi^{cd}U^{\dagger db}_{\mathrm{R}},\\ (\varphi^\dagger)^{ab} &\mapsto U^{ac}_{\mathrm{R}}(\varphi^\dagger)^{cd}U^{\dagger db}_{\mathrm{L}},\end{aligned} \tag{3.18}$$

where $U_{\mathrm{L/R}}$ are unitary $N_{\mathrm{f}} \times N_{\mathrm{f}}$ matrices. Therefore, besides

$$\mathrm{Tr}(\varphi^\dagger\varphi) =: \rho \tag{3.19}$$

we find

$$\{\mathrm{Tr}\phi^i\} =: \{\tilde{\tau}_i\}_{i\geq 2}, \tag{3.20}$$

where $\phi = \varphi^\dagger\varphi - \rho/N_{\mathrm{f}}\mathbb{1}_{N_{\mathrm{f}}}$, to be invariant with respect to the chiral symmetry [46]. With regard to the invariant $\tilde{\tau}_2$, we define

$$\tau := \frac{N_{\mathrm{f}}}{N_{\mathrm{f}}-1}\tilde{\tau}_2. \tag{3.21}$$

In our truncation of the scalar potential, we only consider polynomial terms up to second and first order of ρ and τ, respectively. This corresponds to quartic order in the bosonic fields. The potential in the symmetric regime can be written as

$$U_k^{\mathrm{SYM}}(\rho,\tau) = \bar{m}_k^2\rho + \frac{1}{2}\bar{\lambda}_{1k}\rho^2 + \frac{N_\mathrm{f}-1}{4}\bar{\lambda}_{2k}\tau. \tag{3.22}$$

For the symmetry broken case, $\bar{m}_k^2$ becomes negative and we choose

$$U_k^{\mathrm{SSB}}(\rho,\tau) = \frac{1}{2}\bar{\lambda}_{1k}(\rho-\rho_{0k})^2 + \frac{N_\mathrm{f}-1}{4}\bar{\lambda}_{2k}\tau, \tag{3.23}$$

where ρ_{0k} is the non-vanishing minimum of the potential.

In this truncation, we have ignored the dependency on all contributions of the invariants $\tilde{\tau}_i$ ($i>2$) and of higher polynomial orders of ρ and τ, which correspond to terms $\propto \varphi^n$ with $n \geq 6$. Discarding terms $\propto \varphi^n$ with $n \geq 8$ can be justified by the negative canonical mass dimension of the parametrizing coupling. As long as naive powercounting is not strongly modified by large anomalous dimensions, such terms are irrelevant. For $n=6$ the canonical mass dimension is exactly zero, thus, it is not sure if terms $\propto \varphi^6$ are either relevant or irrelevant upon inclusion of fluctuations. In our further investigations, we will pick up this question again.

We designed the potential with regard to the symmetry breaking pattern $\mathrm{U}(N_\mathrm{f})\otimes\mathrm{U}(N_\mathrm{f}) \to \mathrm{U}(N_\mathrm{f})$ which we wish to investigate in more detail. Nevertheless, we will discuss other symmetry breaking patterns as well in section 3.3. Therefore, it is useful to compute the mass spectra first.

3.2. Mass matrices and flow equation of the potential

As the truncated effective average actions are very similar, the following calculation is close to that in [46]. To obtain the flow equation of the potential, we employ (2.18) in its exact form. Although we perform our later calculations in $2+1$ dimensions, we will first leave d and d_γ unspecified to display some dependencies in a more obvious way. Furthermore, we emphasize that from now on the symbolic distinction U_k^{SYM} and U_k^{SSB} between the potential in the symmetric and symmetry broken regime is dropped and we only write $U_k = U_k(\rho,\tau)$ for both cases. It is convenient for the following calculations to transform the action apart from the scalar potential into momentum space

$$\begin{aligned}\Gamma_k[\psi,\bar{\psi},\varphi,\varphi^\dagger] = &\int \mathrm{d}^d x U_k(\rho,\tau)\\ &+\int \frac{\mathrm{d}^d p}{(2\pi)^d}\Bigg\{ - Z_{\psi,k}\bar{\psi}^a(p)\not{p}\psi^a(p)\\ &+\frac{1}{2}Z_{\varphi,k}p^2\left(\varphi_\mathrm{R}^{ab}(p)\varphi_\mathrm{R}^{ab}(-p)+\varphi_\mathrm{I}^{ab}(p)\varphi_\mathrm{I}^{ab}(-p)\right)\\ &+\mathrm{i}\bar{h}_k\int\frac{\mathrm{d}^d q}{(2\pi)^d}\left[\bar{\psi}_\mathrm{R}^a(p)(\varphi^\dagger)^{ab}(q-p)\gamma_5\psi_\mathrm{L}^b(q) - \bar{\psi}_\mathrm{L}^b(p)\varphi^{ba}(p-q)\gamma_5\psi_\mathrm{R}^a(q)\right]\Bigg\},\end{aligned} \tag{3.24}$$

whose derivatives with respect to the bosonic fields are easier to determine using (3.22) and (3.23) given in space-time coordinates. The fields $\varphi_\mathrm{R}(p)$, $\varphi_\mathrm{I}(p)$ are the Fourier transformed real and imaginary parts of the bosonic fields $\varphi^{ab}(x) = (\varphi_\mathrm{R}^{ab}(x)+\mathrm{i}\varphi_\mathrm{I}^{ab}(x))/\sqrt{2}$ in space-time coordinates. In order to derive the flow equation of the potential, we have to perform the second functional derivative

$$\Gamma_k^{(2)} = \frac{\overrightarrow{\delta}}{\delta\Phi^\mathrm{T}}\Gamma_k\frac{\overleftarrow{\delta}}{\delta\Phi} \qquad \text{with} \qquad \Phi = \begin{pmatrix}\psi\\ \bar{\psi}^\mathrm{T}\\ \varphi_\mathrm{R}\\ \varphi_\mathrm{I}\end{pmatrix} \tag{3.25}$$

of the effective average action. The fields carry indices which run from 1 to N_f implying that the derivative vector has $2N_\mathrm{f}^2 + 2N_\mathrm{f}$ components. To obtain the flow of the scalar potential, we project both sides of the Wetterich equation (2.18) onto $\psi = \bar{\psi} = 0$ and onto space-time independent bosonic fields which means

$$\varphi(p) = \varphi(2\pi)^d\delta(p) \qquad \text{and} \qquad \varphi^\dagger(p) = \varphi^\dagger(2\pi)^d\delta(p) \tag{3.26}$$

in momentum space. A positive effect is the easily treatable diagonal form in momentum space of $\Gamma_k^{(2)}$. For obtaining the full propagator of (2.18), we need a regulator $R_k(p,q)$ satisfying the conditions (2.10)–(2.12). Since it can be interpreted as an additional, scale and momentum dependent mass, we adopt the matrix structure for the regulator[3]

$$R_k(p,q) = \begin{pmatrix} 0 & -R^\mathrm{T}_{\psi,k}(-p)\delta^{ab} & 0 & 0 \\ R_{\psi,k}(p)\delta^{ab} & 0 & 0 & 0 \\ 0 & 0 & R_{\varphi,k}(p)\delta^{ac}\delta^{bd} & 0 \\ 0 & 0 & 0 & R_{\varphi,k}(p)\delta^{ac}\delta^{bd} \end{pmatrix} (2\pi)^d\delta(p-q), \tag{3.27}$$

where $R_{\psi,k}(p) = -Z_{\psi,k}\not{p}r_{\psi,k}(p^2/k^2)$ and $R_{\varphi,k}(p) = Z_{\varphi,k}p^2 r_{\varphi,k}(p^2/k^2)$. In this notation, the conditions (2.10)–(2.12) have to be adapted to the dimensionless shape functions $r_{\psi,k}$ and $r_{\varphi,k}$.

We can now write down the non-vanishing contributions of the inverse propagator matrix $G_k^{-1}(p,q) = \Gamma_k^{(2)}(p,q) + R_k(p,q)$

$$\begin{aligned}
(G_k^{-1})^{12}(p,q) &= \left[-Z_{\psi,k}\delta^{ab}\not{p}^\mathrm{T}(1+r_{\psi,k}) + \mathrm{i}\bar{h}_k\left(\varphi^{ab}(P_\mathrm{L}\gamma_5)^\mathrm{T} - (\varphi^\dagger)^{ab}(P_\mathrm{R}\gamma_5)^\mathrm{T}\right)\right](2\pi)^d\delta(p-q),\\
(G_k^{-1})^{21}(p,q) &= \left[-Z_{\psi,k}\delta^{ab}\not{p}(1+r_{\psi,k}) + \mathrm{i}\bar{h}_k\left((\varphi^\dagger)^{ab}(P_\mathrm{R}\gamma_5) - \varphi^{ab}(P_\mathrm{L}\gamma_5)\right)\right](2\pi)^d\delta(p-q),\\
(G_k^{-1})^{33}(p,q) &= \left[Z_{\varphi,k}p^2\delta^{ac}\delta^{bd}(1+r_{\varphi,k}) + \frac{\delta^2 U_k}{\delta\varphi_\mathrm{R}^{ab}\delta\varphi_\mathrm{R}^{cd}}\right](2\pi)^d\delta(p-q),\\
(G_k^{-1})^{44}(p,q) &= \left[Z_{\varphi,k}p^2\delta^{ac}\delta^{bd}(1+r_{\varphi,k}) + \frac{\delta^2 U_k}{\delta\varphi_\mathrm{I}^{ab}\delta\varphi_\mathrm{I}^{cd}}\right](2\pi)^d\delta(p-q),\\
(G_k^{-1})^{34}(p,q) &= \frac{\delta^2 U_k}{\delta\varphi_\mathrm{R}^{ab}\delta\varphi_\mathrm{I}^{cd}}(2\pi)^d\delta(p-q),\\
(G_k^{-1})^{43}(p,q) &= \frac{\delta^2 U_k}{\delta\varphi_\mathrm{I}^{ab}\delta\varphi_\mathrm{R}^{cd}}(2\pi)^d\delta(p-q).
\end{aligned} \tag{3.28}$$

At first sight, the decoupling of the fermionic and scalar fields is striking and simplifies the inversion of $G_k^{-1}(p,q)$ a lot. The main task now is to evaluate the eigenvalues of the mass matrices $\frac{\delta^2 U_k}{\delta\varphi^{ab}_{\mathrm{R/I}}\delta\varphi^{cd}_{\mathrm{R/I}}}$ which belong to the bosonic part of the inverse propagator. From these eigenvalues, we can read off the mass spectra on the one hand, and on the other hand determine the inverse of $G_k^{-1}(p,q)$. For this purpose, we assume a hermitian, diagonal form of the scalar fields $\varphi^{ab} = \varphi_a\delta^{ab}$ which renders the bosonic part of the inverse propagator hermitian[4]. The exact order of the bosonic fields in the vector Φ can be chosen in such a way that we receive a block diagonal form for the explicit structure of the bosonic, inverse propagator. We may employ then the mathematical theorem that hermitian matrices can always be transformed to a diagonal form by unitary matrices V and $V^\dagger$. The matrices V and $V^\dagger$ actually cancel out of the trace of the Wetterich equation (2.18). The requirement of a hermitian, diagonal scalar field is not as special as one might think at first. To be more precise, it does not give rise to any

[3] The indices a, b and c, d count for the scalar fields φ^{ab} and φ^{cd} in the bosonic part.

[4] Note that the summation convention is not employed for the fields φ_a.

restriction. That can be justified by exploiting the implemented chiral symmetry, see appendix A. It is worth mentioning that the fermionic part of the propagator can be easily inverted for the assumed form of scalar fields.

Applying the chain rule to the mass matrices yields

$$
\begin{aligned}
\frac{\delta^2 U_k}{\delta\varphi_{\mathrm{R}}^{ab}\delta\varphi_{\mathrm{R}}^{cd}} =& U_k'\delta^{ac}\delta^{bd} + 2U_k''\varphi_a\varphi_c\delta^{ab}\delta^{cd} + \dot{U}_k\frac{\delta^2\tau}{\delta\varphi_{\mathrm{R}}^{ab}\delta\varphi_{\mathrm{R}}^{cd}} + \ddot{U}_k\frac{\delta\tau}{\delta\varphi_{\mathrm{R}}^{ab}}\frac{\delta\tau}{\delta\varphi_{\mathrm{R}}^{cd}} \\
&+ \sqrt{2}\dot{U}_k'\left(\varphi_c\delta^{cd}\frac{\delta\tau}{\delta\varphi_{\mathrm{R}}^{ab}} + \varphi_a\delta^{ab}\frac{\delta\tau}{\delta\varphi_{\mathrm{R}}^{cd}}\right), \\
\frac{\delta^2 U_k}{\delta\varphi_{\mathrm{I}}^{ab}\delta\varphi_{\mathrm{I}}^{cd}} =& U_k'\delta^{ac}\delta^{bd} + \dot{U}_k\frac{\delta^2\tau}{\delta\varphi_{\mathrm{I}}^{ab}\delta\varphi_{\mathrm{I}}^{cd}}, \\
\frac{\delta^2 U_k}{\delta\varphi_{\mathrm{R}}^{ab}\delta\varphi_{\mathrm{I}}^{cd}} =& 0.
\end{aligned}
\tag{3.29}
$$

Primes denote derivatives with respect to ρ and dots derivatives with respect to τ. We have already neglected the derivatives of ρ and τ which vanish for the assumed form of the scalar fields. The non-vanishing derivatives which we have used in (3.29) are

$$
\begin{aligned}
\frac{\delta\rho}{\delta\varphi_{\mathrm{R}}^{ab}} =& \sqrt{2}\varphi_a\delta^{ab}, \\
\frac{\delta^2\rho}{\delta\varphi_{\mathrm{R}}^{ab}\delta\varphi_{\mathrm{R}}^{cd}} =& \delta^{ac}\delta^{bd}, \\
\frac{\delta^2\rho}{\delta\varphi_{\mathrm{I}}^{ab}\delta\varphi_{\mathrm{I}}^{cd}} =& \delta^{ac}\delta^{bd}, \\
\frac{\delta\tau}{\delta\varphi_{\mathrm{R}}^{ab}} =& 2\sqrt{2}\delta^{ab}\left(\frac{N_{\mathrm{f}}}{N_{\mathrm{f}}-1}\varphi_a^3 - \frac{1}{N_{\mathrm{f}}-1}\rho\varphi_a\right), \\
\frac{\delta^2\tau}{\delta\varphi_{\mathrm{R}}^{ab}\delta\varphi_{\mathrm{R}}^{cd}} =& 2\delta^{ac}\delta^{bd}\left(\frac{N_{\mathrm{f}}}{N_{\mathrm{f}}-1}(\varphi_a^2+\varphi_b^2) - \frac{1}{N_{\mathrm{f}}-1}\rho\right) \\
&+ \frac{2N_{\mathrm{f}}}{N_{\mathrm{f}}-1}\varphi_a\varphi_c\delta^{bc}\delta^{ad} - \frac{4}{N_{\mathrm{f}}-1}\varphi_a\varphi_c\delta^{ab}\delta^{cd}, \\
\frac{\delta^2\tau}{\delta\varphi_{\mathrm{I}}^{ab}\delta\varphi_{\mathrm{I}}^{cd}} =& 2\delta^{ac}\delta^{bd}\left(\frac{N_{\mathrm{f}}}{N_{\mathrm{f}}-1}(\varphi_a^2+\varphi_b^2) - \frac{1}{N_{\mathrm{f}}-1}\rho\right) \\
&- \frac{2N_{\mathrm{f}}}{N_{\mathrm{f}}-1}\varphi_a\varphi_c\delta^{bc}\delta^{ad}.
\end{aligned}
\tag{3.30}
$$

As for the scalar and fermionic fields before, the real and imaginary parts of the bosonic fields decouple. Thus, the bosonic, inverse propagator decomposes into $(G_k^{-1})^{33}(p,q)$ and $(G_k^{-1})^{44}(p,q)$, which may be treated seperately.

Let us first consider $\frac{\delta^2 U_k}{\delta\varphi_{\mathrm{I}}^{ab}\delta\varphi_{\mathrm{I}}^{cd}}$. We find that only entries for $a=b=c=d$, $(a,b)=(c,d)$ and $(a,b)=(d,c)$, where $a\neq b$ and $c\neq d$, occur. Hence, we choose the order of the fields $\varphi_{\mathrm{I}}^{ab}$ to be in such a way that

$$
\begin{array}{cc}
 & \begin{array}{cccccccccc} \varphi_{\mathrm{I}}^{11} & \varphi_{\mathrm{I}}^{22} & \varphi_{\mathrm{I}}^{33} & \ldots & \varphi_{\mathrm{I}}^{12} & \varphi_{\mathrm{I}}^{21} & \ldots & \varphi_{\mathrm{I}}^{23} & \varphi_{\mathrm{I}}^{32} & \ldots \end{array} \\
\begin{array}{c} \varphi_{\mathrm{I}}^{11} \\ \varphi_{\mathrm{I}}^{22} \\ \varphi_{\mathrm{I}}^{33} \\ \vdots \\ \varphi_{\mathrm{I}}^{12} \\ \varphi_{\mathrm{I}}^{21} \\ \vdots \\ \varphi_{\mathrm{I}}^{23} \\ \varphi_{\mathrm{I}}^{32} \\ \vdots \end{array} &
\begin{pmatrix}
\bullet & & & & & & & & & \\
 & \bullet & & & & & & & & \\
 & & \bullet & & & & & & & \\
 & & & \ddots & & & & & & \\
 & & & & \bullet & \circ & & & & \\
 & & & & \circ & \bullet & & & & \\
 & & & & & & \ddots & & & \\
 & & & & & & & \bullet & \circ & \\
 & & & & & & & \circ & \bullet & \\
 & & & & & & & & & \ddots
\end{pmatrix}
\end{array}
= \frac{\delta^2 U_k}{\delta\varphi_{\mathrm{I}}^{ab}\delta\varphi_{\mathrm{I}}^{cd}}. \tag{3.31}
$$

From the first $N_{\mathrm{f}} \times N_{\mathrm{f}}$ block matrix, we can read off the eigenvalues

$$(M_{\mathrm{I}a})^2 = U_k' + \frac{2}{N_{\mathrm{f}}-1}\dot{U}_k\left(N_{\mathrm{f}}\varphi_a^2 - \rho\right). \tag{3.32}$$

The other $N_{\mathrm{f}}(N_{\mathrm{f}}-1) \times N_{\mathrm{f}}(N_{\mathrm{f}}-1)$ block matrix only consists of small 2×2 matrices. Same color of the dots in such a matrix constitutes same entries. Due to this simple structure, we can easily compute the corresponding eigenvalues

$$(M_{\mathrm{I}ab}^{\pm})^2 = U_k' + \frac{2}{N_{\mathrm{f}}-1}\dot{U}_k\left[N_{\mathrm{f}}\left(\varphi_a^2 + \varphi_b^2 \pm \varphi_a\varphi_b\right) - \rho\right]. \tag{3.33}$$

After having evaluated the mass matrices of the imaginary part of the scalar fields, we determine the eigenvalues of $\frac{\delta^2 U_k}{\delta\varphi_{\mathrm{R}}^{ab}\delta\varphi_{\mathrm{R}}^{cd}}$ in the following with a quite similar procedure. As before, only entries for $(a,b) = (c,d)$ and $(a,b) = (d,c)$ for $a \neq b$ and $c \neq d$ differ from zero. Fields with $a = b$ and $c \neq d$ decouple. Hence, the real bosonic fields with $a \neq b$ are ordered in the same way as the imaginary fields to get at a similar simple form of the mass matrix. For this case, we have the same $N_{\mathrm{f}}(N_{\mathrm{f}}-1)$ eigenvalues

$$(M_{\mathrm{R}ab}^{\pm})^2 = (M_{\mathrm{I}ab}^{\pm})^2 \tag{3.34}$$

as we have found for imaginary fields. On the contrary, the fields $a = b, c = d$ mix providing a more complicated form of the first block matrix

$$
\begin{aligned}
\frac{\delta^2 U_k}{\delta\varphi_{\mathrm{R}}^{aa}\delta\varphi_{\mathrm{R}}^{cc}} = {} & \left[U_k' + \frac{2}{N_{\mathrm{f}}-1}\dot{U}_k(3N_{\mathrm{f}}\varphi_a^2 - \rho)\right]\delta^{ac} \\
& + 2\varphi_a\varphi_c\Bigg[U_k'' + \frac{2}{N_{\mathrm{f}}-1}\dot{U}_k'\left(N_{\mathrm{f}}(\varphi_a^2 + \varphi_c^2) - 2\rho\right) \\
& + \frac{4}{(N_{\mathrm{f}}-1)^2}\ddot{U}_k\left(N_{\mathrm{f}}\varphi_a^2 - \rho\right)\left(N_{\mathrm{f}}\varphi_c^2 - \rho\right) - \frac{2}{N_{\mathrm{f}}-1}\dot{U}_k\Bigg],
\end{aligned} \tag{3.35}
$$

but which is also calculable if we assume a particular configuration of our scalar fields. We assume that the squares of φ_a are equal for $a = 1, \ldots, N_{\mathrm{f}}-1$ in order to be in the more comfortable situation to express the scalar fields only in terms of ρ and τ

$$\rho = (N_{\mathrm{f}}-1)\varphi_1^2 + \varphi_{N_{\mathrm{f}}}^2, \qquad \tau = (\varphi_1^2 - \varphi_{N_{\mathrm{f}}}^2)^2, \tag{3.36}$$

$$\varphi_1^2 = \frac{1}{N_{\mathrm{f}}}(\rho + \sqrt{\tau}), \qquad \varphi_{N_{\mathrm{f}}}^2 = \frac{1}{N_{\mathrm{f}}}(\rho - (N_{\mathrm{f}}-1)\sqrt{\tau}), \tag{3.37}$$

where we require $\varphi_1^2 \geq \varphi_{N_\mathrm{f}}^2$ without any restriction. Actually, we cannot generally choose $\varphi_a^2 = \ldots = \varphi_{N_\mathrm{f}}^2$ since τ would vanish then. This fact demonstrates that a suitable configuration hardly depends on the truncation we have decided for in section 3.1.2. We derive

$$
\begin{aligned}
(M_{\mathrm{R}a})^2 =& A, && \text{multiplicity: } (N_\mathrm{f}-2) \qquad (3.38)\\
(M_{\mathrm{R}N_\mathrm{f}}^{\pm})^2 =& \frac{1}{2}\Big[2A + B + D && \text{multiplicity: } 1 \qquad (3.39)\\
& \pm \sqrt{4(N_\mathrm{f}-1)C^2 + (B-D)^2}\Big],
\end{aligned}
$$

where

$$
\begin{aligned}
A &:= U_k' + \frac{2}{N_\mathrm{f}-1}\dot{U}_k(2\rho + 3\sqrt{\tau}),\\
B &:= 2\varphi_1^2\left[(N_\mathrm{f}-1)U_k'' + 4\dot{U}_k'\sqrt{\tau} + \frac{4}{(N_\mathrm{f}-1)}\ddot{U}_k\tau - 2\dot{U}_k\right],\\
C &:= 2\varphi_1\varphi_{N_\mathrm{f}}\left[U_k'' - \frac{2(N_\mathrm{f}-2)}{N_\mathrm{f}-1}\dot{U}_k'\sqrt{\tau} - \frac{4}{(N_\mathrm{f}-1)}\ddot{U}_k\tau - \frac{2}{N_\mathrm{f}-1}\dot{U}_k\right],\\
D &:= -\frac{6N_\mathrm{f}}{N_\mathrm{f}-1}\dot{U}_k\sqrt{\tau} + 2\varphi_{N_\mathrm{f}}^2\left[U_k'' - 4\dot{U}_k'\sqrt{\tau} + 4\ddot{U}_k\tau - \frac{2}{N_\mathrm{f}-1}\dot{U}_k\right].
\end{aligned}
\tag{3.40}
$$

Putting everything together, we are now able to write down the bosonic part of the potential's flow equation

$$
\begin{aligned}
\left.\frac{\partial U_k}{\partial t}\right|_{\mathrm{Bos}} =& \frac{1}{2}\int \frac{\mathrm{d}^d p}{(2\pi)^d}\partial_t R_{\varphi,k}(p)\\
&\times\Bigg\{\sum_a\left[\frac{1}{Z_{\varphi,k}p^2(1+r_{\varphi,k}) + (M_{\mathrm{I}a})^2} + \frac{1}{Z_{\varphi,k}p^2(1+r_{\varphi,k}) + (M_{\mathrm{R}a})^2}\right]\\
&+\sum_{\substack{a,b\\a<b}}\Bigg[\frac{1}{Z_{\varphi,k}p^2(1+r_{\varphi,k}) + (M_{\mathrm{I}ab}^+)^2} + \frac{1}{Z_{\varphi,k}p^2(1+r_{\varphi,k}) + (M_{\mathrm{I}ab}^-)^2}\\
&+\frac{1}{Z_{\varphi,k}p^2(1+r_{\varphi,k}) + (M_{\mathrm{R}ab}^+)^2} + \frac{1}{Z_{\varphi,k}p^2(1+r_{\varphi,k}) + (M_{\mathrm{R}ab}^-)^2}\Bigg]\Bigg\}.
\end{aligned}
\tag{3.41}
$$

Computing the fermionic part of the flow is straightforward by using $\mathrm{Tr}[(P_\mathrm{L} - P_\mathrm{R})\gamma_5 \not{p}] \propto \mathrm{Tr}\gamma_4\gamma_\mu = 0$ for any $\mu \in \{1,2,3\}$. Therefore, we skip a detailed discussion and finally obtain

$$
\left.\frac{\partial U_k}{\partial t}\right|_{\mathrm{Ferm}} = -\frac{1}{2}d_\gamma \int \frac{\mathrm{d}^d p}{(2\pi)^d}\left[\tilde{\partial}_t\left(Z_{\psi,k}^2 p^2(1+r_{\psi,k})^2\right)\right]\sum_a \frac{1}{Z_{\psi,k}^2 p^2(1+r_{\psi,k})^2 + \bar{h}_k^2\varphi_a^2}. \tag{3.42}
$$

To evaluate the sum for further calculations, we will insert (3.37) assuming the special field configuration and consequently replace the dependency on φ_a by ρ and τ. This will be advantageous for computing the flow equations of the couplings.

3.3. Symmetry breaking patterns and mass spectra

Let us take a break on the way to the determination of the couplings' flow equations and discuss what kinds of spontaneous symmetry breaking exist and which masses are generated then.[5] In reminiscence of our truncation of the scalar potential, the potential is bounded from below for

[5] see also [59].

any value of $\bar{m}_k^2$, positive or negative, if $\bar{\lambda}_{1k} > 0$ and $\bar{\lambda}_{2k} > -2\bar{\lambda}_{1k}/(N_\mathrm{f}-1)$. We first consider the very simple symmetric case. If $\bar{m}_k^2 > 0$, the global minimum of the potential can be found at $\varphi = 0$. One can directly read off the mass $\bar{m}_k^2$ of the $2N_\mathrm{f}^2$ bosons from the eigenvalues which coincides with the mass parameter in (3.22), of course. Since the Yukawa-type term vanishes at the minimum $\frac{\delta^2 U^\mathrm{Yuk}}{\delta\bar{\psi}^a\delta\psi^b}\Big|_{\varphi=0} = 0$, the fermions remain massless.

In the symmetry broken regime $\bar{m}_k^2$ becomes negative. Positive $\bar{\lambda}_{2k}$ implies a particular symmetry breaking pattern we first like to consider. Therefore we use (3.23) in the symmetry broken regime. One can find the absolute minimum to be at $\rho = \rho_{0k}$ and $\tau = 0$. The minimizing field configuration satisfies $\varphi_{0k}^{ab} = \sigma_{0k}\delta^{ab}$. We count $N_\mathrm{f}^2 - 1$ τ-modes

$$(M_{\mathrm{R}a})^2 = (M_{\mathrm{R}N_\mathrm{f}}^+)^2 = (M_{\mathrm{I}ab}^+)^2 = (M_{\mathrm{R}ab}^+)^2 = U_k' + \frac{4\rho_{0k}}{N_\mathrm{f}-1}\dot{U}_k = \rho_{0k}\bar{\lambda}_{2k}, \tag{3.43}$$

one radial mode

$$(M_{\mathrm{R}N_\mathrm{f}}^-)^2 = U_k' + 2U_k''\rho_{0k} = 2\rho_{0k}\bar{\lambda}_{1k} \tag{3.44}$$

and N_f^2 Goldstone modes

$$(M_{\mathrm{I}a})^2 = (M_{\mathrm{I}ab}^-)^2 = (M_{\mathrm{R}ab}^-)^2 = 0. \tag{3.45}$$

The N_f fermions acquire the mass $\rho_{0k}\bar{h}_k^2/N_\mathrm{f}$, which can be verified by computing the eigenvalues of $\frac{\delta^2 U_k^\mathrm{Yuk}}{\delta\bar{\psi}^a\delta\psi^b}\Big|_{\varphi=\varphi_{0k}}$. According to the Goldstone theorem, N_f^2 of the $2N_\mathrm{f}^2$ symmetry generators should be broken due to the N_f^2 massless bosons. Indeed, we recover a remnant $\mathrm{U}(N_\mathrm{f})$ symmetry leaving the non-zero VEV $\sigma_0 \widehat{=} \langle\bar{\psi}_\mathrm{R}^a\gamma_5\psi_\mathrm{L}^a\rangle$ unchanged which can be easily seen if one sets $U_\mathrm{L} = U_\mathrm{R}$ for the transformation matrices. It is worth mentioning that we could also consider $\langle\bar{\psi}^a\gamma_5\psi^a\rangle$ because if $\langle\bar{\psi}_\mathrm{R}^a\gamma_5\psi_\mathrm{L}^a\rangle \neq 0$ then also $\langle\bar{\psi}^a\gamma_5\psi^a\rangle \neq 0$ and vice versa.

Another symmetry breaking pattern arises if $\bar{\lambda}_{2k} < 0$. The minimizing field configuration is given by $\varphi_{0k}^{ab} = \sigma_{0k}\delta^{ab}\delta^{a1}$ for which we observe apart from ρ_{0k} a finite value τ_{0k}, namely $\tau_{0k} = \rho_{0k}^2$. From the eigenvalues of the mass matrices, we can conclude that there are $4N_\mathrm{f} - 3$ Goldstone modes

$$(M_{\mathrm{I}1})^2 = (M_{\mathrm{I}1a}^\pm)^2 = (M_{\mathrm{R}1a}^\pm)^2 = U_k' + 2\rho_{0k}\dot{U}_k = 0, \tag{3.46}$$

where $a = 2, \dots, N_\mathrm{f}$ since at the minimum the condition

$$\frac{\delta U_k}{\delta\varphi_{11}}\bigg|_{\varphi_{11}=\sigma_{0k}} = U_k' + 2\rho_{0k}\dot{U}_k = 0 \tag{3.47}$$

holds [59]. On the other hand, we obtain $2N_\mathrm{f}^2 - 4N_\mathrm{f} + 2$ τ-modes

$$(M_{\mathrm{I}a})^2 = (M_{\mathrm{I}ab}^\pm)^2 = (M_{\mathrm{I}ab}^\pm)^2 = (M_{\mathrm{R}a})^2 = U_k' - \frac{2}{N_\mathrm{f}-1}\rho_0\dot{U}_k, \tag{3.48}$$

where $a, b = 2, \dots, N_\mathrm{f}$ again, and one radial mode with

$$(M_{\mathrm{R}1})^2 = U_k' + 6\rho_{0k}\dot{U}_k + 2\rho_{0k}(U_k'' + 4\rho_{0k}\dot{U}_k' + 4\rho_{0k}^2\ddot{U}_k). \tag{3.49}$$

The remaining boson masses indicate a remnant $\mathrm{U}(N_\mathrm{f}-1)\times\mathrm{U}(N_\mathrm{f}-1)\times\mathrm{U}(1)$ symmetry.

The last case is $\bar{\lambda}_{2k} = 0$ entailing that the potential is independent of τ. The $\mathrm{U}(N_\mathrm{f})\otimes\mathrm{U}(N_\mathrm{f})$ becomes enhanced by an $\mathrm{O}(2N_\mathrm{f}^2)$ symmetry if the coupling $\bar{h}_k$ additionally vanishes. In this case the fermions of this model decouple.[6] We observe then one radial mass $(M_{\mathrm{R}N_\mathrm{f}})^2 = 2\rho_{0k}U_k'' = 2\rho_{0k}\bar{\lambda}_{1k}$ and $2N_\mathrm{f}^2 - 1$ Goldstone modes. Therefore, we find a residual $\mathrm{O}(2N_\mathrm{f}^2 - 1)$ symmetry.

[6] We mention that $\bar{\lambda}_{2k} = 0$ but non-vanishing $\bar{h}_k$ is a not relevant case since a non-zero Yukawa coupling generates a $\bar{\lambda}_{2k}$ coupling during the flow.

3.4. Flow equation of the scalar couplings

First of all, we introduce dimensionless, renormalized couplings. One of the benefits will become clear in our later calculations when we search for fixed points, which are points where the system is scale invariant. Therefore, we define

$$\begin{aligned} h^2 &= Z_\varphi^{-1} Z_\psi^{-2} k^{d-4} \bar{h}^2, \\ \lambda_{1,2} &= Z_\varphi^{-2} k^{d-4} \bar{\lambda}_{1,2}, \\ \kappa &= Z_\varphi k^{2-d} \rho_0, \\ \epsilon &= Z_\varphi^{-1} k^{-2} \bar{m}^2. \end{aligned} \tag{3.50}$$

We suppress the k-dependency in our notation in the following. According to the couplings, we redefine the fields and invariants ρ and τ as well and write

$$\tilde{\rho} = Z_\varphi k^{2-d} \rho, \qquad \tilde{\tau} = Z_\varphi^2 k^{2(2-d)} \tau, \qquad u(\tilde{\rho}, \tilde{\tau}) = k^{-d} U(Z_\varphi^{-1} k^{d-2} \tilde{\rho}, Z_\varphi^{-2} k^{2(d-2)} \tilde{\tau}). \tag{3.51}$$

Instead of treating the wave function renormalizations directly, one can denote the flow in terms of anomalous dimensions

$$\eta_\varphi = -\partial_t \ln Z_\varphi, \qquad \eta_\psi = -\partial_t \ln Z_\psi. \tag{3.52}$$

The flow equation for the dimensionless potential reads

$$\partial_t u(\tilde{\rho}, \tilde{\tau}) = -d u(\tilde{\rho}, \tilde{\tau}) + (d - 2 + \eta_\varphi) \left[\tilde{\rho} \frac{\partial u}{\partial \tilde{\rho}} + 2\tilde{\tau} \frac{\partial u}{\partial \tilde{\tau}} \right] + k^{-d}\, \partial_t U(\rho, \tau)\big|_{\rho = Z_\varphi^{-1} k^{d-2} \tilde{\rho}, \tau = Z_\varphi^{-2} k^{2(d-2)} \tilde{\tau}} \,. \tag{3.53}$$

From this flow equation, it is now very easy to derive the couplings' scale dependency since we have already computed the last term. For this purpose, we perform derivatives of the left hand side with respect to $\tilde{\rho}$ or $\tilde{\tau}$ at the minimum. Projecting onto these minimizing values, we suppress contributing parts of other higher polynomial terms and implement the special symmetry breaking pattern in our equations, namely the symmetry breaking $\mathrm{U}(N_\mathrm{f}) \otimes \mathrm{U}(N_\mathrm{f}) \to \mathrm{U}(N_\mathrm{f})$. In the symmetric regime the evolution equations read[7]

$$\begin{aligned} \partial_t \epsilon = \frac{\partial(\partial_t u)}{\partial \tilde{\rho}}\bigg|_{(0,0)} &= -(2 - \eta_\varphi)\epsilon - 2v_d \Big\{ [2(N_\mathrm{f}^2 + 1)\lambda_1 + (N_\mathrm{f}^2 - 1)\lambda_2] l_1^d(\epsilon; \eta_\varphi) \\ &\quad - d_\gamma h^2 l_1^{(\mathrm{F})d}(\eta_\psi) \Big\}, \end{aligned} \tag{3.54}$$

$$\begin{aligned} \partial_t \lambda_1 = \frac{\partial^2(\partial_t u)}{\partial \tilde{\rho}^2}\bigg|_{(0,0)} &= (d - 4 + 2\eta_\varphi)\lambda_1 + 2v_d \Big\{ [2(N_\mathrm{f}^2 + 4)\lambda_1^2 \\ &\quad + (N_\mathrm{f}^2 - 1)\lambda_2(2\lambda_1 + \lambda_2)] l_2^d(\epsilon; \eta_\varphi) - \frac{d_\gamma}{N_\mathrm{f}} h^4 l_2^{(\mathrm{F})d}(\eta_\psi) \Big\}, \end{aligned} \tag{3.55}$$

$$\begin{aligned} \partial_t \lambda_2 = \frac{\partial(\partial_t u)}{\partial \tilde{\tau}}\bigg|_{(0,0)} &= (d - 4 + 2\eta_\varphi)\lambda_2 + 2v_d \Big\{ [12\lambda_1\lambda_2 + 2(N_\mathrm{f}^2 - 3)\lambda_2^2] l_2^d(\epsilon; \eta_\varphi) \\ &\quad - 2\frac{d_\gamma}{N_\mathrm{f}} h^4 l_2^{(\mathrm{F})d}(\eta_\psi) \Big\}, \end{aligned} \tag{3.56}$$

[7] see [46].

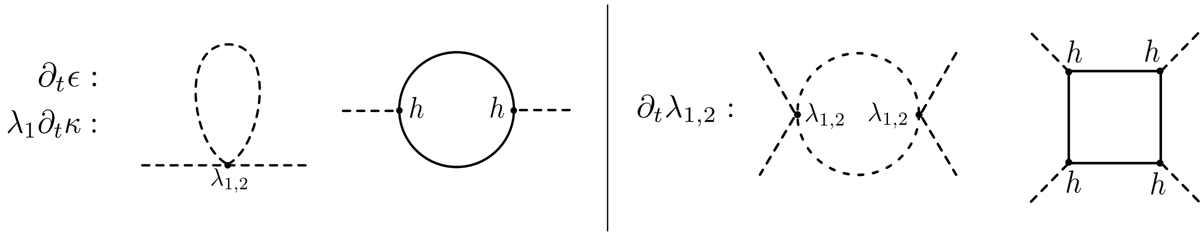

Figure 3.1.: The Feynman diagrams depict the flow equations of the scalar couplings in both regimes. Inner lines correspond to full propagators.

and in the symmetry broken regime

$$\partial_t\kappa = -\frac{1}{\lambda_1}\frac{\partial(\partial_t u)}{\partial\tilde{\rho}}\bigg|_{(\kappa,0)} =(2-d-\eta_\varphi)\kappa + 2v_d\bigg\{N_\mathrm{f}^2 l_1^d(\eta_\varphi) + 3l_1^d(2\kappa\lambda_1;\eta_\varphi) + (N_\mathrm{f}^2-1)\left[1+\frac{\lambda_2}{\lambda_1}\right]l_1^d(\kappa\lambda_2;\eta_\varphi) - d_\gamma\frac{h^2}{\lambda_1}l_1^{(\mathrm{F})d}(\kappa h^2/N_\mathrm{f};\eta_\psi)\bigg\}, \tag{3.57}$$

$$\partial_t\lambda_1 = \frac{\partial^2(\partial_t u)}{\partial\tilde{\rho}^2}\bigg|_{(\kappa,0)} =(d-4+2\eta_\varphi)\lambda_1 + 2v_d\bigg\{N_\mathrm{f}^2\lambda_1^2 l_2^d(\eta_\varphi) + 9\lambda_1^2 l_2^d(2\kappa\lambda_1;\eta_\varphi) + (N_\mathrm{f}^2-1)[\lambda_1+\lambda_2]^2 l_2^d(\kappa\lambda_2;\eta_\varphi), - \frac{d_\gamma}{N_\mathrm{f}}h^4 l_2^{(\mathrm{F})d}(\kappa h^2/N_\mathrm{f};\eta_\psi)\bigg\} \tag{3.58}$$

$$\partial_t\lambda_2 = \frac{\partial(\partial_t u)}{\partial\tilde{\tau}}\bigg|_{(\kappa,0)} =(d-4+2\eta_\varphi)\lambda_2 + 2v_d\bigg\{\frac{N_\mathrm{f}^2}{4}\lambda_2^2 l_2^d(\eta_\varphi) + \frac{9}{4}(N_\mathrm{f}^2-4)\lambda_2^2 l_2^d(\kappa\lambda_2;\eta_\varphi) - \frac{1}{2}N_\mathrm{f}^2\lambda_2^2 l_{1,1}^d(0,\kappa\lambda_2;\eta_\varphi) + 3[\lambda_2+4\lambda_1]\lambda_2 l_{1,1}^d(2\kappa\lambda_1,\kappa\lambda_2;\eta_\varphi) - 2\frac{d_\gamma}{N_\mathrm{f}}h^4 l_2^{(\mathrm{F})d}(\kappa h^2/N_\mathrm{f};\eta_\psi)\bigg\}, \tag{3.59}$$

where $v_d^{-1} := 2^{d+1}\pi^{d/2}\Gamma(d/2)$. For our special case $d=3$ we obtain $v_3 = 1/8\pi^2$. The threshold functions $l_n^{(\dots)d}(\dots)$ inherit the residual momentum integration coming from the trace of the Wetterich equation. Additionally, they carry information about the particular regularization scheme encoded in the choice of the shape functions $r_{\psi,k}$ and $r_{\varphi,k}$. Their definition and their explicit form can be looked up in appendix B.

The first part of each flow equation derives from the renormalization and rescaling of the couplings and do not encode any particular interactions. For interpreting the interaction contributions, Feynman diagrams are a helpful tool, see figure 3.1. In the symmetric regime, all the bosonic propagators carry the same mass ϵ. Fermionic fluctuations are massless, thus, there only exists one kind of bosonic and fermionic propagator which is encoded in the threshold functions. By contrast, in the spontaneous symmetry broken regime, the bosonic fluctuations may carry different masses from the radial mode, the τ-mode or remain massless due to the Goldstone bosons. These types of fluctuations may couple which happens in (3.59). Referring to the other equations, we only have loops of one type of bosons. Apart from prefactors, the contribution of the different bosons is proportional to their number. Note that due to the non-zero VEV the fermions now acquire a mass as well.

3.5. Flow equation of the scalar anomalous dimension

For the computation of the flow of the scalar anomalous dimension, we need to introduce a different structure of the scalar matrix fields because the kinetic term, which we are interested in, would vanish for constant fields. To be able to project $\partial_t \Gamma_k$ onto $\partial_t Z_\varphi$, we choose the spatially varying configuration

$$\varphi^{ab}(x) = \varphi\delta^{ab} + [\delta\varphi \mathrm{e}^{iQx} + \delta\varphi^* \mathrm{e}^{-iQx}]\Sigma_{ab} = (\varphi^{ab})^*(x), \tag{3.60}$$

where $\Sigma_{ab} = \delta^{a1}\delta^{b2} - \delta^{a2}\delta^{b1}$ and Q is an external momentum. In momentum space, the field reads

$$\begin{aligned}\varphi^{ab}(p) &= \varphi\delta(p)\delta^{ab} + [\delta\varphi\delta(p-Q) + \delta\varphi^*\delta(p+Q)]\Sigma_{ab} \\ &=: \varphi\delta(p)\delta^{ab} + \Delta(p,Q)\Sigma_{ab}.\end{aligned} \tag{3.61}$$

Since the fermions do not play any role, we set $\bar\psi = \psi = 0$. Thus, we obtain the evolution equation of the wave function renormalization by computing

$$\partial_t Z_\varphi = \frac{1}{\Omega_d} \lim_{Q^2\to 0} \frac{1}{4Q^2} \left(\lim_{\delta\varphi,\delta\varphi^*\to 0} \frac{\partial}{\partial(\delta\varphi\delta\varphi^*)} \partial_t \Gamma_k - X \right), \tag{3.62}$$

where $\Omega_d = (2\pi)^d \delta(0)$ denotes the space-time volume. The right hand side is evaluated by subtracting all Q-independent terms summarized in X. As before the fermionic and the bosonic parts of the inverse, full propagator $G_k^{-1} = \Gamma_k^{(2)} + R_k$ do not mix and can be treated separately [46]. It is convenient to decompose

$$\Gamma_k^{(2)} = \Gamma_{k,0}^{(2)} + \Delta\Gamma_k^{(2)} \tag{3.63}$$

into a part $\Gamma_{k,0}^{(2)}$ independent of $\delta\varphi$ and $\delta\varphi^*$ and into $\Delta\Gamma_k^{(2)}$ carrying all contributions of $\delta\varphi$ and $\delta\varphi^*$. Exploiting this decomposition, the following expansion

$$\begin{aligned}\mathrm{Tr}\left[\left(\Gamma_k^{(2)} + R_k\right)^{-1} \partial_t R_k\right] =& \mathrm{Tr}\left[\left(\Gamma_{k,0}^{(2)} + R_k\right)^{-1} \partial_t R_k\right] \\ &+ \mathrm{Tr}\left[\tilde\partial_t \left\{ \left(\Gamma_{k,0}^{(2)} + R_k\right)^{-1} \Delta\Gamma_k^{(2)} \right\}\right] \\ &- \frac{1}{2}\mathrm{Tr}\left[\tilde\partial_t \left\{ \left(\Gamma_{k,0}^{(2)} + R_k\right)^{-1} \Delta\Gamma_k^{(2)} \left(\Gamma_{k,0}^{(2)} + R_k\right)^{-1} \Delta\Gamma_k^{(2)} \right\}\right] \\ &+ \mathcal{O}(\Delta^3)\end{aligned} \tag{3.64}$$

can be terminated at quadratic order since higher terms would vanish in the limit $\delta\varphi, \delta\varphi^* \to 0$ anyway. As already mentioned, the trace of the fermionic and bosonic part may be evaluated separately. Inserting both into the Wetterich equation (2.18) determines the flow of the effective action. We drop a more detailed discussion of the calculation since the most important ideas are already treated in section 3.2 or can be looked up in [46]. All in all, by insertion of the corresponding potential's minimum, we obtain

$$\eta_\varphi = 4d_\gamma \frac{v_d}{d} h^2 m_4^{(\mathrm{F})d}(0;\eta_\psi) \tag{3.65}$$

for the symmetric regime and

$$\begin{aligned}\eta_\varphi =& 8\frac{v_d}{d}\kappa\left\{2\lambda_1^2 m_{2,2}^d(0,2\kappa\lambda_1;\eta_\varphi) + \frac{N_\mathrm{f}^2-2}{4}\lambda_2^2 m_{2,2}^d(0,\kappa\lambda_2;\eta_\varphi)\right\} \\ &+ 4d_\gamma \frac{v_d}{d} h^2 m_4^{(\mathrm{F})d}(\kappa h^2/N_\mathrm{f};\eta_\psi)\end{aligned} \tag{3.66}$$

for the symmetry broken regime. For the threshold functions, we again refer to appendix B.

The corresponding contributions can be illustrated by use of Feynman diagrams, see figure 3.2. In the symmetric case, we do not observe any coupling of the VEV since $\sigma_0 = 0$. Only fermionic fluctuations of vanishing mass contribute. In the symmetry broken case, loops of Goldstone bosons mixed with bosons of radial or τ-mass occur to which the VEV couples as transmitted by λ_1 or λ_2.

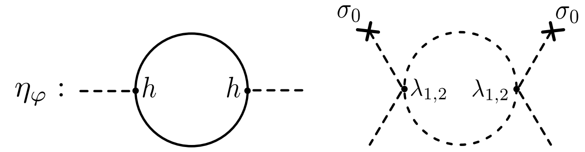

Figure 3.2.: The Feynman diagrams depict the flow equation of the scalar anomalous dimension in both regimes. Inner lines correspond to full propagators.

3.6. Flow of the Yukawa coupling and fermion anomalous dimension

For our next purpose, the determination of the flow equation of the Yukawa coupling and fermion anomalous dimension, we need a non-vanishing fermion field. Therefore, we assume

$$\begin{aligned} \varphi^{ab}(x) &= \varphi\delta^{ab}, \\ \psi^a(x) &= \psi^a \mathrm{e}^{iQx}, \\ \bar{\psi}^a(x) &= \bar{\psi}^a \mathrm{e}^{-iQx}. \end{aligned} \tag{3.67}$$

The following steps are similar to the calculation in the preceding section. Therefore, we only give the most important ideas. For more details we refer again to [46]. For the flow equation of h and Z_ψ, we need terms proportional to bilinears of ψ. Hence, it is obvious that a similar seperation of $\Gamma_k^{(2)}$ into a ψ-field independent and ψ-field dependent part coming from the mixed scalar-fermionic functional derivatives is advantageous. Analogously, we use an expansion reminiscent of (3.64) to determine the flow of the fermionic part of the effective action. Inserting the potential's minimum and taking the limit $Q^2 \to 0$, we can immediately read off the evolution equation for the fermion anomalous dimension

$$\begin{aligned} \eta_\psi =& \frac{4}{N_\mathrm{f}} \frac{v_d}{d} h^2 \Big\{ N_\mathrm{f}^2 m_{1,2}^{(\mathrm{FB})d}(\kappa h^2/N_\mathrm{f}, \epsilon; \eta_\psi, \eta_\varphi) + m_{1,2}^{(\mathrm{FB})d}(\kappa h^2/N_\mathrm{f}, \epsilon + 2\kappa\lambda_1; \eta_\psi, \eta_\varphi) \\ &+ (N_\mathrm{f}^2 - 1) m_{1,2}^{(\mathrm{FB})d}(\kappa h^2/N_\mathrm{f}, \epsilon + \kappa\lambda_2; \eta_\psi, \eta_\varphi) \Big\}, \end{aligned} \tag{3.68}$$

and for the Yukawa coupling

$$\begin{aligned} \partial_t h^2 =& (d - 4 + 2\eta_\psi + \eta_\varphi) h^2 - \frac{4}{N_\mathrm{f}} v_d h^4 \Big\{ N_\mathrm{f}^2 l_{1,1}^{(\mathrm{FB})d}(\kappa h^2/N_\mathrm{f}, \epsilon; \eta_\psi, \eta_\varphi) \\ &- (N_\mathrm{f}^2 - 1) l_{1,1}^{(\mathrm{FB})d}(\kappa h^2/N_\mathrm{f}, \epsilon + \kappa\lambda_2; \eta_\psi, \eta_\varphi) \\ &- l_{1,1}^{(\mathrm{FB})d}(\kappa h^2/N_\mathrm{f}, \epsilon + 2\kappa\lambda_1; \eta_\psi, \eta_\varphi) \Big\}. \end{aligned} \tag{3.69}$$

For obtaining the equations in the symmetric or symmetry broken regime, set $\kappa = 0$ or $\epsilon = 0$, respectively. It is convenient to use h^2 instead of h in further investigations since all contributions including the Yukawa coupling are quadratic or quartic in h. Even its flow can be expressed by the squared Yukawa coupling $\partial_t h^2$. The terms contributing to the flow of the Yukawa coupling and fermion anomalous dimension are visualized in figure 3.3. The flow of η_ψ consists of mixed fermionic and bosonic fluctuations. The number of bosons of each type coincides with the prefactors of the mixed propagators in the symmetry broken regime. The same holds for the Yukawa coupling.

It is worth mentioning that (3.69) does not include all possible terms the presence of which has been discussed in [60]. In fact, for the flow to the IR physics, these terms are important. However, for the fixed point structure in three dimensions they are expected to introduce only small quantitative corrections.

We emphasize that the system of flow equations holds for $N_\mathrm{f} \geq 2$. For $N_\mathrm{f} = 1$ the theory does not contain any contribution of λ_2 since $\tau = 0$. Accordingly, to obtain the equations for this case, the λ_2 evolution equation and all λ_2 contributions as well have to be neglected which is in most cases automatically done if we set $N_\mathrm{f} = 1$. Contrary to naive expectations, we found out that it does not seem to be possible to smoothly connect the results of both cases $N_\mathrm{f} = 1$ and $N_\mathrm{f} \geq 2$.

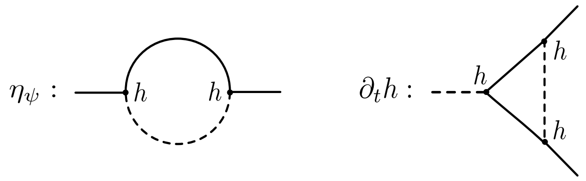

Figure 3.3.: The Feynman diagrams depict the flow equation of the fermion anomalous dimension and Yukawa coupling in both regimes. Inner lines correspond to full propagators.

4. Fixed point structure

We have computed the flow equations and discussed the mass quantities in the different regimes. However, this is only the necessary beginning of a rigorous investigation of our theory to understand the rich dynamics of the system in a profound way. The fixed point structure is important since the theory becomes independent of the artificial UV cutoff at these points. Additionally, fixed points are known to be related to critical phenomena like phase transitions. With regard to the dimensionless, renormalized couplings of our model, fixed points arise as zeros of (3.54)–(3.59) and (3.69) inserting the anomalous dimensions.

We aim at a complete picture of the structure of these points in dependency on N_f. Therefore, we concentrate on both the large N_f and the finite N_f case. For the large N_f limit, we can work out a fairly explicit picture of the fixed point structure. By contrast, in the situation of finite N_f, the equations are so involved especially for the symmetry broken case, that we cannot yet exclude the existence of further fixed points. Nevertheless, we are sure to be able to present a basic picture of the most important properties of the model.

With a short retrospection to the previous chapter, the fixed point structure reveals the fact of $N_\mathrm{f} = 1$ and $N_\mathrm{f} \geq 2$ being two rather distinct models. We are not able to find counter parts of the fixed points for $N_\mathrm{f} = 1$ in our model for higher flavor numbers. Therefore, we refer to [27] for a study of the case $N_\mathrm{f} = 1$ and drop it in our following investigations.

For our studies, we need to fix the dimension $d = 3$ and $d_\gamma = 4$ and decide for certain regulator shape functions $r_{\psi,k}$ and $r_{\varphi,k}$. Therefore, we choose the linear cutoff fulfilling the optimization criterion [61]. A benefit of this choice is that the residual loop integrals can be solved analytically. For more details and the explicit structure of the threshold functions, see appendix B.

4.1. The symmetric regime

We start with the investigation of the fixed point structure in the easier one of both regimes: the symmetric regime. Because of the vanishing VEV, the evolution equations do not encounter so many nonlinearities compared to the symmetry broken case.

4.1.1. First approach: the large N_f limit

To get a feel for the equations we will work with, we first consider the approximate case $N_\mathrm{f} \to \infty$. To be sure that the anomalous dimension η_ψ remains finite which is important for a good truncation of our model, h^2 needs to scale as $\propto 1/N_\mathrm{f}$. This assumption results in η_φ being zero in this limit. For the equation (3.54) to be able to generate non-trivial zeros, the N_f^2 dependency of the second term must be compensated by λ_1 and λ_2. Thus, we assume $\lambda_{1,2} \propto 1/N_\mathrm{f}^2$. Finally, we obtain

$$\partial_t \epsilon = -(2-\eta_\varphi)\epsilon - 2v_d\{2\lambda_1' + \lambda_2'\} l_1^d(\epsilon;\eta_\varphi), \tag{4.1}$$
$$\partial_t \lambda_1' = (d-4+2\eta_\varphi)\lambda_1' + 2v_d\{2\lambda_1'^2 + 2\lambda_1'\lambda_2' + \lambda_2'^2\} l_2^d(\epsilon;\eta_\varphi), \tag{4.2}$$
$$\partial_t \lambda_2' = (d-4+2\eta_\varphi)\lambda_2' + 4v_d \lambda_2'^2 l_2^d(\epsilon;\eta_\varphi), \tag{4.3}$$
$$\partial_t h'^2 = (d-4+2\eta_\psi+\eta_\varphi)h'^2, \tag{4.4}$$
$$\eta_\psi = 8\frac{v_d}{d} h'^2 m_{1,2}^{(\mathrm{FB})d}(0,\epsilon;\eta_\psi,\eta_\varphi), \tag{4.5}$$
$$\eta_\varphi = 0, \tag{4.6}$$

where $h'^2 = h^2 N_\mathrm{f}$ and $\lambda_{1,2}' = \lambda_{1,2} N_\mathrm{f}^2$. In this approximation, we have ignored that the threshold functions could also show a damping behavior for a certain N_f dependency of the couplings. However, such a behavior would probably only produce unphysical solutions since the structure of the threshold functions depends on the special choice of the regulator, but the existence of fixed points should not.

For obtaining solutions of non-zero h'^2, we derive from (4.4) the condition

$$1 = 2\eta_{\psi*} + \eta_{\varphi*} \qquad (\text{for } d=3) \tag{4.7}$$

from which one easily deduces that the fermion anomalous dimension needs to be $\eta_{\psi*} = 1/2$ and $h_*'^2$ has to be chosen such that this can be fulfilled by (4.5). Additionally, we discover the trivial solution $h_*'^2 = 0$ of (4.5). With regard to (4.1), we note that at least one of the couplings $\lambda_{1,2*}$ has to be negative. However, for both equations (4.2) and (4.3), there cannot exist any negative solution. Thus, we find only the two solutions $\epsilon_* = \lambda_{1*}' = \lambda_{2*}' = 0$ and $h_*'^2 = 0$ or $h_*'^2 = d(16 v_d m_{1,2}^{(\mathrm{FB})d}(0,0;0.5,0))^{-1} \approx 14.804$.

Remembering that these are the solutions in the large N_f limit, vanishing couplings do not have to be exactly zero. They also could decrease faster with growing N_f than we had assumed. Considering $\epsilon = \epsilon'/N_\mathrm{f}$ and $\lambda_{1,2} = \lambda_{1,2}''/N_\mathrm{f}^3$, we derive

$$\partial_t \epsilon' = -(2-\eta_\varphi)\epsilon' - 2v_d\Big\{(2\lambda_1'' + \lambda_2'') l_1^d(0;\eta_\varphi) - d_\gamma h'^2 l_1^{(\mathrm{F})d}(\eta_\psi)\Big\}, \tag{4.8}$$
$$\partial_t \lambda_1'' = (d-4+2\eta_\varphi)\lambda_1'' - 2v_d d_\gamma h'^4 l_2^{(\mathrm{F})d}(\eta_\psi), \tag{4.9}$$
$$\partial_t \lambda_2'' = (d-4+2\eta_\varphi)\lambda_2'' - 4v_d d_\gamma h'^4 l_2^{(\mathrm{F})d}(\eta_\psi), \tag{4.10}$$
$$\partial_t h'^2 = (d-4+2\eta_\psi+\eta_\varphi)h'^2, \tag{4.11}$$
$$\eta_\psi = 8\frac{v_d}{d} h'^2 m_{1,2}^{(\mathrm{FB})d}(0,0;\eta_\psi,\eta_\varphi), \tag{4.12}$$
$$\eta_\varphi = 0. \tag{4.13}$$

There we obtain the two fixed points:

FP(SYM)	ϵ_*'	λ_{1*}''	λ_{2*}''	$h_*'^2$	$\eta_{\psi*}$	$\eta_{\varphi*}$
G	0	0	0	0	0	0
1	1.313	-25.908	-51.815	14.804	0.5	0

In addition to the trivial, Gaussian fixed point FP(SYM)G, we obtain another fixed point FP(SYM)1 which belongs to the non-trivial solution we have found above. In fact, there are only these two reasonable large N_f schemes producing another solution besides the Gaussian fixed point. Hence, in the symmetric regime the system only generates two fixed points, which exist for large flavor numbers, one of them being trivial.

With regard to the non-trivial solution, the negative values of λ_{1*} and λ_{2*} render the bosonic potential unbounded from below, see section 3.3. It is not clear if such solutions should be dropped as unphysical artifacts of the equations or if the potential could become stable within a better truncation and thus, the solutions should be considered. For our further investigation, we make the compromise not to generally forbid negative values of $\lambda_{1,2}$, but to critically estimate the physical meaning of their existence since the flow to the IR physics might drive the couplings to physical values which are the quantities to be measured. That will be discussed in the next sections as well. By contrast, we emphasize that we do not allow negative values for h^2 since an imaginary Yukawa coupling violates the Osterwalder-Schrader positivity of our model and therefore is quite unphysical. Additionally, the flow equation (3.69) has the property that the Yukawa coupling h^2 can never cross zero during the flow because of an invariant[8] subspace $h^2 \equiv 0$. Thus, there is no hope that the flow of such a fixed point could drive the coupling constant to physical values.

4.1.2. Fixed points for finite N_f

After having understood the system for large N_f, we search for fixed points for finite $N_\mathrm{f} \geq 2$. Some of these solutions may vanish for increasing N_f because they go over into the symmetry broken regime to be discussed below or annihilate with other fixed points.

To gain first insight into the finite N_f case, we consider the purely bosonic system with decoupled fermions $h^2 \equiv 0$. We immediately find that the equations (3.55) and (3.56) only produce one trivial and one non-trivial solution with positive $\lambda_{1*}(\epsilon_*)$, but vanishing $\lambda_{2*}(\epsilon_*)$ for all positive values of ϵ_* independently of the flavor number. Inserting $\lambda_{1,2*}(\epsilon_*)$ into β_ϵ (see (3.54)) reveals that only the trivial case at $\epsilon_* = 0$ is a solution. That means we do need the fermionic contribution to obtain non-trivial fixed points in the symmetric regime. Therefore, we now consider the full system with non-decoupling fermions.

From the equation (3.69), we again read off the condition (4.7) which must be fulfilled to obtain solutions of non-zero h^2. Inserting the explicit solutions of (3.65) and (3.68) for η_φ and η_ψ, we find from (4.7) h_*^2 as a function of ϵ_*

$$\begin{aligned} h_*^2(\epsilon_*) =& \frac{3\pi^2}{8N_\mathrm{f}}\Big[5 + 10\epsilon_* + 5\epsilon_*^2 + 4N_\mathrm{f} \\ & \pm \sqrt{25(1 + 4\epsilon_* + 6\epsilon_*^2 + 4\epsilon_*^3 + \epsilon_*^4) + 8N_\mathrm{f}(1 + 2\epsilon_* + \epsilon^2{}_* + 2N_\mathrm{f})}\Big]. \end{aligned} \tag{4.14}$$

Here, we have already inserted the specific structure of the threshold functions for the linear cut off. We only find acceptable solutions for the negative root. "Acceptable" means that the anomalous dimensions are $|\eta_{\varphi*}|, |\eta_{\psi*}| \lesssim 1$. Too large anomalous dimensions may signal the breakdown of the derivative expansion. A more technical argument is that the threshold functions could vanish or become negative depending on the special choice of the regulator which would result in regulator dependent solutions then. The function h_*^2 of ϵ_* is bounded from below by $3\pi^2\Big[5 + 4N_\mathrm{f} - \sqrt{25 + 8N_\mathrm{f} + 16N_\mathrm{f}^2}\Big]/8N_\mathrm{f}$ and from above by $6\pi^2/5$. Thus, we do not have to worry about negative solutions of h_*^2. We recover the non-trivial large N_f fixed point FP(SYM)1 and find a second one FP(SYM)2 which only exists near $N_\mathrm{f} = 3$. In fact, expanding the range of N_f over all real numbers ≥ 2, we see that both fixed points arise at $N_\mathrm{f} \approx 2.77$ and the second one annihilates with another one in the symmetry broken regime, which we discuss later, at $N_\mathrm{f} \approx 3.06$.

By computing the eigenvalues of the stability matrix $\frac{\partial \beta_{g_i}}{\partial g_j}|_{g*}$, we obtain the critical exponents. For FP(SYM)1, there are three exponents with positive real part, the two smaller ones are complex conjugate to each other.[9] The two complex exponents causes that the flow spirals

[8] If the flow is exactly initiated in an invariant subspace, it will never leave this subspace.

[9] We emphasize that for complex critical exponents the real part decides about the corresponding direction to be relevant or irrelevant.

around the fixed point. For increasing N_{f}, the imaginary part decreases and the two exponents are converging to the same value, namely $\theta_{2,3} \to 1$.[10] The biggest, real exponent converges to $\theta_1 \to 2$. For FP(SYM)2, we determine two real and positive exponents.

Explicit values characterizing the fixed points can be read off from table 4.1. Figure 4.1 depicts the dependency of the couplings, anomalous dimensions and the critical exponent[11] $\nu = 1/\theta_1$ on the flavor number. For large N_{f}, one can see the behavior of FP(SYM)1 predicted by our earlier investigations. Because of the reasons already mentioned for FP(SYM)1, we accept the bosonic potential being unbounded from below at FP(SYM)2 for now.

To be sure that we have found all important solutions, let us briefly summarize the numerical methods we used. By giving several starting points to the method "FindRoot" of Mathematica, we have looked individually for solutions in the full system. Besides, we have applied the method "NSolve" to obtain the whole system of solutions.

4.2. The regime of spontaneous symmetry breaking

In the last section we have discussed the fixed point structure of the symmetric regime. As already mentioned, in the symmetry broken regime the search for fixed points will become more difficult since the coupling of the VEV gives rise to a higher degree of nonlinearity of the flow equations.

4.2.1. First approach: the large N_{f} limit

To get a first impression of the structure of the flow equations, it is helpful to consider the large N_{f} limit before treating the full system for finite N_{f}. For this purpose, we have to analyze how the couplings scale with respect to N_{f}. Starting again with η_ψ, we recognize that at least $h^2 \propto 1/N_{\mathrm{f}}$ leads to a finite fermionic anomalous dimension. Regarding (3.57), the contributions of the Goldstone bosons can only be compensated if we assume $\kappa \propto N_{\mathrm{f}}^2$. For finite masses and to keep the threshold functions from an unphysical influence, the couplings $\lambda_{1,2}$ have to decrease at least like $\propto 1/N_{\mathrm{f}}^2$. Within the limit $N_{\mathrm{f}} \to \infty$, we finally obtain

$$\partial_t \kappa' = (2 - d - \eta_\varphi)\kappa' + 2v_d \Big\{ l_1^d(\eta_\varphi) + \Big(1 + \frac{\lambda_2'}{\lambda_1'}\Big) l_1^d(\kappa'\lambda_2'; \eta_\varphi) \Big\}, \tag{4.15}$$

$$\partial_t \lambda_1' = (d - 4 + 2\eta_\varphi)\lambda_1' + 2v_d \Big\{ {\lambda_1'}^2 l_2^d(\eta_\varphi) + (\lambda_1' + \lambda_2')^2 l_2^d(\kappa'\lambda_2'; \eta_\varphi) \Big\}, \tag{4.16}$$

$$\begin{aligned}\partial_t \lambda_2' =& (d - 4 + 2\eta_\varphi)\lambda_2' + 2v_d \Big\{ \frac{1}{4}{\lambda_2'}^2 l_2^d(\eta_\varphi) + \frac{9}{4}{\lambda_2'}^2 l_2^d(\kappa'\lambda_2'; \eta_\varphi) \\ & - \frac{1}{2}{\lambda_2'}^2 l_{1,1}^d(0, \kappa'\lambda_2'; \eta_\varphi) \Big\},\end{aligned} \tag{4.17}$$

$$\begin{aligned}\partial_t h'^2 =& (d - 4 + 2\eta_\psi + \eta_\varphi)h'^2 - 4v_d h'^4 \Big\{ l_{1,1}^{(\mathrm{FB})d}(\kappa' h'^2, 0; \eta_\psi, \eta_\varphi) \\ & - l_{1,1}^{(\mathrm{FB})d}(\kappa' h'^2, \kappa'\lambda_2'; \eta_\psi, \eta_\varphi) \Big\},\end{aligned} \tag{4.18}$$

$$\eta_\psi = 4\frac{v_d}{d} h'^2 \Big\{ m_{1,2}^{(\mathrm{FB})d}(\kappa' h'^2, 0; \eta_\psi, \eta_\varphi) + m_{1,2}^{(\mathrm{FB})d}(\kappa' h'^2, \kappa'\lambda_2'; \eta_\psi, \eta_\varphi) \Big\}, \tag{4.19}$$

$$\eta_\varphi = 2\frac{v_d}{d} \kappa' {\lambda_2'}^2 m_{2,2}^d(0, \kappa'\lambda_2'; \eta_\varphi), \tag{4.20}$$

where $\kappa' = \kappa/N_{\mathrm{f}}^2$. For the other couplings the notation above holds. At first sight, the coupling of the VEV leads to a non-vanishing scalar anomalous dimension. It is obvious that the sum rule

[10] For clarification we always assume $\theta_1 > \theta_2 > \theta_3 > \theta_4$ in the following.

[11] We will explain in section 5.2 for which reason we may identify $\nu = 1/\theta_1$ although the fixed points in general possess more than one relevant direction.

Table 4.1.: Fixed point values of the couplings, anomalous dimensions and critical exponents in the symmetric regime.

FP(SYM)	N_f	ϵ_*	λ_{1*}	λ_{2*}	h_*^2	$\eta_{\psi*}$	$\eta_{\varphi*}$	θ_i
1	3	0.379	0.3635	-4.317	5.890	0.279	0.442	(2.841, 0.361 ± 0.473 i)
	4	0.340	-0.194	-1.594	4.743	0.326	0.348	(2.892, 0.701 ± 0.468 i)
	5	0.272	-0.141	-0.711	3.750	0.365	0.270	(2.834, 0.850 ± 0.426 i)
	10	0.130	-0.022	-0.067	1.717	0.440	0.119	(2.511, 1.045 ± 0.286 i)
2	3	0.021	1.499	-2.051	3.956	0.357	0.286	(2.262, 0.564)

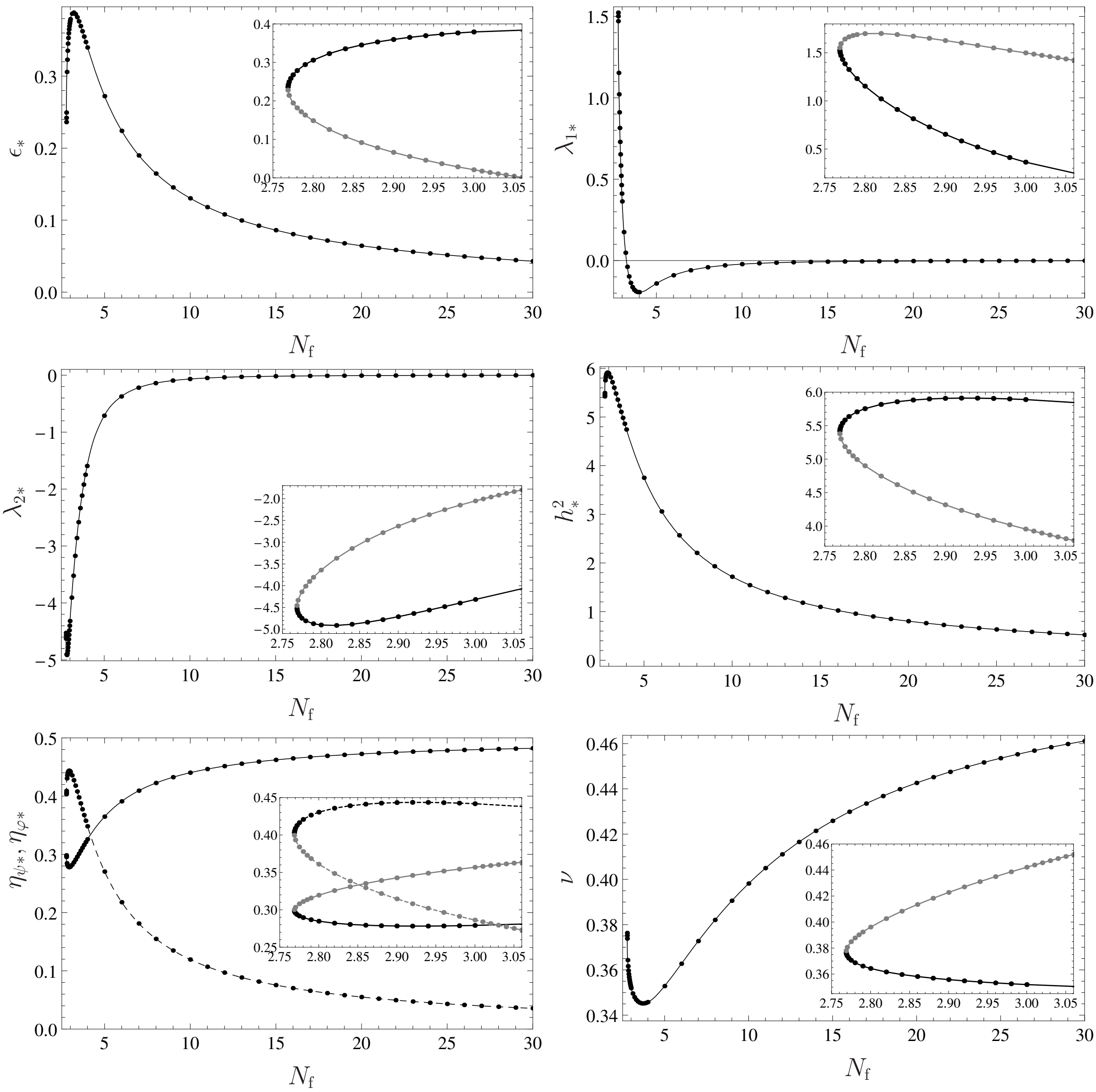

Figure 4.1.: Coupling constants, anomalous dimensions η_ψ (solid) and η_φ (dashed) and the critical exponent $\nu = 1/\theta_1$ of FP(SYM)1 (black) and FP(SYM)2 (gray) in dependency on N_f. The insets show an extract of $N_\mathrm{f} \approx 3$.

(4.7) for the anomalous dimensions does not hold in the large N_f limit. This can be constituted by the fact that the terms of the mixed propagators carrying massless Goldstone bosons and τ-masses cannot compensate each other. Similar reasons hold for finite N_f.

A big benefit of treating the evolution equations in this limit is the decoupling of the bosonic equations from the fermionic ones. Thus, we can look for zeros in the bosonic sector first and then check for the zeros of (4.18). Moreover, since the propagators carrying radial masses are suppressed within this limit, (4.16) is simply quadratic in λ_1'. Hence, the solution λ_{1*}' can be expressed as a function of λ_{2*}' and κ_*'

$$\begin{aligned}\lambda_{1*}' = &-\frac{(d-4+2\eta_{\varphi*})+4v_d\lambda_{2*}' l_2^d(\kappa_*'\lambda_{2*}';\eta_{\varphi*})}{4v_d(l_2^d(\eta_{\varphi*})+l_2^d(\kappa_*'\lambda_{2*}';\eta_{\varphi*}))} \\ &\pm \underbrace{\sqrt{\left(\frac{(d-4+2\eta_{\varphi*})+4v_d\lambda_{2*}' l_2^d(\kappa_*'\lambda_{2*}';\eta_{\varphi*})}{4v_d(l_2^d(\eta_{\varphi*})+l_2^d(\kappa_*'\lambda_{2*}';\eta_{\varphi*}))}\right)^2 - \frac{(\lambda_{2*}')^2 l_2^d(\kappa_*'\lambda_{2*}';\eta_{\varphi*})}{l_2^d(\eta_{\varphi*})+l_2^d(\kappa_*'\lambda_{2*}';\eta_{\varphi*})}}}_{=:\sqrt{a(\kappa_*',\lambda_{2*}')}}\,.\end{aligned} \tag{4.21}$$

Fixed points exist for a non-negative radicand. We now switch to the modified coupling $\kappa' \to \zeta' := \kappa'\lambda_2'$. The scalar anomalous dimension then reads

$$\eta_\varphi = \frac{\lambda_2'\zeta'}{12\pi^2(1+\zeta')^2}. \tag{4.22}$$

Multiplying (4.15) with λ_2', (4.17) with κ' and setting them to zero, we can translate the equations of the original coupling set to the ones of the new set $(\zeta', \lambda_1', \lambda_2')$. The resulting modified equation (4.17) becomes quadratic in λ_2' inserting the result (4.22) for η_φ. Note that this is a regulator dependent statement, for the sharp cut off the equation would be linear in λ_2'. As the existence of fixed points should not depend on the specific regulator function, we already know that one of these solutions λ_{2*}' is not physical. For any ζ_*', we obtain

$$\begin{aligned}\lambda_{2*}' = &\frac{6\pi^2(1+\zeta_*')^2}{\zeta_*'(8+2\zeta_*'^2+\zeta_*'^3)}\Big[5(4+\zeta_*')(2+\zeta_*'^2) \\ &\pm\sqrt{5(320+128\zeta_*'+308\zeta_*'^2+152\zeta_*'^3+88\zeta_*'^4+36\zeta_*'^5+5\zeta_*'^6)}\Big].\end{aligned} \tag{4.23}$$

Inserting λ_{2*}' in (4.22) identifies the solution with the positive root to be the artificial one because $\eta_{\varphi*} > 4$ for all $\zeta_*' > -1$. At this point we emphasize that we only search for fixed points in the range $\zeta' > -1$. Otherwise the threshold functions $l_2^d(\ldots)$ would become singular or negative, which generates unreasonable solutions. As the solution λ_{2*}' with the negative root is positive over the whole range and κ_*' has to be positive as well, we will not find any true fixed point for $\zeta' < 0$. Inserting λ_{1*}' and λ_{2*}' as functions of ζ_*' into the modified equation (4.15), we plot $f(\zeta') := \lambda_2'\beta_{\kappa'}(\zeta', \lambda_1', \lambda_2')$ for $\zeta' > 0$, see figure 4.2. We see that there exists no true fixed point since the function f is negative in the range of an existing solution λ_{1*}'.

However, note that we have excluded the case $\lambda_{2*}' = 0$ so far, which is indeed a zero of (4.17). Inserting $\lambda_{2*}' = 0$ in (4.21), we obtain one solution for λ_1', the other one $\lambda_{1*}' = 0$ would cause a singular function $\beta_{\kappa'}$. Considering (4.15), it is obvious that it must have one zero at a certain positive value κ_*, since $\beta_{\kappa'}$ is linear in κ' with a negative slope and the κ' independent term is positive. For completeness, it is worth emphasizing that for the other case $\kappa' = 0$ of vanishing ζ', we do not find any solution.

Now we involve again the fermionic equations. For $\lambda_{2*}' = 0$, the fermion anomalous dimension reads

$$\eta_{\psi*} = \frac{1}{3\pi^2}\frac{h_*'^2}{(1+\kappa_*' h_*'^2)}. \tag{4.24}$$

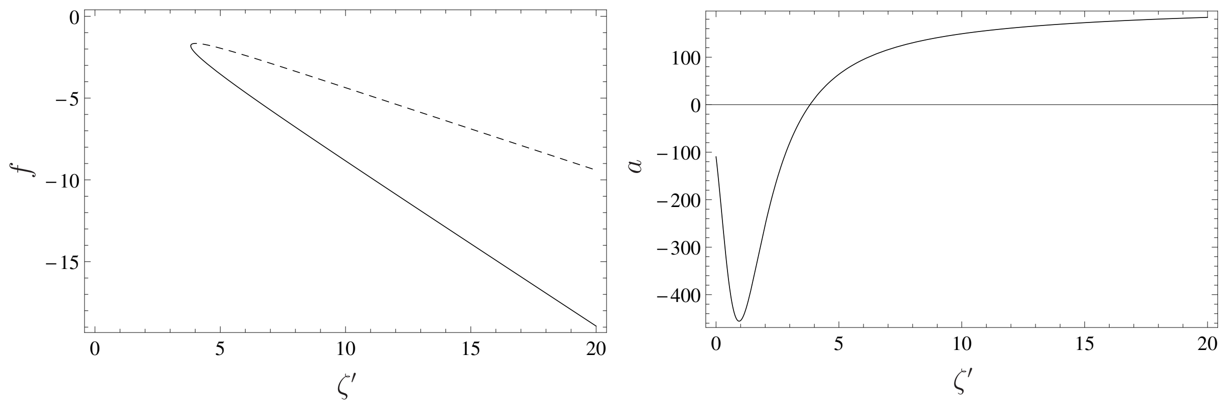

Figure 4.2.: Search for zeros of the function $f(\zeta')$ (left panel) for non-complex values of λ'_{1*}: $a \geq 0$ (right panel). The positive and negative root of λ'_{1*} gives rise to the solid and dashed line, respectively.

As τ-modes are massless within this limit, (4.18) simplifies to the corresponding flow equation in the symmetric case. Therefore, the sum rule for the anomalous dimensions hold which entails the condition $\eta_{\psi*} = 1/2$ again for nonzero h'^2_*. Finally, we obtain two solutions

FP(SSB)	κ'_*	λ'_{1*}	λ'_{2*}	h'^2_*	$\eta_{\psi*}$	$\eta_{\varphi*}$
1a	0.034	14.804	0	0	0	0
1b	0.034	14.804	0	29.609	0.5	0

which we labeled FP(SSB)1a,b. These labels already indicate that the two fixed points have a certain relationship, since FP(SSB)1b can be understood as a copy of FP(SSB)1a in the full system with non-vanishing Yukawa interaction.

By the examination of the large N_f limit for $\lambda_2 = \lambda''_2/N_\mathrm{f}^3$, where only propagators with vanishing bosonic masses contribute, we see that the non-zero $h'^2 = 29.609$ matches to a non-zero $\lambda''_2 = -25.908$ and that the other solution with vanishing Yukawa and λ_2 coupling is the well known Wilson-Fisher fixed point which we have already mentioned in chapter 2. We have not found further reasonable solutions within other schemes of large N_f scaling of the couplings.

4.2.2. Fixed points for finite N_f: the bosonic sector

We have gained a first impression of the equations' dynamics in the spontaneous symmetry broken regime. Before considering the full system for finite N_f, we first investigate the case of decoupling fermions $h^2 \equiv 0$. Inserting the scalar anomalous dimension into our flow equations, we derive λ_{1*} and λ_{2*} from (3.58) and (3.59) depending on κ_*. For $N_\mathrm{f} = 2$, we find that the consideration of the range $\kappa_* < 1$ is sufficient because for higher values, the dynamics of the system does not change significantly anymore. Figure 4.3 depicts the dependency of β_κ on κ having inserted our solutions of λ_1 and λ_2. We have only selected solutions for which $\eta_\varphi \lesssim 2$. From the diagram, we read off the zeros κ_* and compute the corresponding solutions for the other couplings, see table 4.2.

The fixed point FP(SSB)1a is the Wilson-Fisher fixed point that we have already discovered in the large N_f limit. FP(SSB)2a and FP(SSB)2b arise for $N_\mathrm{f} = 2$ and annihilate each other at $N_\mathrm{f} \approx 2.17$. It is worth mentioning that the potential is stable, although $\lambda_{2*} < 0$. Nevertheless, the kind of symmetry breaking pattern is not yet clear and depends on the IR behavior. Thus, hoping that the dimensionless, renormalized τ-mass within our considered symmetry breaking pattern becomes positive in the IR flow, we preliminarily accept also negative masses.

The remaining solutions exist for all $N_\mathrm{f} \geq 2$, but did not occur in the large N_f limit.

Table 4.2.: Fixed point values of the couplings and the anomalous dimensions in the purely bosonic system for $N_\mathrm{f} = 2$.

FP(SSB)	κ_*	λ_{1*}	λ_{2*}	h_*^2	$\eta_{\psi*}$	$\eta_{\varphi*}$
1a	0.129	3.346	0	0	0	0.028
2a	0.050	2.646	-4.158	0	0	0.038
2b	0.119	3.859	-1.746	0	0	0.042
A	0.431	-1.707	-1.210	0	0	0.429
B	0.578	-0.492	-3.633	0	0	0.157
C	0.072	-15.052	0	0	0	0.803

That indicates that some terms in the flow equations behave in a singular way. The radial mass of FP(SSB)A-C converges to $2\kappa\lambda_1 \to -1$ for increasing N_f which gives rise to a completely different amount of leading terms. Additionally, for each solution we find one negative mass smaller than minus one entailing that some of the threshold functions become negative. This induces a regulator dependent existence of the solutions FP(SSB)A-C. Thus, this is a good reason to drop them.

We emphasize that by repeating this examination for $N_\mathrm{f} = 5$, we only discover the solutions discussed here.

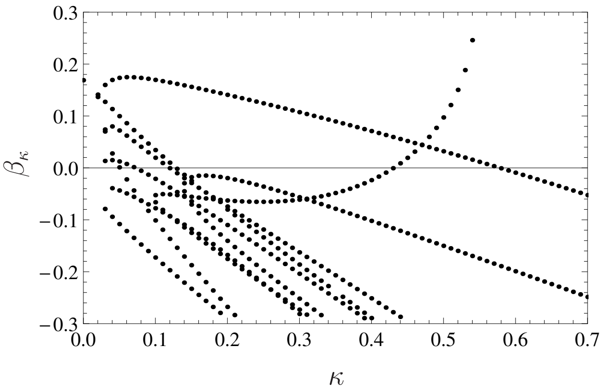

Figure 4.3.: Search for zeros of $\beta_\kappa(\kappa)$ for $\eta_\varphi \lesssim 2$ and different solutions of λ_1 and λ_2 for $N_\mathrm{f} = 2$.

4.2.3. Fixed points for finite N_f: the full system

After a short excursion into the purely bosonic system, we come back to our actual goal to determine fixed point solutions of the full system, especially for non-vanishing Yukawa interactions. By applying “FindRoot” to the flow equations for several N_f, we are able to scan the space of solutions. The results are listed in table 4.3. The plots in figure 4.4 show the dependency of the couplings, anomalous dimensions and critical exponent $\nu = 1/\operatorname{Re}\theta_1$ on N_f.

The Wilson-Fisher fixed point FP(SSB)1a and the fixed point FP(SSB)1b show the dependency on N_f that we have already discussed within the large N_f limit. Additionally, we find the fixed point FP(SSB)3 arising with FP(SSB)1b at $N_\mathrm{f} \approx 2.81$ that annihilates with FP(SYM)2 at the regime boundary for $N_\mathrm{f} \approx 3.06$. Besides FP(SSB)2a,b, there is a second pair of fixed points FP(SSB)4a,b which vanish at $N_\mathrm{f} \approx 3.25$.

For the Wilson-Fisher fixed point, we obtain three positive critical exponents due to a more general symmetry in comparison to O(N) models,[12] for which $\theta_{1,2,3} \to 1$ for increasing N_f. For FP(SSB)1b we find two relevant directions whose exponents converge to one as well. In comparison to the Wilson-Fisher fixed point FP(SSB)1a, there is one relevant direction less since the relevant Yukawa type term of FP(SSB)1a becomes irrelevant at FP(SSB)1b. We believe that flows starting close to FP(SSB)1a and generating a Yukawa type interaction may be dominated by FP(SSB)1b. The fixed point FP(SSB)3 is the only one we have found with solely one relevant direction apart from FP(SSB)4a for some non-integer flavor numbers $N_\mathrm{f} > 3$. The other fixed points have at least two relevant directions, partly with complex exponents. The plots 4.4 depict that the behavior of the critical exponent ν considerably changes if the complex spectrum becomes real. For these N_f, the curves show a kink. With regard to FP(SSB)4a,

[12]Note that the flavor numbers of the O(N) model and of our U(N_f) ⊗ U(N_f) model are not the same.

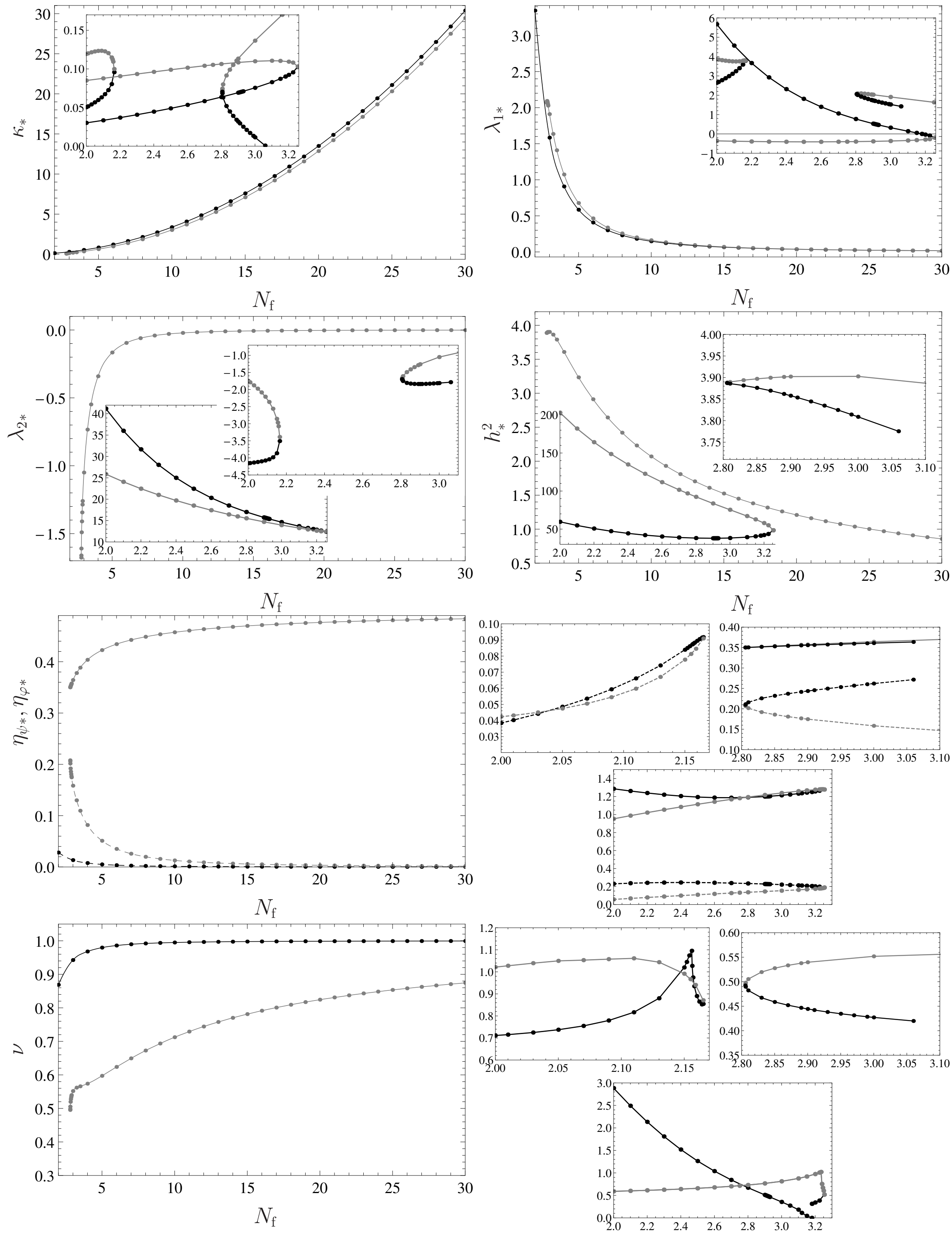

Figure 4.4.: Coupling constants, anomalous dimensions η_ψ (solid) and η_φ (dashed) and the critical exponent $\nu = 1/\operatorname{Re}\theta_1$ of FP(SSB)1a (black) and FP(SSB)1b (gray) in the big boxes for $N_\mathrm{f} = 2 - 30$, FP(SSB)3 (black) and FP(SSB)1b (gray) in the small boxes for $N_\mathrm{f} \approx 2.8 - 3.1$, FP(SSB)2a (black) and FP(SSB)2b (gray) in the small boxes for $N_\mathrm{f} \approx 2 - 2.2$, FP(SSB)4a (black) and FP(SSB)4b (gray) in the small boxes for $N_\mathrm{f} \approx 2 - 3.3$.

Table 4.3.: Fixed point values of the couplings, the anomalous dimensions and critical exponents in the spontaneous symmetry broken regime.

FP(SSB)	N_f	κ_*	λ_{1*}	λ_{2*}	h_*^2	$\eta_{\psi *}$	$\eta_{\varphi *}$	θ_i
1a	2	0.129	3.3465	0	0	0	0.028	(1.151, 0.972, 0.386)
	3	0.296	1.584	0	0	0	0.013	(1.061, 0.987, 0.723)
	4	0.532	0.907	0	0	0	0.008	(1.033, 0.992, 0.844)
	5	0.836	0.585	0	0	0	0.005	(1.021, 0.995, 0.900)
	10	3.368	0.148	0	0	0	0.001	(1.005, 0.999, 0.975)
1b	3	0.137	1.910	-1.050	3.903	0.364	0.158	(1.812, 0.440)
	4	0.356	1.073	-0.341	3.608	0.404	0.082	(1.743, 0.637)
	5	0.633	0.678	-0.166	3.234	0.423	0.051	(1.674, 0.699)
	10	3.023	0.162	-0.021	2.070	0.457	0.013	(1.404, 0.827)
2a	2	0.050	2.646	-4.158	0	0	0.038	(1.406 ± 0.865 i, 0.962)
2b	2	0.119	3.859	-1.746	0	0	0.042	(0.979, 0.958)
3	3	0.012	1.524	-1.811	3.809	0.361	0.262	(2.341)
4a	2	0.030	5.672	41.197	59.571	1.286	0.230	(0.347 ± 1.773 i)
	3	0.076	0.323	14.636	38.257	1.214	0.221	(2.817 ± 3.173 i)
4b	2	0.085	-0.361	25.863	203.026	0.952	0.057	(1.694 ± 1.524 i)
	3	0.110	-0.367	13.949	75.396	1.240	0.154	(1.231 ± 1.360 i)

we see a discontinuity instead of a kink that comes from θ_1 increasing to infinity and then changing its sign. Therefore, the formerly second largest exponent is then the largest one. For emerging or annihilating solutions, we observe that a relevant direction of the one fixed point and an irrelevant direction of its complement become marginal at the certain value of N_f due to the parabolic structure of the flow equations. In figure 4.5 the situation for two annihilating fixed points is depicted. The quantity g_i stands for a certain coupling constant or a projection on a certain direction in theory space. The arrows indicate the relevance or irrelevance of the corresponding direction. On the contrary, for FP(SSB)3 this behavior does not hold since quantities at the regime boundary are not differentiable in general.

For all fixed points listed in table 4.3, we see that the boson and fermion masses are bigger then minus one leaving all threshold functions positive. Nevertheless, for all fixed points, despite of FP(SSB)1a and FP(SSB)4a for $2 \le N_\mathrm{f} \lesssim 3$, we have negative boson masses and at FP(SSB)3,4b the potential turns out to be unstable. With regard to these cases, we refer to our arguments we have already used above to justify the consideration of these fixed points.

For clarification, we have dropped the obviously unphysical solutions with masses smaller than minus one which we have found as well. It is remarkable that for each physical or non-physical solution which we have obtained for arbitrarily large N_f in the symmetry broken regime, there is one with decoupling fermions $h_*^2 = 0$ and the other one with non-vanishing h_*^2 that can be associated to each other by similar values of non-vanishing coupling constants.

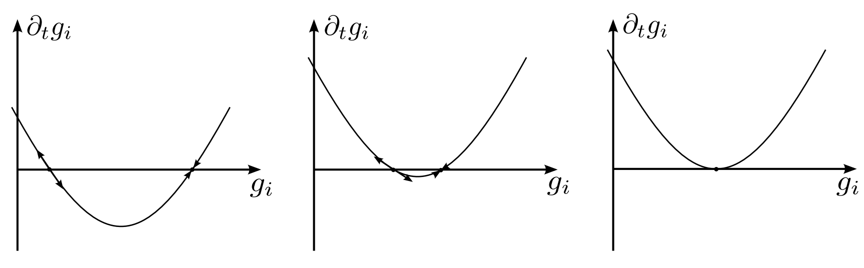

Figure 4.5.: Annihilation of two fixed points for increasing N_f.

4.3. Summary

We have determined the fixed point structure of both regimes for large and finite N_f and introduced some criteria to isolate true fixed points from artificial solutions of our system. For summarizing our results both in the symmetric and symmetry broken regime, figure 4.6 is very instructive. Although our truncation is not very complicated, the model gives rise to a rich fixed point structure, especially for small flavor numbers. Altogether, we obtain nine potential fixed points whose properties will be investigated in our further analysis. Three of them exist for all flavor numbers, the other ones annihilate for some special N_f.

Besides FP(SSB)3, we did not find any further fixed point with only one relevant direction. Such fixed points are suspected to exhibit a second order phase transition and therefore are of special interest. By contrast, fixed points with more than one relevant direction are expected to be associated with first order phase transitions.

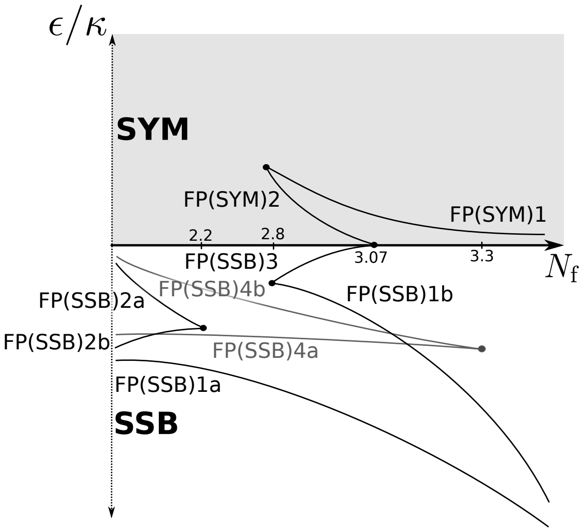

Figure 4.6.: Sketch of the fixed point structure of the symmetric and symmetry broken regime as a function of N_f. The fixed point FP(SSB)1a is the Wilson-Fisher fixed point known from O(N) symmetric models.

In reminiscence of the previous chapter, we come back to the discussion about the quality of our truncation. We neglected the invariant $\tilde{\tau}_3$ occuring for $N_\mathrm{f} \geq 3$ and terms $\propto \rho^3$ and $\propto \rho\tau$ parametrized by couplings of zero canonical mass dimension. One may ask if the fixed points would exhibit an additional relevant direction including such contributions. Such a term would be very important for further analysis then. Considering the scaling term at the beginning of each flow equation, this question may simplify to a question for the sign of the anomalous dimensions. That is a very rough picture since the values of the fixed points and the rest of the flow equations do also have an influence on the values of the critical exponents. However, assuming that picture, we conclude that additional terms $\propto \varphi^6$ are not relevant because of the positive sign of the anomalous dimensions requiring that the structure of the flow equations would not change significantly.

That assumption is certainly true for the Wilson-Fisher fixed point, since nearly all critical exponents are smaller than the canonical mass dimension one of the coupling constants. The direction whose exponent is bigger than one is mostly dominated by κ compared to all other directions. Therefore, the reason for this comparatively large exponent can be read off from (3.57), where the scalar anomalous dimension contributes with a negative sign. For FP(SSB)1b, except for the largest one again, all other critical exponents are smaller than the canonical mass dimension of the couplings as well. Additionally, there is one relevant direction less in comparison to the Wilson-Fisher fixed point FP(SSB)1a supporting our reasoning. The size of the largest critical exponent we suppose to be a result of the negative sign of λ_2, especially for small N_f, which we expect to become positive in higher truncations and therefore let the exponent decrease. The same holds for FP(SSB)2a and FP(SSB)3. All critical exponents of FP(SSB)2b are smaller than the canonical masses of the couplings for almost all N_f which reveals our presumption above. With regard to FP(SYM)1,2, the directions with the largest critical exponent exhibit the biggest ϵ component of all directions. Hence, their large values may be explained by the large canonical mass dimension two of ϵ. The positive real part of the other exponents of FP(SYM)1 are slightly bigger than one for $N_\mathrm{f} \geq 8$, which is the canonical mass dimension of the other couplings. Thus, for these flavor numbers, there is a little uncertainty if the assumption we made above holds. However, for FP(SYM)2 the remaining positive exponents are smaller than one which supports the viewpoint that additional terms $\propto \varphi^6$ obey our assumption.

Concerning FP(SSB)4a,b, we see first signs of being non-physical in the large coupling constants, anomalous dimensions and negative λ_{1*} value of FP(SSB)4b, although FP(SSB)4a is the only fixed point of purely positive couplings for $2 \leq N_\mathrm{f} \lesssim 3$. Therefore, we marked FP(SSB)4a,b in figure 4.6 with a gray color. We will come back to this issue in the next chapter.

5. Flow analysis

By employing the approximate criterion that the dimensionless, renormalized, bosonic UV masses have to be larger than minus one, we have extracted a small number of solutions which we have started to discuss in the previous chapter. Nevertheless, it remains difficult to isolate fixed points exhibiting reasonable IR physics from those which do not. Therefore, we now investigate the flow from the UV physics of large momenta to the IR physics by successively integrating out all degrees of freedom. This will offer us a deeper insight into the dynamics of the equations and some difficulties due to our chosen truncation.

5.1. Overview of the flow in the vicinity of the fixed points

To investigate the IR behavior of our system at the fixed points, we start in the UV taking a little step of δg_Λ into the relevant directions. From these directions, we know that they dominate the flow behavior towards the IR. Thus, we hope to get a good insight into the flow properties towards the long-range physics during our examination.

FP(SSB)1a: the Wilson-Fisher fixed point

We start our analysis with the Wilson-Fisher fixed point. As already mentioned, the Wilson-Fisher fixed point is a scale invariant solution of $\mathrm{O}(N)$ symmetric models. Therefore, the Wilson-Fisher fixed point lies in the $\mathrm{O}(2N_\mathrm{f}^2)$ symmetric, invariant subspace of our $\mathrm{U}(N_\mathrm{f}) \otimes \mathrm{U}(N_\mathrm{f})$ symmetric theory. In this subspace, the fermions decouple, which means $h^2 \equiv 0$, and additionally $\lambda_2 \equiv 0$ guarantees the existence of the enhanced symmetry. We find one relevant direction lying in the $\mathrm{O}(2N_\mathrm{f}^2)$ symmetric subspace. There is an extension of the invariant subspace if we allow a non-zero λ_2 coupling. That reduces the enhanced $\mathrm{O}(2N_\mathrm{f}^2)$ symmetry to the $\mathrm{U}(N_\mathrm{f})\otimes\mathrm{U}(N_\mathrm{f})$ symmetry. The Yukawa interaction term still vanishes in this subspace which disconnects both parts $h^2 < 0$ and $h^2 > 0$ of the full theory space. A second relevant direction is associated with this subspace. Finally, perturbing around the purely bosonic, $\mathrm{U}(N_\mathrm{f}) \otimes \mathrm{U}(N_\mathrm{f})$ symmetric subspace, the flow pushes us into the full theory space due to a third relevant direction. After these introductory words, we go through these subspaces and discuss the occurring flow properties in more detail.

The following examination relates to the case $N_\mathrm{f} = 2$, but is not expected to be much different for higher values of N_f. As the $\mathrm{O}(2N_\mathrm{f}^2)$ symmetric subspace is protected from the influence of the other relevant directions, the flow in the whole subspace is fully determined by the largest exponent $\theta_1 = 1.15$. In this subspace, we find both the symmetric and the ordered phase depending on the sign of the first component $\Delta\kappa$ of the eigenvector corresponding to the relevant direction, where the UV starting value is $g_{i\Lambda} = g_{i*} + \Delta g_i$ for the coupling g_i. That can be easily understood since fixed points with relevant and irrelevant directions always lie on the critical hyperplane separating both phases and the first relevant direction runs through this plane. Flowing into the symmetric regime we observe converging values of the bare mass $\bar{m}^2$ and renormalized mass $\bar{m}_\mathrm{R}^2 = Z_\varphi^{-1}\bar{m}^2$ for $k \to 0$ which only differ by the wave function renormalization Z_φ. See figure 5.1 (left panel) for the flow of the couplings and masses. In the symmetry broken phase, we are faced with a common problem of the polynomial truncation of the scalar potential: The contribution of the Goldstone bosons does not decouple during the flow because of vanishing masses in the threshold functions. Thus, we do not observe the

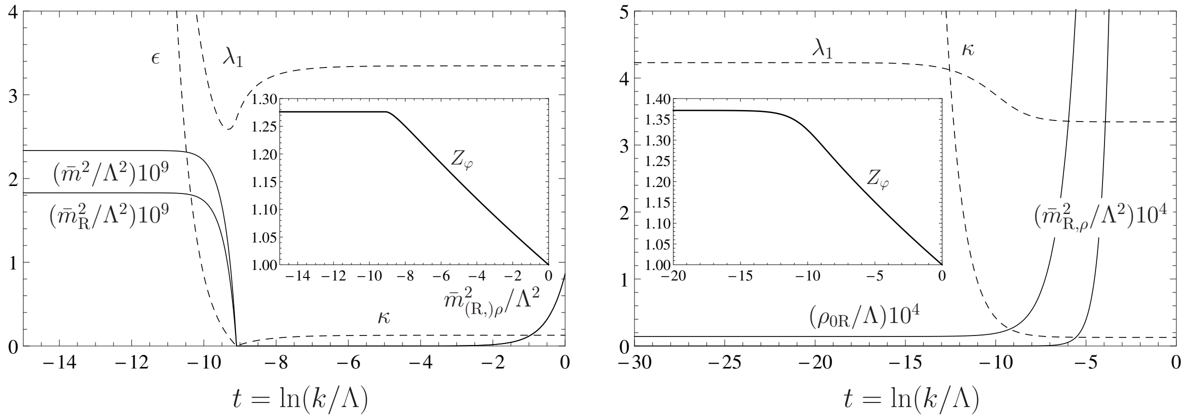

Figure 5.1.: Flow at the Wilson-Fisher fixed point in the $O(2N_f^2)$ symmetric subspace for $N_f = 2$. The non-vanishing coupling constants (dashed), the VEV (dashed), the masses (solid) and the wave function renormalization (small plots) are depicted. The UV starting point is shifted by a distance of $\delta g_\Lambda = 10^{-5}$ from the fixed point into the direction $\vec{v}_1$ with $\theta_1 = 1.15$. Left panel: Starting in the symmetric phase. Right panel: Starting in the ordered phase.

expected scaling behavior of $\lambda_1(k)$ for small momenta. Instead, the dimensionless coupling converges to an attractive, partial fixed point. Converging to such a partial fixed point affects the renormalized radial mass $\bar{m}^2_{R,\rho} = k^2 2\kappa\lambda_1(k)$ to be zero for $k \to 0$. Thus, we need to find an IR stopping criterion that defines where the Goldstone modes should decouple and the flow is closest to the expected scaling behavior. We will justify in section 5.3 that the inflection point $t_{\lambda_1} = \ln(k_{\lambda_1}/\Lambda)$ of $\lambda_1(k = \Lambda e^t)$ is a good choice. We emphasize that for fixing this inflection point, it is advisable to consider λ_1 as a function of $t = \ln(k/\Lambda)$. Nevertheless, we will often refer to k_{λ_1} in the following. It is worth mentioning that the scaling behavior of the dimensionless VEV κ is not distorted by the Goldstone bosons. Therefore, the renormalized, dimensional VEV can be determined by taking the limit of $\rho_{0R}(k \to 0) = k\kappa(k \to 0)$. In figure 5.1 (right panel) the flow behavior in the ordered phase is depicted.

We consider now the purely bosonic, $U(N_f) \otimes U(N_f)$ symmetric, invariant subspace with $h^2 \equiv 0$. If we differ only a little from the relevant direction with the critical exponent $\theta_3 = 0.39$, the flow is highly influenced by the other one because of the large difference between the positive exponents. We mention that it is next to impossible to avoid this within numerical calculations. We locate the symmetry broken phase in the relevant direction with positive $\lambda_{2\Lambda}$. While the τ-mass is generated, the fermion mass remains zero. We emphasize that $\lambda_2(k)$ suffers from the same artificial non-decoupling as $\lambda_1(k)$. Therefore, we determine the τ-mass $\bar{m}^2_{R,\tau} = k^2\kappa\lambda_2(k)$ at k_{λ_1} as well. We drop the other case with negative $\lambda_{2\Lambda}$ using a similar argument as we have given for h^2 at the end of subsection 4.1.1: If we are situated in the bosonic subspace, the flow will never drive the λ_2 coupling to positive values due to the invariant, $O(2N_f^2)$ symmetric subspace. This can be also seen from the flow equations. Note that this is a general statement which holds for the symmetric regime as well. Thus, it is impossible to obtain reasonable flow behavior in this direction that fits to our symmetry breaking pattern within the present truncation.

The direction with $\theta_2 = 0.97$ leads out of any invariant subspace since $\Delta h^2 \neq 0$. Although the λ_2 component of this vector vanishes, the non-zero h^2 component generates an increasing λ_2 coupling during the flow. Due to our arguments given at the end of subsection 4.1.1, it is reasonable to consider only the case $h^2_\Lambda > 0$. In this direction, we flow into the symmetric regime, see figure 5.2. In contrast to the flow in the $O(2N_f^2)$ symmetric subspace, the wave function renormalization $Z_\varphi(k)$ grows rapidly even for small k because of the fluctuations of the massless fermions. This phenomenon is a generic effect occurring in three dimensions, which can be technically explained as follows: With regard to (3.65), we observe that η_φ only decreases if $h^2(k)$ decreases. Thus, if $h^2(k \to 0)$ is non-zero, the wave function renormalization will never

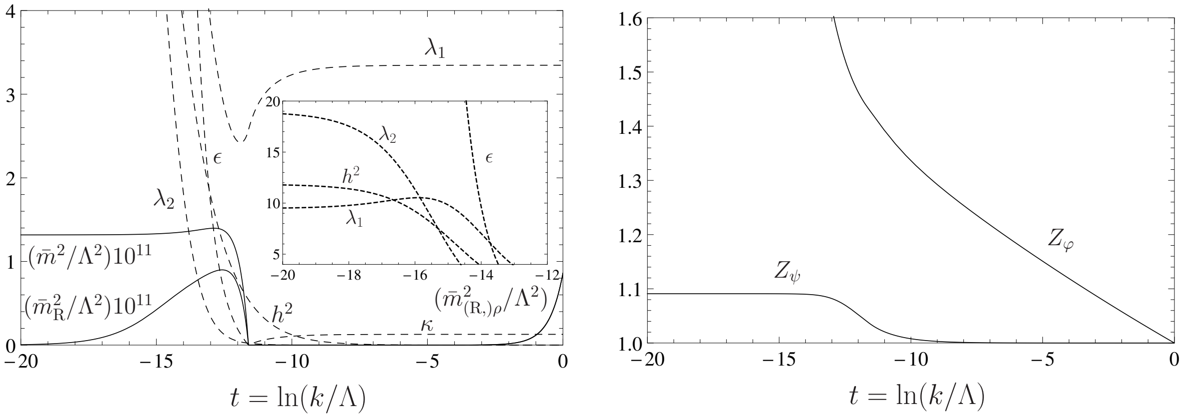

Figure 5.2.: Flow at the Wilson-Fisher fixed point in the full theory space for $N_{\mathrm{f}} = 2$. The non-vanishing coupling constants (dashed), the VEV (dashed) and the masses (solid) (right panel) and the wave function renormalizations (left panel) are depicted. The UV starting point is shifted by a distance of $\delta g_\Lambda = 10^{-5}$ from the fixed point into the direction $\vec v_2$ with $\theta_2 = 0.97$.

approach a certain limit. For non-vanishing Yukawa coupling h_Λ^2, we observe a convergence of $h^2(k)$ during the flow to an attractive, partial fixed point in the symmetric regime. Thus, we find $\eta_\varphi \to 1$, which ensures the convergence of $h^2(k)$. Only $\bar m^2$ approaches a non-vanishing value. To obtain the IR quantity $\bar m_{\mathrm{R}}^2$, we need to find a suitable definition. This problem has been treated in [24, 25]. There the ratio $r_c = k/\bar m_{\mathrm{R}}$ is introduced by which the renormalized mass can be defined

$$\bar m_{\mathrm{R}}^2 = k_c^2(\epsilon(k_c) - \epsilon^{cr}(k_c)), \qquad k_c = r_c \bar m_{\mathrm{R}}. \tag{5.1}$$

The quantity ϵ^{cr} denotes ϵ on the critical trajectory and is replaced by $2(\kappa\lambda_1)^{cr}$ if we start in the ordered regime. In our investigations, we will insert the fixed point values for the critical mass since we measure $\bar m_{\mathrm{R}}^2$ as a function of the distance to the fixed point in section 5.2. In the following, we will use (5.1) in every case where $\bar m_{\mathrm{R}}^2$ converges to zero, otherwise we simply employ the IR limit of $\bar m_{\mathrm{R}}^2$ as we did before.

For finite $h^2(k)$, we can read off from the flow equations that the couplings $\lambda_{1,2}(k)$ converge to finite values in the symmetric regime as well. That is in contrast to zero $h^2(k)$, where we observe the typical $\propto 1/k$ scaling behavior.

The artificial problems due to non-decoupling of Goldstone modes and the generic $3d$ effect of the diverging, bosonic wave function renormalization occur at the other fixed points as well. Therefore, we will not go too much into detail in the following.

FP(SSB)1b

For FP(SSB)1b, we obtain two relevant directions. As the Yukawa coupling h_*^2 is non-zero, we do not find an invariant subspace close to this fixed point. Near the fixed point, we always start with negative value $\lambda_{2\Lambda}$. Thus, we hope to obtain positive values at the end of our flow at least.

We especially consider the case $N_{\mathrm{f}} = 3$ in what follows. Going along the relevant direction with the largest exponent $\theta_1 = 1.81$ and negative $\Delta\kappa$, the flow leads into the symmetric regime where $\lambda_2(k) > 0$. Here we are faced with the same problem of increasing $Z_\varphi(k)$ due to $h^2 \nrightarrow 0$. Otherwise, for $\Delta\kappa > 0$ and $\Delta\lambda_2 < 0$, we stay in the symmetry broken regime, but approach $\kappa\lambda_2 \to -1$ which is quite unphysical because the threshold functions of masses $\kappa\lambda_2$ diverge.

The other relevant direction, where $\theta_2 = 0.44$, leads us exclusively into the symmetric regime with positive $\lambda_2(k)$ again, which is probably due to the high influence of the first relevant direction. As for increasing flavor numbers the difference between both critical exponents decreases, this behavior might slightly change. In fact, we locate an ordered phase in the second relevant

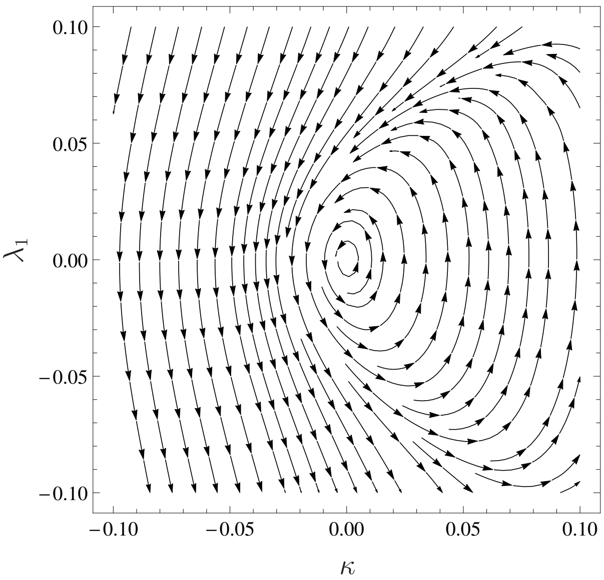

Figure 5.3.: Phase diagram of FP(SSB)2a at (0,0) in the plane spanned by both relevant directions with $\mathrm{Re}\,\theta_{1,2} = 1.4$. Only the κ and λ_1 components of the trajectories are depicted.

direction for increasing N_f without any occurring divergencies. That may be a hint that the existence of the ordered phase with reasonable flow behavior is not to be excluded for smaller N_f as well, but harder to detect.

FP(SSB)2a

Due to $h_*^2 = 0$, this fixed point is situated in the bosonic, $\mathrm{U}(N_\mathrm{f}) \otimes \mathrm{U}(N_\mathrm{f})$ symmetric subspace. Two of three relevant directions lie in this subspace which correspond to complex exponents[13] $\mathrm{Re}\,\theta_{1,2} = 1.4$. We expect a flow behavior which depends on the initial conditions in a very sensitive way. See figure 5.3 where the plane of the phase space spanned by both relevant directions is depicted. We observe spiral shaped trajectories. If we modify our UV starting value only a little, we may arrive in a totally different region of our theory space. We confirmed this fact in our analysis. However, since we always start with negative $\lambda_{2\Lambda}$ in the vicinity of this fixed point, we do not obtain any reasonable flow behavior in the bosonic subspace fitting to our symmetry breaking pattern.

Leaving the invariant subspace along the other relevant direction with non-complex exponent $\theta_3 = 0.96$ for positive $\Delta\lambda_2$, $\Delta\kappa$ and h_Λ^2, the flow leads into the symmetry broken regime with reasonable flow behavior because $\lambda_1(k)$ and $\lambda_2(k)$ converge to positive values. The scaling of the generated fermion mass $\bar{m}_{\mathrm{R},f}^2$ does not suffer from the Goldstone bosons since only mixed fermionic and bosonic fluctuations contribute, and can be read off from the finite limit of $k^2\kappa h^2(k)/N_\mathrm{f}$.

FP(SSB)2b

This fixed point is situated in the bosonic, $\mathrm{U}(N_\mathrm{f}) \otimes \mathrm{U}(N_\mathrm{f})$ symmetric subspace $h^2 \equiv 0$. In this subspace, where the relevant direction with critical exponent $\theta_1 = 0.98$ dominates the flow behavior, we determine a symmetric and a symmetry broken phase. However, remembering the fixed point FP(SSB)2a, we do not get reasonable flow behavior as well. Nevertheless, we will

[13]We mention that the real and the imaginary part of the corresponding eigenvectors are taken as the relevant directions in case of complex exponents.

consider the flow behavior in the symmetric phase for the evaluation of the critical exponents in section 5.2 since the needed quantities do not directly depend on $\lambda_2(k)$.

Following the direction with $\theta_2 = 0.96$ and positive $\Delta\lambda_2$, h^2_Λ and negative $\Delta\kappa$ out of the subspace, we find the symmetric phase with $\eta_\varphi \to 1$ and positive converging $\lambda_{1,2}(k)$. We also can find an ordered phase in the full theory space extending our examinations over the mere consideration of the relevant directions. However, we do not observe a reasonable behavior in the ordered phase that fits to our symmetry breaking pattern.

FP(SSB)3

The flow in the vicinity of this fixed point is dominated by only one relevant direction with $\theta_1 = 2.34$. That is a very comfortable situation because we can be sure that there is no other flow behavior in any direction than the one we observe for the relevant direction. In the symmetric phase with $\Delta\kappa < 0$, we arrive at positive converging $\lambda_{1,2}(k)$ while $Z_\varphi(k)$ is diverging, in the symmetry broken phase with $\Delta\kappa > 0$, the τ-mass approaching minus one renders the flow singular. All in all, we unfortunately do not observe physically reliable flow behavior in both phases close to the phase transition.

FP(SSB)4a,b

For both fixed points, the two relevant exponents are complex for $N_\mathrm{f} = 2, 3$ which entails a complicated structure of the phase diagrams. Yet, for both fixed points, we do not observe any reasonable IR physics as we have already supposed in the previous chapter. Either the fermion anomalous dimension rises to too large values, especially for FP(SSB)4a or we reach singularities, especially for FP(SSB)4b. At the regime boundary, the continuation of the flow from the symmetry broken regime into the symmetric regime fails.

Actually, we could not expect any reasonable IR behavior, especially for FP(SSB)4b, since starting from $\lambda_{1\Lambda} < 0$, $\lambda_1(k)$ has to become positive to ensure stability. However, when λ_1 crosses zero, singularities arise at least in the present truncation. Due to that behavior, we do not expect that FP(SSB)4a,b may become reasonable fixed points within a higher truncation with our symmetry breaking pattern and are thus no longer considered in our following investigations.

FP(SYM)1

We obtain three relevant directions for this fixed point, two of them belong to complex exponents. Our following observations are related to the case $N_\mathrm{f} = 3$. However, we do not think that the flow behavior significantly changes for increasing flavor numbers. Along the first relevant direction with $\theta_1 = 2.84$, we find the symmetric phase for $\Delta\epsilon > 0$ where $\lambda_2(k)$ satisfactorily becomes larger than zero and $\eta_\varphi \to 1$ again. For $\Delta\epsilon < 0$ we are situated in the symmetry broken phase, where the continuation of the flow in the symmetry broken regime fails, which might be an effect of our truncation. For the other directions with complex exponents, we can report on similar observations. However, opposed to our previous statements, the flow behavior seems to be insensitive to our starting point along these directions.

FP(SYM)2

For the flow starting along the direction with the largest positive exponent $\theta_1 = 2.26$, we approach $\kappa\lambda_2 \to -1$ in the ordered phase for $\Delta\epsilon < 0$, but obtain positive values for $\lambda_{1,2}(k)$ and diverging $Z_\varphi(k)$, due to non-zero Yukawa coupling $h^2(k)$, in the symmetric phase for $\Delta\epsilon > 0$. As the exponent $\theta_2 = 0.56$ of the other direction is much smaller, we expect high influence of the first one. Following this direction, we locate the symmetric phase exhibiting the same behavior as in the case before.

Finally, it is worth mentioning that for all fixed points the limits of the converging couplings are the same if we are situated in the same phase and subspace for the same flavor number. This indicates that we have some attractive IR behavior which often dominates the IR flow.

All in all, it is hard to decide about the physical reliability of the fixed points from the results of the flow analysis. Besides FP(SSB)4a,b which we could exclude, we are not able to give clear reasons for the occurrence of unreasonable flow behavior for each fixed point within our present truncation. With regard to the singularity $\kappa\lambda_2 \to -1$ for example, we can only guess that it occurs due to the negative λ_{2*} values of the fixed points, which may probably become positive within another truncation including higher polynomial orders.

5.2. Critical exponents

After having investigated the flow in the vicinity of all fixed points, we determine their critical exponents. For this purpose, we compute the observable IR quantities shifting the UV starting point of the flow by a varying distance of δg_Λ into the considered relevant direction. That is a good check for our calculations since we can derive the exponents from the positive θ_is and the anomalous dimension $\eta_{\varphi*}$ as well. Additionally, we are able to test the reliability of our definitions of those quantities that could not be determined by simply taking the limit $k \to 0$.

In the following, we restrict ourselves to the directions with the largest exponents θ_i and those which are a little bit smaller at most. We expect that the scaling and hyperscaling relations for one relevant direction hold since starting in such a direction, the flow does not notice anything of the other directions. Therefore, we will observe the critical behavior of phase transitions of second order.

Referring to the mass and bare mass in the symmetric regime, we define the critical exponents, cf. [24, 25],

$$\nu = \frac{1}{2} \lim_{\delta g_\Lambda \to 0} \frac{\partial \ln \bar{m}_\mathrm{R}^2}{\partial \ln \delta g_\Lambda} \qquad \text{and} \qquad \gamma = \lim_{\delta g_\Lambda \to 0} \frac{\partial \ln \bar{m}^2}{\partial \ln \delta g_\Lambda}, \tag{5.2}$$

where δg_Λ denotes the distance from the fixed point in the chosen direction. In general δg_Λ stands for the distance from the phase boundary. In the ordered phase, we employ $\bar{m}_{\mathrm{R},\rho}^2$ and $\bar{m}_\rho^2 = Z_\varphi \bar{m}_{\mathrm{R},\rho}^2$ instead of $\bar{m}_\mathrm{R}^2$ and $\bar{m}^2$, respectively. From the relation between the renormalized mass and the bare mass and exploiting the hyperscaling relation $\gamma = \nu(2 - \eta_{\varphi*})$, we derive, cf. [24],

$$-\eta_{\varphi*}\nu = \lim_{\delta g_\Lambda \to 0} \frac{\partial \ln Z_\varphi}{\partial \ln \delta g_\Lambda}. \tag{5.3}$$

In the ordered phase, we can additionally determine the thermodynamical exponent β defined by, cf. [25],

$$\beta = \frac{1}{2} \lim_{\delta g_\Lambda \to 0} \frac{\partial \ln \sigma_0^2}{\partial \ln \delta g_\Lambda}, \tag{5.4}$$

where $\sigma_0^2 = \frac{1}{N_\mathrm{f}} \rho_{0\mathrm{R}}/Z_\varphi = \frac{1}{N_\mathrm{f}} \rho_0$. For consistency, we may check the hyperscaling relation $\beta = \nu(d - 2 + \eta_{\varphi*})/2$ and compute $\gamma = \nu(2 - \eta_{\varphi*})$ for completeness. We now have repeated the full set of critical exponents we like to compute.

In the disordered phase, if $h^2 \nrightarrow 0$, we observe that the value of $\bar{m}_\mathrm{R}^2$ depends on the ratio r_c reflecting the regulator dependency. Therefore, we fix $r_c = 0.01$ for our investigations as it has been done in [24, 25]. However, it is worth emphasizing that we could have chosen another value smaller than one as well. Thus, we cannot give absolute results for $\bar{m}_\mathrm{R}^2$. Nevertheless, we obtain convenient dependency on δg_Λ. In this sense, we take Z_φ at the scale k_c as well if diverging. It is worth mentioning that the exponent γ does not depend upon whether we compute $\bar{m}^2$ at k_c or $k \to 0$.

Table 5.1.: Critical exponents, scaling and hyperscaling relations. The scaling and hyperscaling relations are fulfilled up to the sixth decimal place at least.

FP	N_f	$\theta\|_{\mathrm{FP}}$	$1/\theta\|_{\mathrm{FP}}$	$\nu\|_{\mathrm{Flow}}$	$\eta_{\varphi*}\|_{\mathrm{FP}}$	$\eta_{\varphi*}\|_{\mathrm{Flow}}$	γ	β	$\nu(2-\eta_{\varphi*})$	$\nu(1+\eta_{\varphi*})/2$
(SSB)										
1a	2	1.151 (SSB)	0.869	0.869	0.028	0.028	1.713	0.447	1.713	0.447
		1.151 (SYM)	0.869	0.869	0.028	0.028	1.713	-	1.713	0.447
		0.972 (SYM)	1.029	1.029	0.028	0.028	2.029	-	2.029	0.529
1b	3	1.812 (SYM)	0.552	0.552	0.158	0.158	1.016	-	1.016	0.320
2a	2	0.962 (SSB)	1.040	1.040	0.038	0.038	2.040	0.540	2.040	0.540
2b	2	0.979 (SYM)	1.021	1.021	0.042	0.042	2.000	-	2.000	0.532
		0.958 (SYM)	1.044	1.044	0.042	0.042	2.044	-	2.044	0.544
3	3	2.341 (SYM)	0.427	0.427	0.262	0.262	0.742	-	0.742	0.269
(SYM)										
1	3	2.841 (SYM)	0.352	0.352	0.442	0.442	0.548	-	0.548	0.254
2	3	2.262 (SYM)	0.442	0.442	0.286	0.286	0.758	-	0.758	0.284

In the symmetry broken phase, we evaluate the quantities $\bar{m}^2_{\mathrm{R},\rho}$ and $\bar{m}^2_{\rho}$ at k_{λ_1}. Taking σ_0^2 and Z_φ at k_{λ_1} or $k \to 0$ does not result in any difference for the critical exponents. The table 5.1 shows the critical exponents, scaling and hyperscaling relations for those integer flavor numbers at which the fixed points arise. The notation "FP" and "Flow" distinguishes between the exponents we obtain by inserting θ_i into the scaling relations or simply evaluating η_φ at the fixed point and those we have computed by integrating out the flow. The subscripts "SYM" and "SSB" clarify if the flow is computed in the disordered or ordered phase. Note, that we have not found reasonable flow behavior along the direction of the largest exponents in the symmetric phase as well as in the symmetry broken phase for the most fixed points. Therefore, the critical exponent β can only be computed using the hyperscaling relation in those cases where we have only observed reliable flow behavior in the symmetric phase.

It is remarkable that all critical exponents are in very good agreement to each other and fulfill the hyperscaling relations (up to the sixth decimal place at least). We have not listed the largest critical exponent of FP(SSB)2a. Besides non-reliable flow behavior, we add that its determination using (5.2)-(5.4) is technically demanding. By contrast, the critical exponent of the last relevant direction could be determined to be in good agreement with $1/\theta_3$, showing that it is not affected very much by the other directions.

5.3. Critical behavior and universality of phase transitions

Having obtained an impression of the flow behavior in the vicinity of the fixed points, we are now able to look for phase transitions. Within our examinations the order, which determines the critical and universal behavior, is of special interest. As our model is well established, there are some publications, for example [59] where the bosonic part of our model is treated beyond the polynomial truncation of our potential.

5.3.1. Search for physically reliable phase transitions

With regard to the Wilson-Fisher fixed point, we find reasonable phase transitions in all subspaces. For non-vanishing Yukawa coupling constant, we in fact did not observe a symmetry broken phase in previous examinations. However, the existence of the ordered phases in the invariant subspaces indicates rightly that there nevertheless might be one. Another suitable phase transition we find close to the fixed point FP(SSB)1b. As we have already supposed, physically reliable flow in the ordered phase without running into any divergencies is harder to detect and can only be observed if we start very close to the phase transition. At the fixed point FP(SSB)2a, we cannot completely exclude that there might exist a suitable, observable phase transition within our truncation, although this is very unlikely. However, as already mentioned, an investigation of this phase transition would be technically demanding. Therefore, we drop further investigations of FP(SSB)2a. For FP(SSB)2b, we can be sure that there is no physically reliable phase transition in the bosonic subspace $h^2 \equiv 0$ due to our observations above. For $h^2 > 0$ starting in the spontaneous symmetry broken phase, we observe that $\lambda_2(k)$ is always negative. Therefore, we do not have any phase transition exhibiting physical flow behavior close to FP(SSB)2b within our truncation. As we have obtained only one relevant direction for FP(SSB)3, but did not detect a symmetry broken phase without running into the singularity $\kappa\lambda_2 \to -1$, we are not able to find any physically reliable phase transition within our present truncation.

Close to the fixed point FP(SYM)1, we observe that the $\lambda_{1,2}$ couplings decrease if we start in the ordered phase, resulting in negative values of $\lambda_{1,2}(k)$ when we arrive at the regime boundary. This effects that the continuation of the flow in the symmetry broken regime fails. Therefore, we do not detect an ordered phase with reasonable flow behavior in the vicinity of FP(SYM)1. Thus, there is no observable phase transition within our truncation. At FP(SYM)2, we do not observe any reliable flow behavior in the symmetry broken phase as well. That observation from the flow analysis is supported by considering the phase diagrams in the vicinity of this fixed point. Arriving at the regime boundary, we expect to approach either the singularity $\kappa\lambda_2 \to -1$ in the ordered regime or that the continuation of the flow immediately fails.

Thus, we conclude that there are only phase transitions with reasonable flow properties in their vicinity at the Wilson-Fisher fixed point and FP(SSB)1b.

5.3.2. Detailed investigation of phase transitions

Both fixed points, the Wilson-Fisher fixed point FP(SSB)1a and FP(SSB)1b, have more than only one relevant direction. Therefore, if we are not located in any invariant subspace with only one relevant direction, we very likely observe phase transitions of first order. Hence, we only find a phase transition of second order in the $\mathrm{O}(2N_\mathrm{f}^2)$ symmetric subspace $\lambda_2, h^2 \equiv 0$ at the Wilson-Fisher fixed point [59]. Pausing at this point and remembering our truncation, we have to admit that at the beginning of our investigations, we hoped to find some more second order phase transitions since the polynomial expansion of the potential is actually not suitable for first order phase transitions. In fact, during the flow into another regime, we do not know when we arrive at the regime boundary because the VEV or the bosonic mass coupling $\bar{m}^2$ are not zero, but rather discontinuous there. Actually, we would need to compare both the potential's local minima at $\rho = 0$ and $\rho = \rho_0$, assuming that the minimum at $\rho = 0$ persists. Thus, we anticipate that we will not be able to prove the order of the phase transition, to determine the exact position of the phase transition and compute all the characterizing quantities correctly. However, using earlier results as a benchmark for our calculations, we are in the comfortable situation to explore those things which we can examine within our truncation and apply our experiences to new investigations. That will be the plan for our following examinations. Our benchmark model is the pure bosonic model treated in [59], which coincides with our model in the $\mathrm{U}(N_\mathrm{f}) \otimes \mathrm{U}(N_\mathrm{f})$ symmetric subspace $h^2 \equiv 0$.

Finally, it is worth emphasizing that the following calculations are made in the ordered phase. On the one hand, starting in the disordered phase close to the first order phase transition, we observe that the λ_1 coupling approaches zero for some RG "time" during the flow into the symmetric regime which causes unphysical flow behavior. This is due to our truncation. On the other hand, it will become obvious during the following discussion that we are not able to produce meaningful results for first order phase transitions from only measuring the two

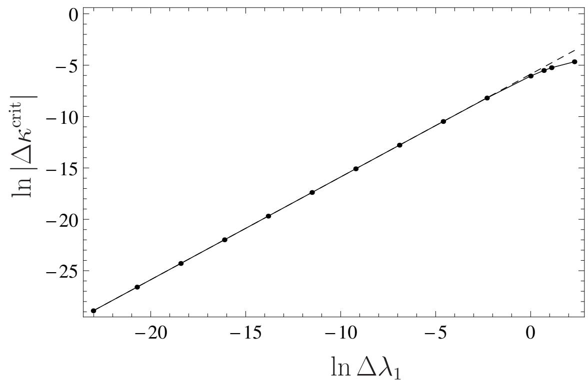

(a) The dependency of $\Delta\kappa^{\text{crit}}$ on $\Delta\lambda_1$: From the intersection of the linear slope with the y-axis, the value of the constant ratio $\Delta\kappa^{\text{crit}}/\Delta\lambda_1$ for small $\Delta\lambda_1$ can be computed

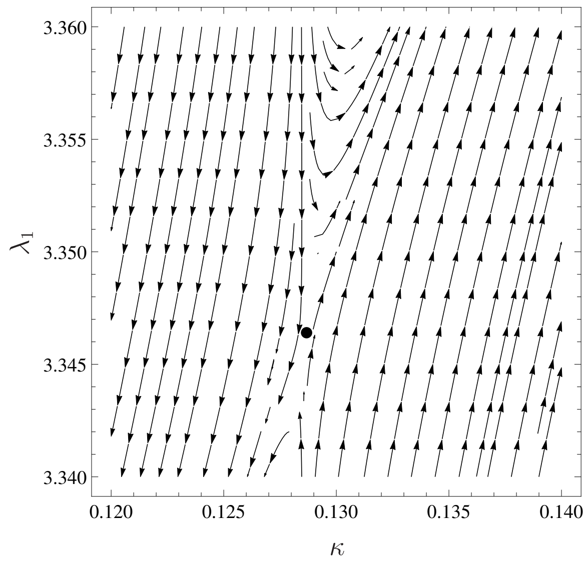

(b) Phase diagram in the vicinity of the Wilson-Fisher fixed point. For small $\Delta\lambda_1$ the separatrix is linear and corresponds to the irrelevant direction. The ratio $\Delta\kappa^{\text{crit}}/\Delta\lambda_1$ agrees with the ratio of the first components of the eigenvector corresponding to this direction.

Figure 5.4.: The separatrix in the invariant, $\mathrm{O}(2N_\mathrm{f}^2)$ symmetric subspace close to the Wilson-Fisher fixed point.

non-vanishing quantities $\bar{m}_\mathrm{R}^2$ and $\bar{m}^2$ in the symmetric phase.

FP(SSB)1a: the Wilson-Fisher fixed point

The following investigations are made again for $N_\mathrm{f} = 2$, but we believe that the qualitative statements hold for higher flavor numbers as well. We start with the second order phase transition in the invariant, $\mathrm{O}(2N_\mathrm{f}^2)$ symmetric subspace. To gain first impressions, we compute the critical value $\kappa^{\text{crit}} = \kappa_* + \Delta\kappa^{\text{crit}}$, for which we encounter the phase transition, for different starting values $\lambda_{1\Lambda} = \lambda_{1*} + \Delta\lambda_1$. Figure 5.4a is a logarithmic plot of the dependency of $\Delta\kappa^{\text{crit}}$ on $\Delta\lambda_1$. Close to the fixed point, the slope converges to one which displays the ratio $\Delta\kappa^{\text{crit}}/\Delta\lambda_1$ being constant. That fits to the phase diagram 5.4b where we can clearly identify the linear separatrix corresponding to the remaining irrelevant direction. The ratio $\Delta\kappa^{\text{crit}}/\Delta\lambda_1 \approx -0.00281$ is in very good agreement with the ratio of both components of the eigenvector corresponding to the irrelevant direction. It is worth mentioning that for rising $\lambda_{1\Lambda}$, the dependency of $\Delta\kappa^{\text{crit}}$ deviates more and more from the observed linearity near the Wilson-Fisher fixed point.

We check the critical flow behavior for three different UV values $\lambda_{1\Lambda} \in \{\lambda_{1*} + 10^{-5}, \lambda_{1*} + 10^{-3}, \lambda_{1*} + 1\}$. Figure 5.5 depicts the expected dependency of $\bar{m}_{\mathrm{R},\rho}^2$ and $\rho_{0\mathrm{R}}$ on $\delta\kappa_\Lambda = \kappa_\Lambda - \kappa^{\text{crit}}$. The linear behavior of the logarithmic plot is typical for second order phase transitions, since the VEV arises and increases continuously and the curvature of the potential vanishes at the critical value κ^{crit}. Close to the separatrix, we can verify the critical exponents we have already computed and listed in table 5.1. For this, we identified $\delta g_\Lambda = \delta\kappa_\Lambda$. It is worth mentioning that we confirmed these exponents starting in the symmetric phase as well, but we do not extend the discussion to the disordered phase at this point. The critical exponents ν and β as well as $\eta_{\varphi*}$ are in very good agreement with those given in [59]. The exponents ν and β differ by $1 - 1.5\%$ from our values, the anomalous dimension $\eta_{\varphi*}$ approximately by 20%. These differences are likely to arise from our simple polynomial expansion. Universality can be seen from the existence of the critical exponents and from the ratio $\bar{m}_{\mathrm{R},\rho}/\rho_{0\mathrm{R}}$ which becomes independent of the starting

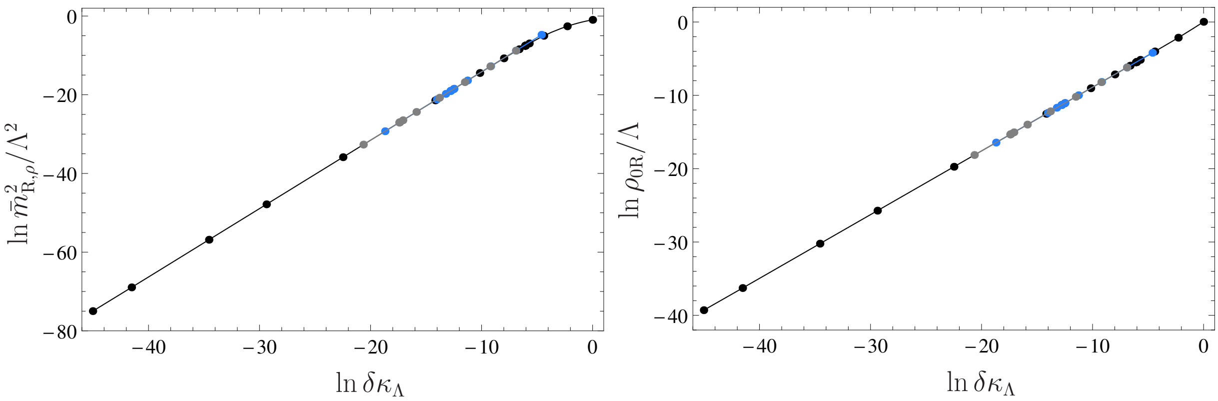

Figure 5.5.: Dependency of $\bar{m}^2_{\mathrm{R},\rho}$ and $\rho_{0\mathrm{R}}$ on $\delta\kappa_\Lambda$ for $\Delta\lambda_1 = 10^{-5}$ (gray), $\Delta\lambda_1 = 10^{-3}$ (blue), $\Delta\lambda_1 = 1$ (black).

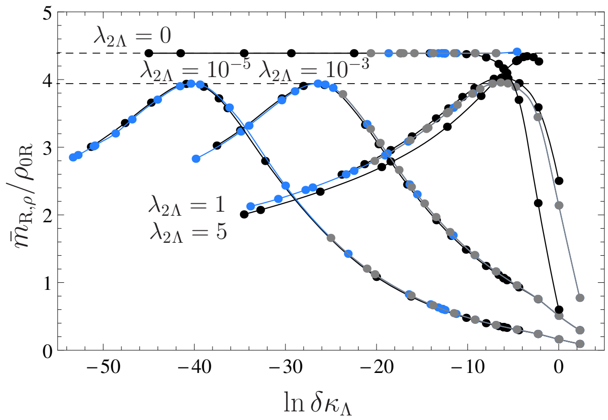

Figure 5.6.: Dependence of $\bar{m}_{\mathrm{R},\rho}/\rho_{0\mathrm{R}}$ on $\delta\kappa_\Lambda$ for $\Delta\lambda_1 = 10^{-5}$ (gray), $\Delta\lambda_1 = 10^{-3}$ (blue), $\Delta\lambda_1 = 1$ (black). For non-vanishing $\lambda_{2\Lambda}$, but small $\lambda_{2\Lambda}/\lambda_{1\Lambda} \ll 1$ the universality is manifest in the same values of the maxima.

point near the phase transition, see figure 5.6 for $\lambda_{2\Lambda} = 0$. This means, measuring one of both quantities, the other one can be well predicted. This can be explained as follows: If we start very close to the phase transition, the flow is driven near the fixed point for some RG "time". Close to the fixed point, the irrelevant couplings have enough "time" to cancel. Thus, the flow looses its memory on the initial conditions and the IR quantities exhibit universal behavior [59]. It is in accordance with our expectations that the universal behavior can be first seen for smaller $\delta\kappa_\Lambda$ for increasing starting value of $\lambda_{1\Lambda}$.

It is worth emphasizing that we in fact used the VEV at k_{λ_1} for computing the ratio $\bar{m}_{\mathrm{R},\rho}/\rho_{0\mathrm{R}}$. Doing this, we hope that the fluctuations, that are still present at k_{λ_1} and influence the scaling behavior of $\bar{m}_{\mathrm{R},\rho}$, are better compensated since $\rho_{0\mathrm{R}}$ suffers in the similar way from the fluctuations at k_{λ_1}. In this case the VEV at k_{λ_1} deviates from that at $k \to 0$ by 38%.

Based on these results, one may ask if the universality holds for non-vanishing $\lambda_{2\Lambda}$ in a certain vicinity of the higher symmetric, invariant subspace. May we find critical exponents describing critical behavior or a universal, constant ratio of two quantities as well? In [59] the answer of this question is yes and our next goal is to confirm this answer within our truncation as far as we can. As initial values of our following flow analysis, we choose $\lambda_{2\Lambda} \in \{10^{-5}, 10^{-3}, 1, 5\}$ and $\lambda_{1\Lambda} \in \{\lambda_{1*} + 10^{-5}, \lambda_{1*} + 10^{-3}, \lambda_{1*} + 1\}$, computing the flow to the IR physics for variable $\delta\kappa_\Lambda$. With the fact in mind that we are now concerned with phase transitions of first order, we actually should see jumps of the masses and the VEV at $\delta\kappa_\Lambda \to 0$ and therefore observe finite values of our quantities close to the phase transition in figure 5.7. However, because of reasons we have already given at the beginning of this section, we do not. Nevertheless, plotting $\rho_{0\mathrm{R}}$ as a function of $\delta\kappa_\Lambda$, we see that the curves for rising $\lambda_{2\Lambda}$ differs increasingly from the case $\lambda_{2\Lambda} = 0$

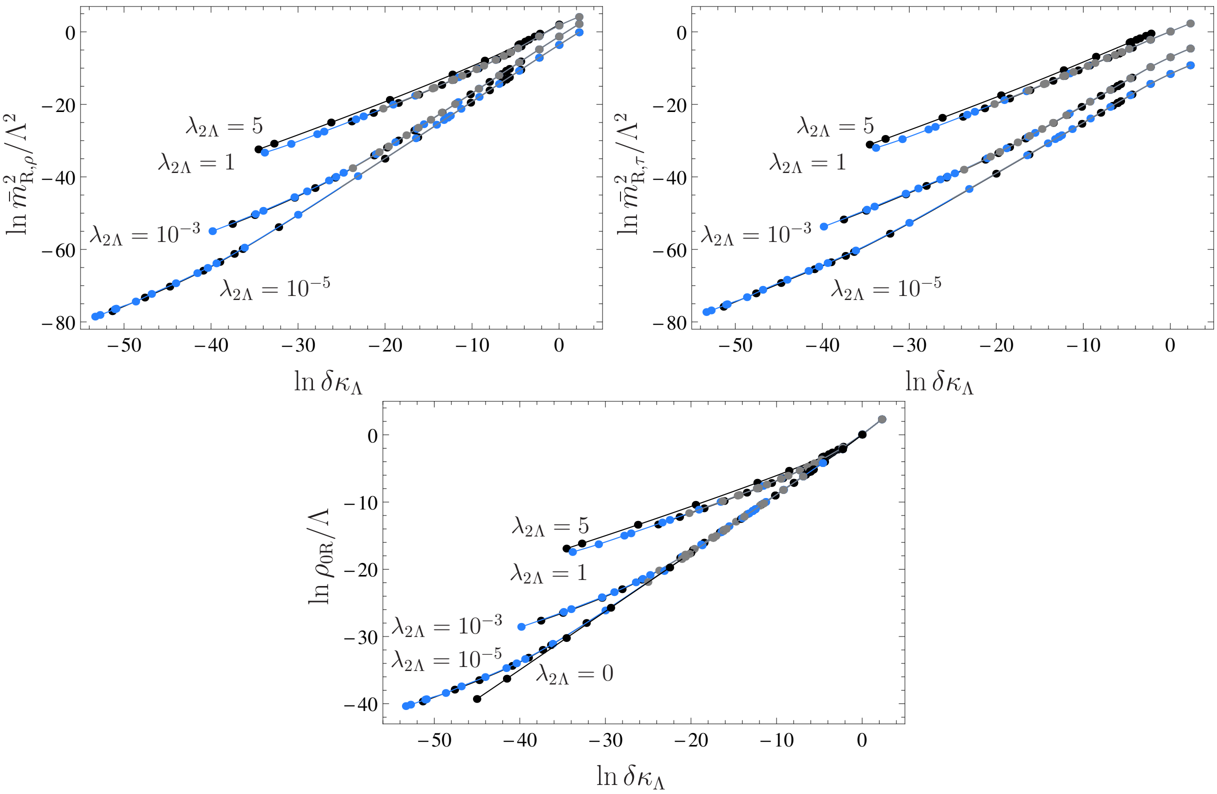

Figure 5.7.: Dependence of $\bar{m}^2_{\mathrm{R},\rho}$, $\bar{m}^2_{\mathrm{R},\tau}$ and $\rho_{0\mathrm{R}}$ on $\delta\kappa_\Lambda$ for $\Delta\lambda_1 = 10^{-5}$ (gray), $\Delta\lambda_1 = 10^{-3}$ (blue), $\Delta\lambda_1 = 1$ (black).

due to the increasing strength of the first order phase transition.

In [59], the universality is visible in the critical exponents ζ and ϑ defined by the critical behavior of

$$\rho_{0\mathrm{R}}^{\mathrm{crit}} \propto (\lambda_{2\Lambda})^{\vartheta} \qquad \text{and} \tag{5.5}$$

$$\rho_{0}^{\mathrm{crit}} \propto (\lambda_{2\Lambda})^{2\zeta}, \tag{5.6}$$

where the subscript denotes the quantity to be taken at the phase transition $\delta\kappa_\Lambda = 0$. One finds the same hyperscaling relation as for ν and β, namely $\zeta = \vartheta(1+\eta_{\varphi *})/2$. Additionally, the amplitude ratio $\bar{m}^{\mathrm{crit}}_{\mathrm{R},\rho}/\rho^{\mathrm{crit}}_{0\mathrm{R}}$ turns out to be universal for $\lambda_{2\Lambda}/\lambda_{1\Lambda} \ll 1$. Summarizing, it is easy to remember that the universality is recovered in this case by considering the quantities at $\delta\kappa_\Lambda = 0$ as functions of $\lambda_{2\Lambda}$ instead of as functions of $\delta\kappa_\Lambda$ like for second order transitions.

As we cannot determine the exact value of any quantity at $\delta\kappa_\Lambda = 0$, we have plotted the ratio $\bar{m}_{\mathrm{R},\rho}/\rho_{0\mathrm{R}}$ for running $\delta\kappa_\Lambda$, see figure 5.6. We have used again $\rho_{0\mathrm{R}}$ taken at k_{λ_1}, differing only by at most 8% from $\rho_{0\mathrm{R}}$ at $k \to 0$. At first sight, it is obvious that the ratio after reaching a maximum decreases. To understand this behavior, let us go more into depth and discuss how the flows of the couplings behave and influence each other. On this occasion, it is time to come back to the IR stopping scale k_{λ_1} for more details. In figure 5.8, besides the dimensionless renormalized couplings, the derivative of the logarithm of the coupling $\partial_t \ln g_i = \partial_t g_i/g_i$ with $g_i \in \{\kappa, \lambda_1, \lambda_2\}$ as a function of t is depicted. To get a better insight, we use the logarithmic scale t in our further line of argument. For $\kappa(t)$, the scaling behavior is almost perfectly fulfilled at t_{λ_1}, the fluctuations are almost completely suppressed by the rising masses. If $\delta\kappa_\Lambda$ is not too small, the minimal values of $\partial_t \ln \lambda_{1,2}$ are found in a relative small vicinity around t_{λ_1}. At these minima, the control of the scaling term over the fluctuations is best fulfilled, which can be comprehended with regard to the flow equations. For pure scaling behavior of the couplings

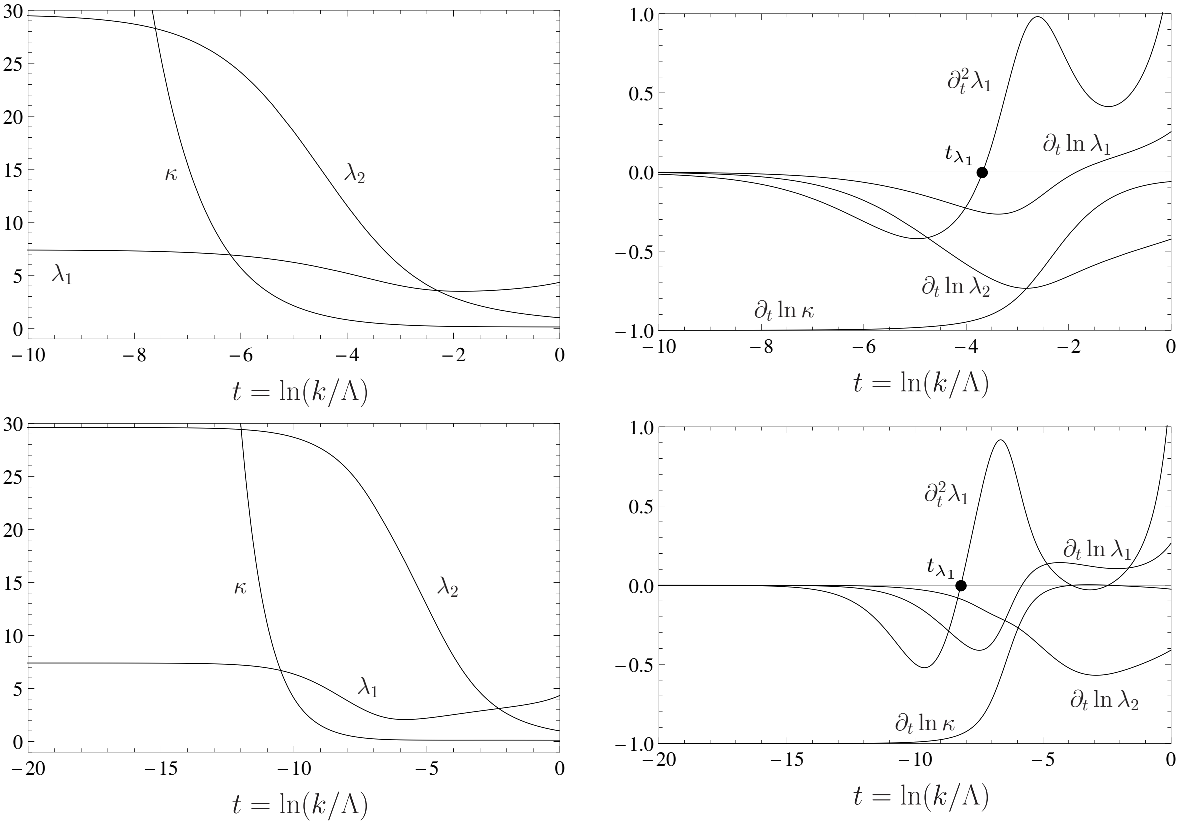

Figure 5.8.: Flow of the couplings and their derivatives for $\Delta\lambda_1 = \lambda_{2\Lambda} = 1$ and $\delta\kappa_\Lambda = 3.8 \times 10^{-3}$ (upper diagrams) and $\delta\kappa_\Lambda = 1.4 \times 10^{-6}$ (lower diagrams). The IR stopping scale t_{λ_1} can be read off from the zero of $\partial_t^2 \lambda_1$.

$\lambda_{1,2}$, $\partial_t \ln \lambda_{1,2}$ would approach minus one. However, the minima are usually bigger, especially for λ_1 and λ_2 for decreasing $\delta\kappa_\Lambda$. We could have employed these points as IR stopping scale as well. However, compared to t_{λ_1} lying close to these points, this would not make any sizable difference in our rather qualitative examinations. We emphasize that these findings generally hold for the earlier cases where we have already employed the IR stopping scale criterion as well. For first order phase transitions, all this changes at a certain $\delta\tilde{\kappa}_\Lambda$ where our IR stopping scale criterion becomes unreliable. In this range of $\delta\tilde{\kappa}_\Lambda$, we observe that the inflection point of $\lambda_1(t)$ becomes larger than that of $\lambda_2(t)$ and the minima of $\partial_t \ln \lambda_{1,2}$, especially that of $\partial_t \ln \lambda_2$, move away from t_{λ_1} and from each other. This starts to happen in the range where $\bar{m}_{\mathrm{R},\rho}/\rho_{0\mathrm{R}}$ approaches its maximum. Let us define the above introduced $\delta\tilde{\kappa}_\Lambda$ to be $\delta\kappa_\Lambda$ at this maximum. These observations are very technical, but give rise to the following fact: While the IR stopping criterion is getting unreliable, the τ-mass becomes too small. The τ-modes act therefore in a similar way like Goldstone bosons. Thus, the resulting radial mass decreases with respect to $\rho_{0\mathrm{R}}$, whereas the VEV is not affected. Hence, the decrease of the ratio can be finally traced back to the non-decoupling of the Goldstone bosons for $t \to -\infty$.

We concentrate on the maxima of $\bar{m}_{\mathrm{R},\rho}/\rho_{0\mathrm{R}}$ and find that for $\lambda_{2\Lambda}/\lambda_{1\Lambda} \ll 1$ their absolute values are all the same. The values themselves do not fit to the universal ratio given in [59] where $\bar{m}^{\mathrm{crit}}_{\mathrm{R},\rho}/\rho^{\mathrm{crit}}_{0\mathrm{R}} = 1.69$, but we can derive the universal behavior qualitatively for those flows which start close to the invariant subspace. Furthermore, the quantities $\rho_{0\mathrm{R}}$ and ρ_0 taken at $\delta\tilde{\kappa}_\Lambda$ lie on a line for the same $\lambda_{1\Lambda}$, but different $\lambda_{2\Lambda}$ in the logarithmic plot 5.9. If we consider both as a good approximation for $\rho^{\mathrm{crit}}_{0\mathrm{R}}$ and ρ^{crit}_0, we can determine the critical exponents ζ and ϑ with an accuracy of one decimal place from the slope. It turns out that these exponents deviate significantly in our truncation from those given in [59], but fulfill the hyperscaling relation (see

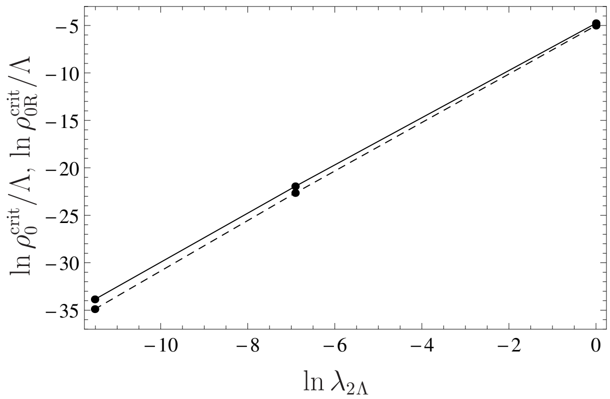

Figure 5.9.: Dependency of $\rho_{0\mathrm{R}}^{\mathrm{crit}}$ (solid) and ρ_0^{crit} (dashed) on $\lambda_{2\Lambda}$ for $\Delta\lambda_1 = 10^{-3}$. From the slope we can derive the critical exponents ϑ and ζ.

table 5.2), which is a good indication for consistency.

Table 5.2.: Critical exponents and hyperscaling relation.

	ζ	ϑ	$\eta_{\varphi *}$	ζ/ϑ	$(1+\eta_{\varphi *})/2$
Berges et al. (2002) [59]	0.988	1.93	0.022	0.513	0.511
our results	≈ 1.3	≈ 2.6	0.028	0.5	0.514

Summarizing our findings, we are not able to verify the order of the actual first order phase transition and measure any quantities at $\delta\kappa_\Lambda = 0$, but we can qualitatively observe universality. We will not extend our investigations to the full space $h^2 > 0$ close to the Wilson-Fisher fixed point since the flow starting near that fixed point with $\Delta h^2 > 0$ may be dominated by the fixed point FP(SSB)1b for $N_\mathrm{f} \geq 3$. To this end we will concentrate on the flow behavior at FP(SSB)1b in the following.

The fixed point FP(SSB)1b

In the last section, we recovered universality for weak first order phase transitions at the Wilson-Fisher fixed point close to an invariant, $\mathrm{O}(2N_\mathrm{f}^2)$ symmetric subspace. One might ask if there still exists universality without any invariant subspace giving rise to a second order phase transition. At FP(SSB)1b, we do not have such an invariant subspace which is therefore a good candidate to examine this question. The following calculations are made for the flavor number $N_\mathrm{f} = 3$.

The procedure is the same as for the Wilson-Fisher fixed point except for the fact that we consider the influence of the additional operator with the coupling h^2. We choose the UV couplings as $\lambda_{2\Lambda} \in \{\lambda_{2*} + 10^{-3}, \lambda_{2*} + 10^{-2}, \lambda_{2*} + 10^{-1}, \lambda_{2*} + 1, \lambda_{2*} + 5\}$, $\lambda_{1\Lambda} \in \{\lambda_{1*}, \lambda_{1*} + 10^{-5}, \lambda_{1*} + 10^{-3}, \lambda_{1*} + 10^{-1}\}$ and $h_\Lambda^2 \in \{h_*^2, h_*^2 + 10^{-5}, h_*^2 + 10^{-1}\}$. As $\lambda_{2*} < 0$, we only find the ordered phase close to the phase transition without exhibiting any singular flow behavior. Figure 5.10 depicts the VEV $\rho_{0\mathrm{R}}$ and the bosonic and fermionic masses in dependency on $\delta\kappa_\Lambda$. Again, we do not see the behavior of the quantities typical for first order phase transitions. We compute the amplitude $\bar{m}_{\mathrm{R},\rho}/\rho_{0\mathrm{R}}$ in the same way as for the Wilson-Fisher fixed point. By contrast, we take $\bar{m}_{\mathrm{R},f}$ and $\rho_{0\mathrm{R}}$ at $k \to 0$ for $\bar{m}_{\mathrm{R},f}/\rho_{0\mathrm{R}}$. Both ratios are represented as functions of $\delta\kappa_\Lambda$ in figure 5.11. It can be seen that there is almost no difference between the curves if we vary h_Λ^2 or $\lambda_{1\Lambda}$ within our range. Interestingly, the curves again exhibit maxima. For that fixed point, we consider the two amplitudes to proof that the occurrence of the curves' maxima has nothing to do with the chosen IR stopping scale.

However, let us intersperse a few comments on the couplings' flow and the IR stopping scale t_{λ_1} as we did for the Wilson-Fisher fixed point since some aspects are slightly different. As

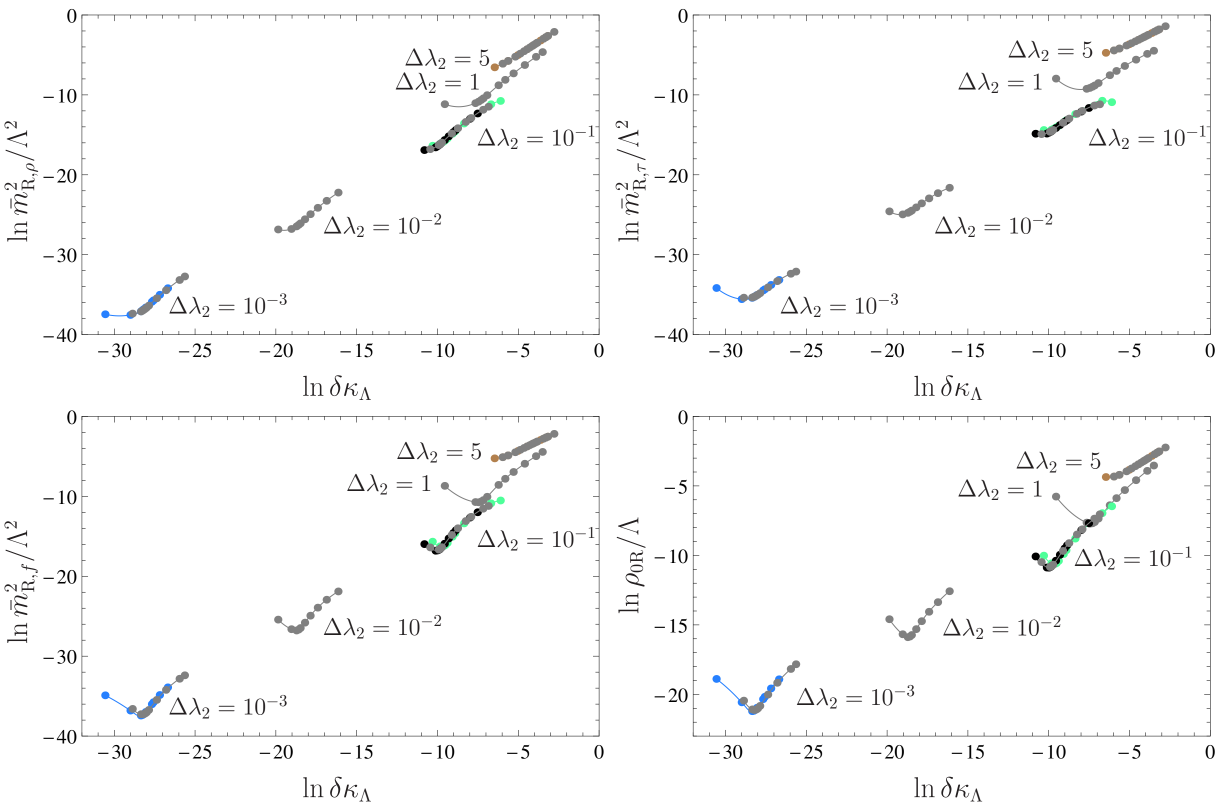

Figure 5.10.: Dependency of $\bar{m}^2_{\mathrm{R},\rho}$, $\bar{m}^2_{\mathrm{R},\tau}$, $\bar{m}^2_{\mathrm{R},f}$ and $\rho_{0\mathrm{R}}$ on $\delta\kappa_\Lambda$ for $\Delta\lambda_1 = 10^{-5}$ (gray), $\Delta\lambda_1 = 10^{-3}$ (blue), $\Delta\lambda_1 = 10^{-1}$ (black), $\Delta h^2 = 10^{-5}$ (brown), $\Delta h^2 = 10^{-1}$ (green).

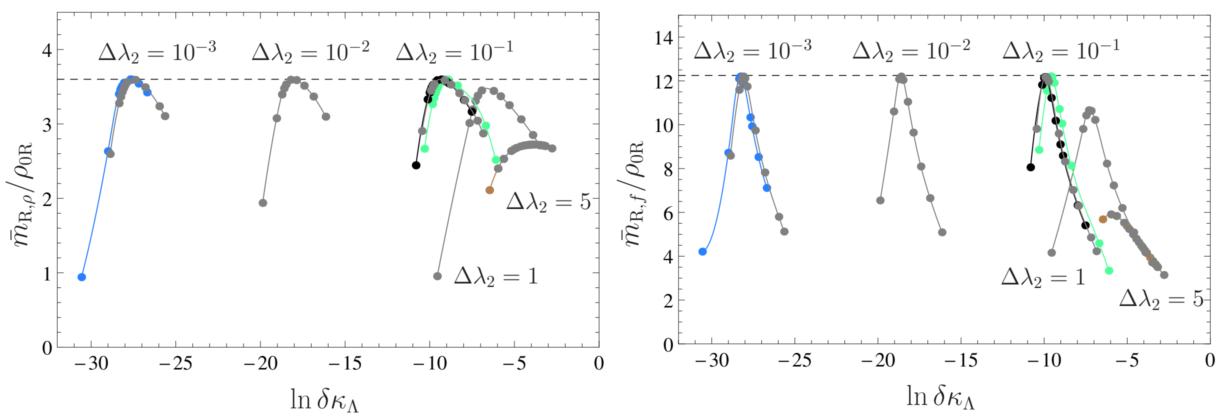

Figure 5.11.: Dependency of $\bar{m}_{\mathrm{R},\rho}/\rho_{0\mathrm{R}}$ and $\bar{m}_{\mathrm{R},f}/\rho_{0\mathrm{R}}$ on $\delta\kappa_\Lambda$ for $\Delta\lambda_1 = 10^{-5}$ (gray), $\Delta\lambda_1 = 10^{-3}$ (blue), $\Delta\lambda_1 = 10^{-1}$ (black), $\Delta h^2 = 10^{-5}$ (brown), $\Delta h^2 = 10^{-1}$ (green). For $\Delta\lambda_2/\lambda_{1\Lambda} \ll 1$ and $\Delta\lambda_2/h^2_\Lambda \ll 1$ the universality is manifest in the same values of the maxima.

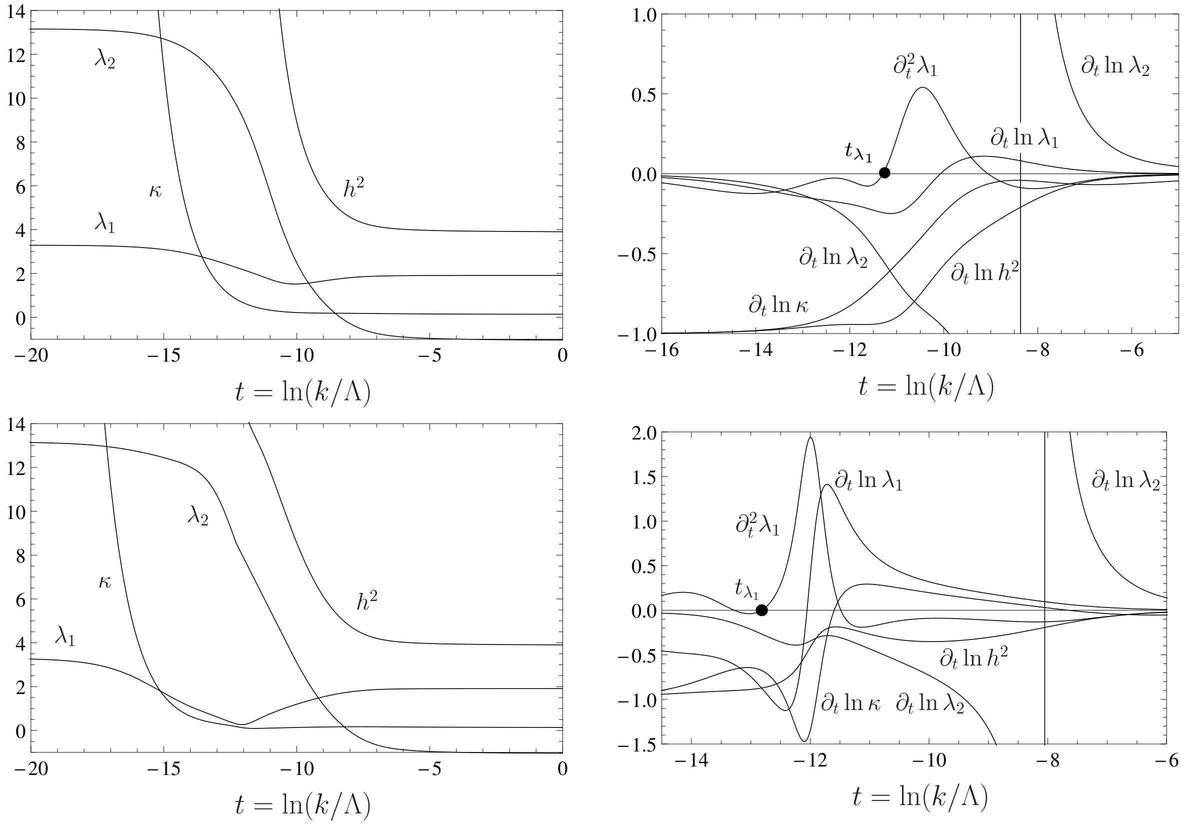

Figure 5.12.: Flow of the couplings and their derivatives for $\Delta\lambda_1 = 10^{-5}$, $\Delta\lambda_2 = 10^{-2}$ and $\delta\kappa_\Lambda = 10^{-7}$ (upper diagrams) and $\delta\kappa_\Lambda = 2.4 \times 10^{-9}$ (lower diagrams). The IR stopping scale t_{λ_1} can be read off from the zero of $\partial_t^2\lambda_1$.

it can be seen in figure 5.12, the λ_1 coupling decreases before converging to the partial fixed point, which entails that the radial mass becomes very small during the flow. With regard to the flow function β_κ, the small radial mass causes κ to lower before taking on its scaling behavior. Therefore, the VEV converges later with respect to the IR stopping scale t_{λ_1}. This behavior strengthens during the approach to the phase transition and gives rise to up to four times bigger values of $\rho_{0\mathrm{R}}$ at t_{λ_1} compared to those evaluated at $t \to -\infty$. Working conversely, the fermionic contribution exerts more influence for small enough $\delta\kappa_\Lambda$. Moreover, the VEV read off at $t \to -\infty$ increases. As we have mentioned for the Wilson-Fisher fixed point, we find the minimum of $\partial_t \ln \lambda_1$ close to the inflection point t_{λ_1}, which is a good argument for the choice of t_{λ_1}. We emphasize that the minimum can be again interpreted as the dominance of the scaling term if $\delta\kappa_\Lambda$ is not too small, although we have fermionic contributions, due to the damping influence of the fermionic mass. As almost all $\lambda_{2\Lambda} < 0$, it is difficult to find a similar argument for the IR stopping scale with regard to λ_2. However, approaching the phase transition we can observe a rising value of $\partial_t \ln \lambda_2$ at t_{λ_1}, indicating a too small τ-mass. Therefore, the radial mass decreases with respect to $\rho_{0\mathrm{R}}$ as for the Wilson-Fisher fixed point. Finally, both scalar masses effect the fermionic mass to decrease as compared to $\rho_{0\mathrm{R}}$ if we start close to the phase transition. It is worth mentioning that for too small $\delta\kappa_\Lambda$, we are not able to determine t_{λ_1} anymore since the flow is getting singular due to vanishing λ_1 for some RG "time" which is finally an effect of our truncation.

Similar to the Wilson-Fisher fixed point, the equal maxima of $\bar{m}_{\mathrm{R},\rho}/\rho_{0\mathrm{R}}$ and $\bar{m}_{\mathrm{R},f}/\rho_{0\mathrm{R}}$ embody universal behavior which is derived for $\Delta\lambda_2/\lambda_{1\Lambda} \ll 1$ and $\Delta\lambda_2/h_\Lambda^2 \ll 1$. We do not expect to obtain good approximations for the universal ratios. We compute the critical exponents ζ and ϑ using (5.5) and (5.6), where we substitute $\lambda_{2\Lambda}$ for $\Delta\lambda_2$. The quantities $\rho_{0\mathrm{R}}$ and ρ_0 taken at

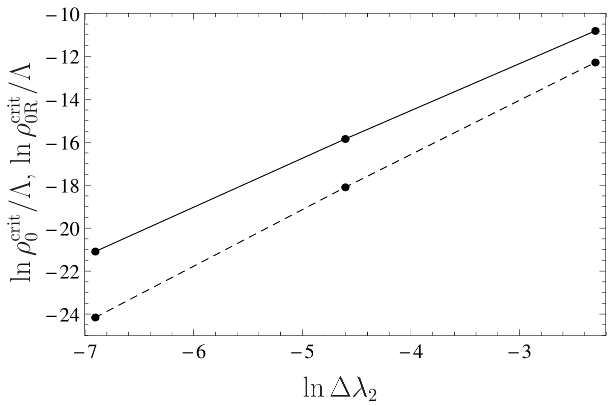

Figure 5.13.: Dependency of $\rho_{0\mathrm{R}}^{\mathrm{crit}}$ (solid) and ρ_0^{crit} (dashed) on $\Delta\lambda_2$ for $\Delta\lambda_1 = 10^{-5}$. From the slope we can derive the critical exponents ϑ and ζ.

$\delta\tilde{\kappa}_\Lambda$ again lie on a line, see figure 5.13. The slope and therefore the exponents do not depend on whether we employ the maximum of $\bar{m}_{\mathrm{R},\rho}/\rho_{0\mathrm{R}}$ or $\bar{m}_{\mathrm{R},f}/\rho_{0\mathrm{R}}$. We have to be very careful evaluating the reliability of the critical exponents given in table 5.3. We may expect that the given values are not fully reliable estimates, but an indication of consistency is that the hyperscaling relation is fulfilled.

Table 5.3.: Critical exponents and hyperscaling relation.

ζ	ϑ	$\eta_{\varphi*}$	ζ/ϑ	$(1+\eta_{\varphi*})/2$
≈ 1.3	≈ 2.2	0.158	0.6	0.579

To summarize, within our technical capabilities, we do find universality at the fixed point FP(SSB)1b, although there is no invariant subspace exhibiting a phase transition of higher order. We emphasize that our findings lead to a very interesting result which, however, should be checked by means of better adapted methods.

6. Summary and conclusions

In this work, we have investigated a chiral $\mathrm{U}(N_\mathrm{f}) \otimes \mathrm{U}(N_\mathrm{f})$ symmetric fermion system in order to check possible relations to the fixed point corresponding to the second order phase transition which was found in [40–45] at sufficiently small N_f. To this end, we have employed the renormalization group (RG) method. For a quantitative examination of this phase transition, we have considered a partially bosonized action. In order to truncate the effective average action, we worked at next-to-leading order in a systematic derivative expansion. With regard to the bosonic potential, we have employed a polynomial expansion consisting of the two invariants ρ and τ up to second and first order respectively, which correspond to φ^4 interactions. Additionally, we have implemented the $\mathrm{U}(N_\mathrm{f}) \otimes \mathrm{U}(N_\mathrm{f}) \to \mathrm{U}(N_\mathrm{f})$ symmetry breaking pattern while computing the RG equations of the dimensionless, renormalized couplings. Within the search for fixed points, we have found some arguments for the irrelevance of φ^6 terms for most of the fixed points. However, to be absolutely sure, we would have to include terms of higher polynomial orders within our calculations. In order to investigate the whole fixed point structure, we have started with the large N_f case, where we have employed large N_f scaling schemes that appeared to be natural. In the symmetric regime, the contribution of the fermions is indispensable for obtaining any non-trivial solution. In the symmetry broken regime, the bosonic equations decouple. Within this approximation, we have shown a fairly explicit picture of the fixed point structure. We have found one fixed point FP(SYM)1 in the symmetric regime and two fixed points FP(SSB)1a,b in the symmetry broken regime, one of them corresponding to the Wilson-Fisher fixed point exhibiting an enhanced $\mathrm{O}(2N_\mathrm{f}^2)$ symmetry. Finally, we have considered the finite N_f case. In the symmetry broken case, it has turned out to be advantageous to examine the purely bosonic sector at first and then take again the fermions into account. Hence, we have found solutions where the fermions decouple as well as where the Yukawa-type interaction does not vanish. All in all, we have obtained a rich fixed point structure of emerging and annihilating solutions, especially for small $N_\mathrm{f} \geq 2$. However, we had to be careful to estimate their physical reliability since the λ_2 coupling of almost all fixed points is negative. In order to select the physically reliable solutions, we therefore have introduced some criteria. To gain deeper insight, we have integrated out the flow in the vicinity of the fixed points. We have not found any reasonable flow behavior at the fixed points FP(SSB)4a,b. Due to the non-decoupling of the Goldstone bosons, we have introduced an IR stopping scale k_{λ_1} for the evaluation of the radial mass and the τ-mass in the symmetry broken phase. Additionally, we observed the generic $3d$ effect $\eta_\varphi \to 1$ for non-zero h^2 in the symmetric phase to which end we have employed a definition of $\bar{m}_\mathrm{R}^2$ from [24, 25] in these cases. These definitions were used within the calculation of the critical exponents by integrating out the flow starting in the relevant directions from each fixed point. These exponents have turned out to be in good agreement with those computed from the eigenvalues of the stability matrix. Furthermore, they fulfill the hyperscaling relations to high accuracy. After having obtained a good overview of the properties of each fixed point within our truncation, we have searched for suitable phase transitions. Unfortunately, we have only found one phase transition of second order in the invariant, $\mathrm{O}(2N_\mathrm{f}^2)$ symmetric subspace at the Wilson-Fisher fixed point which shows reasonable flow behavior. We could confirm the expected universal behavior and determine the critical exponents in good agreement with [59] close to the phase transition. However, with regard to the numerical predictions of [40–45], we did not find a suitable fixed point exhibiting a second order phase transition. As almost all fixed points we have found possess more than one relevant direction, it is very unlikely that one of them was observed by numerical means and the only fixed point with one relevant direction solely exists for $N_\mathrm{f} \approx 3$. Therefore, the numerical calculations are likely to observe a phase transition in a different universality class.

As most of the fixed points have more than one relevant direction, the other found phase transitions are very likely of first order. However, the polynomial expansion of the potential is not suitable for first order phase transitions. Therefore, we have used the purely bosonic $\mathrm{U}(N_\mathrm{f}) \otimes \mathrm{U}(N_\mathrm{f})$ symmetric model in [59] as a benchmark test. We have found out that we are nevertheless able to observe universality of the first order phase transition at the Wilson-Fisher fixed point. We could not confirm the universal ratio $\bar{m}^{\mathrm{crit}}_{\mathrm{R},\rho}/\rho^{\mathrm{crit}}_{0\mathrm{R}}$ and the exponents ϑ, ζ, although their values fulfill the hyperscaling relation. However, we could infer the qualitative occurrence of universality from the same values of the maxima of $\bar{m}_{\mathrm{R},\rho}/\rho_{0\mathrm{R}}(\delta\kappa_\Lambda)$ for $\lambda_{2\Lambda}/\lambda_{1\Lambda} \ll 1$. This observation has offered an unexpected opportunity to us: To our knowledge, it is still an open question if the emergence of universality is bounded to the existence of an invariant subspace exhibiting a second order phase transition. A very interesting result of our investigations at the fixed point FP(SSB)1b is that we have observed similar behavior at the first order phase transition for $\Delta\lambda_2/\lambda_{1\Lambda} \ll 1$ and $\Delta\lambda_2/h^2_\Lambda \ll 1$ indicating universal behavior. The critical exponents, whose values we may expect not to be fully reliable estimates, nevertheless fulfill the hyperscaling relation. It would be very exciting to confirm these results by means of better adapted methods. We hope to have given some impetus for this.

Bibliography

[1] D. V. Shirkov. “Fifty years of the renormalization group.” *CERN Courier* (2001).

[2] E. C. Stueckelberg and A. Petermann. “The normalization group in quantum theory.” *Helv.Phys.Acta* 24 (1951), pp. 317–319.

[3] E. Stueckelberg and A. Petermann. “Normalization of constants in the quanta theory.” *Helv.Phys.Acta* 26 (1953), pp. 499–520.

[4] M. Gell-Mann and F. E. Low. “Quantum Electrodynamics at Small Distances.” *Phys. Rev.* 95 (1954), pp. 1300–1312.

[5] N. N. Bogoliubov and D. V. Shirkov. “Charge renormalization group in quantum field theory.” *Nuovo Cimento* 3 (1956), pp. 845–863.

[6] N. N. Bogoliubov and D. V. Shirkov. “The multiplicative renormalization group in the quantum theory of fields.” *Soviet Physics JETP-USSR* 3 (1956), pp. 57–64.

[7] N. N. Bogoliubov and D. V. Shirkov. *Introduction to the theory of quantized fields.* Wiley-Interscience, New York, 1959.

[8] K. G. Wilson. “Renormalization Group and Critical Phenomena. I. Renormalization Group and the Kadanoff Scaling Picture.” *Phys. Rev. B* 4 (1971), pp. 3174–3183.

[9] L. P. Kadanoff. “Scaling laws for Ising models near T_c.” *Physics (Long Island City, N. Y.)* 2 (1966), p. 263.

[10] D. Shirkov. “The Bogoliubov renormalization group” (1996). arXiv:`hep-th/9602024 [hep-th]`.

[11] B. Rosenstein et al. “Four-fermion theory is renormalizable in 2+1 dimensions.” *Phys. Rev. Lett.* 62 (1989), pp. 1433–1436.

[12] J. Zinn-Justin. “Four-fermion interaction near four dimensions.” *Nuclear Physics B* 367 (1991), pp. 105 –122.

[13] B. Rosenstein et al. “Dynamical symmetry breaking in four-fermion interaction models.” *Physics Reports* 205 (1991), pp. 59 –108.

[14] S. Hands et al. “Four-Fermi Theories in Fewer Than Four Dimensions.” *Annals of Physics* 224 (1993), pp. 29 –89.

[15] J. Gracey. “The Nambu-Jona-Lasinio model at $O(1/N^2)$.” *Phys.Lett.* B308 (1993), pp. 65–69. arXiv:`hep-th/9305012 [hep-th]`.

[16] J. A. Gracey. “The conformal bootstrap equations for the four fermi interactionnn in arbitrary dimensions.” *Zeitschrift für Physik C Particles and Fields* 59 (1993), pp. 243–249.

[17] J. Gracey. “On the $O(1/N^2)$ β-function of the Nambu-Jona-Lasinio model with non-abelian chiral symmetry.” English. *Zeitschrift für Physik C Particles and Fields* 61 (1994), pp. 115–124.

[18] J. Gracey. “Computation of $\beta'(\mathrm{g(c)})$ at $O(1/N^2)$ in the $O(N)$ Gross-Neveu model in arbitrary dimensions.” *Int.J.Mod.Phys.* A9 (1994), pp. 567–590. arXiv:`hep-th/9306106 [hep-th]`.

[19] J. A. Gracey. "The β-function of the chiral Gross-Neveu model at $O\ (1/N^2)$." *Phys. Rev. D* 50 (1994), pp. 2840–2847.

[20] I. M. Barbour et al. "Strongly coupled lattice gauge theory with dynamical fermion mass generation in three dimensions." *Phys. Rev. D* 58 (1998).

[21] S. Christofi and C. Strouthos. "Three dimensional four-fermion models - A Monte Carlo study." *JHEP* 05 (2007).

[22] T. Banks et al. "Strong-coupling calculations of lattice gauge theories: $(1 + 1)$-dimensional exercises." *Phys. Rev. D* 13 (1976), pp. 1043–1053.

[23] L. Susskind. "Lattice fermions." *Phys. Rev. D* 16 (1977), pp. 3031–3039.

[24] L. Rosa et al. "Critical Exponents of the Gross-Neveu Model from the Effective Average Action." *Phys. Rev. Lett.* 86 (2001), pp. 958–961.

[25] F. Höfling et al. "Phase transition and critical behavior of the $d = 3$ Gross-Neveu model." *Phys. Rev. B* 66 (2002).

[26] C. Wetterich. "Exact evolution equation for the effective potential." *Physics Letters B* 301 (1993), pp. 90 –94.

[27] L. Janssen. "Critical phenomena in 2+1-dimensional relativistic fermion systems." PhD thesis. Theoretisch-Physikalisches Institut, Friedrich-Schiller-Universität Jena, 2012.

[28] P. R. Wallace. "The Band Theory of Graphite." *Phys. Rev.* 71 (1947), pp. 622–634.

[29] A. H. Castro Neto et al. "The electronic properties of graphene." *Rev. Mod. Phys.* 81 (2009), pp. 109–162.

[30] K. S. Novoselov et al. "Electric field effect in atomically thin carbon films." *Science* 306 (2004), pp. 666–669.

[31] A. K. Geim and S. Novoselov. "The rise of graphene." *Nature Materials* 6 (2007), pp. 183–191.

[32] A. C. Neto et al. "Drawing conclusions from graphene." *Physics World* 19 (2006), pp. 33–37.

[33] M. I. Katsnelson et al. "Chiral tunneling and the Klein paradox in graphene." *Nature Physics* 2 (2006), pp. 620–625.

[34] M. Katsnelson and K. Novoselov. "Graphene: New bridge between condensed matter physics and quantum electrodynamics." *Solid State Communications* 143 (2007), pp. 3–13.

[35] O. Klein. "Die Reflexion von Elektronen an einem Potentialsprung nach der relativistischen Dynamic von Dirac." *Zeitschrift für Physik C Particles and Fields* 53 (1929), p. 157.

[36] M. I. Katsnelson. "Zitterbewegung, chirality, and minimal conductivity in graphene." *Eur. Phys. J. B* 51 (2006), pp. 157–160.

[37] J. Tworzydło et al. "Sub-Poissonian Shot Noise in Graphene." *Phys. Rev. Lett.* 96 (2006).

[38] E. Schroedinger. "Über die kräftefreie Bewegung in der relativistischen Quantenmechanik." *Sitzber. Preuss. Akad. Wiss. Phys.-Math. Kl.* 24 (1930), p. 418.

[39] W. E. Thirring. "A soluble relativistic field theory." *Annals of Physics* 3 (1958), pp. 91–112.

[40] L. Del Debbio and S. Hands. "The Three Dimensional Thirring Model for $N_\mathrm{f} = 4$ and $N_\mathrm{f} = 6$." *Nuclear Physics B* 552 (1999), 339–362.

[41] L. Del Debbio and S Hands. "Monte Carlo simulation of the three dimensional Thirring model." *Physics Letters B* 373 (1996), pp. 171 –177.

[42] L. Del Debbio et al. “Three-dimensional thirring model for small N_{f}.” *Nuclear Physics B* 502 (1997), pp. 269 –308.

[43] S. Chandrasekharan and A. Li. “Fermion Bags, Duality, and the Three Dimensional Massless Lattice Thirring Model.” *Phys. Rev. Lett.* 108 (2012).

[44] S. Christofi et al. “Critical flavor number in the three dimensional Thirring model.” *Phys. Rev. D* 75 (2007).

[45] S. Christofi et al. “Phase diagram of the three dimensional Thirring model: A Monte Carlo study.” *PoS* LAT2006 (2006), p. 217. arXiv:`hep-lat/0703016 [HEP-LAT]`.

[46] D.-U. Jungnickel and C. Wetterich. “Effective action for the chiral quark-meson model.” *Phys. Rev. D* 53 (1996), pp. 5142–5175.

[47] H. Gies. “Introduction to the functional RG and applications to gauge theories.” *Lect.Notes Phys.* 852 (2012), pp. 287–348. arXiv:`hep-ph/0611146 [hep-ph]`.

[48] J. Braun. “Fermion interactions and universal behavior in strongly interacting theories.” *Journal of Physics G: Nuclear and Paricle Physics* 39 (2012), p. 033001.

[49] M. E. Peskin and D. V. Schroeder. *An Introduction to Quantum Field Theory.* Westview Press, 1995.

[50] J. Zinn-Justin. *Quantum Field Theory and Critical Phenomena.* 4th ed. Clarendon Press Oxford, 2002.

[51] J. M. Pawlowski. “Aspects of the functional renormalisation group.” *Annals Phys.* 322 (2007), pp. 2831–2915. arXiv:`hep-th/0512261 [hep-th]`.

[52] K. G. Wilson and M. E. Fisher. “Critical Exponents in 3.99 Dimensions.” *Phys. Rev. Lett.* 28 (1972), pp. 240–243.

[53] J. Goldstone. “Field theories with superconductor solutions.” *Nuovo Cimento* 19 (1961), pp. 154–164.

[54] J. Goldstone et al. “Broken Symmetries.” *Phys. Rev.* 127 (1962), pp. 965–970.

[55] M. E. Fisher and R. J. Burford. “Theory of Critical-Point Scattering and Correlations. I. The Ising Model.” *Phys. Rev.* 156 (1967), pp. 583–622.

[56] D. S. Ritchie and M. E. Fisher. “Theory of Critical-Point Scattering and Correlations. II. Heisenberg Models.” *Phys. Rev. B* 5 (1972), pp. 2668–2692.

[57] H. B. Tarko and M. E. Fisher. “Theory of critical point scattering and correlations. III. The Ising model below T_c and in a field.” *Phys. Rev. B* 11 (1975), pp. 1217–1253.

[58] F. Gehring. “Fixpunkt-Struktur von verallgemeinerten Gross-Neveu-Modellen in drei Raumzeitdimensionen.” MA thesis. Friedrich-Schiller-Universität Jena, 2013.

[59] J. Berges et al. “Nonperturbative renormalization flow in quantum field theory and statistical physics.” *Phys.Rept.* 363 (2002), pp. 223–386. arXiv:`hep-ph/0005122 [hep-ph]`.

[60] H. Gies and M. M. Scherer. “Asymptotic safety of simple Yukawa systems.” *Eur. Phys. J. C* 66 (2010), pp. 387–402.

[61] D. F. Litim. “Optimized renormalization group flows.” *Phys. Rev. D* 64 (2001).

A. Details on the computation of the flow equations

In section 3.2 with regard to the computation of the bosonic potential's flow equation, we assume a hermitian, diagonal form of the scalar fields. We now show that this assumption does not give rise to any restriction.

Think of some arbitrary scalar $N_\mathrm{f} \times N_\mathrm{f}$ matrix field φ. It is obvious that

$$A = (\varphi^\dagger \varphi)^{1/2} \tag{A.1}$$

is a hermitian matrix, which is therefore diagonalizable and that

$$B = \varphi(\varphi^\dagger \varphi)^{-1/2} \tag{A.2}$$

is unitary. The root of the matrix $\varphi^\dagger\varphi$ is defined in the way that $\varphi^\dagger\varphi = (\varphi^\dagger\varphi)^{1/2}(\varphi^\dagger\varphi)^{1/2}$. We denote the diagonalized matrix computed from A as

$$D_A := CAC^\dagger, \tag{A.3}$$

where $C \in \mathrm{U}(N_\mathrm{f})$ is unitary. Exploiting the $\mathrm{U}(N_\mathrm{f}) \otimes \mathrm{U}(N_\mathrm{f})$ symmetry transformation

$$\varphi \mapsto U_\mathrm{L} \varphi U_\mathrm{R}^\dagger \tag{A.4}$$

with $U_\mathrm{L}, U_\mathrm{R} \in \mathrm{U}(N_\mathrm{f})$, we may bring the arbitrarily chosen field φ into a diagonal form

$$\varphi' = U_\mathrm{L} \varphi U_\mathrm{R}^\dagger = U_\mathrm{L} B A U_\mathrm{R}^\dagger = CAC^\dagger = D_A, \tag{A.5}$$

where we have used $U_\mathrm{L} = CB^{-1}$ and $U_\mathrm{R} = C$.

B. The regulator and threshold functions[1]

The fermionic and bosonic regulator functions $R_{\psi/\varphi,k}$ can be denoted in terms of dimensionless shape functions $r_{\psi/\varphi,k}$

$$R_{\psi,k}(p) = -Z_{\psi,k}\not{p}\, r_{\psi,k}\left(\frac{p^2}{k^2}\right) \quad \text{and} \quad R_{\varphi,k}(p) = Z_{\varphi,k}p^2 r_{\varphi,k}\left(\frac{p^2}{k^2}\right). \tag{B.1}$$

In our work, we employ the linear cutoff, satisfying the optimization criterion [61],

$$r_{\psi,k}(y) = \left(\frac{1}{\sqrt{y}} - 1\right)\Theta(1-y) \quad \text{and} \quad r_{\varphi,k}(y) = \left(\frac{1}{y} - 1\right)\Theta(1-y). \tag{B.2}$$

The threshold functions are single integrals due to the one-loop structure of the Wetterich equation. Without inserting of any specific regulator function, they read

$$l_n^{(\mathrm{F/B})d}(\omega;\eta_{\psi/\varphi}) = -\frac{1}{2}k^{2n-d}\tilde{\partial}_t \int_0^\infty \mathrm{d}x\, x^{\frac{d}{2}-1}[P_{\psi/\varphi,k}(x) + \omega k^2]^{-n}, \tag{B.3}$$

$$l_{n_1,n_2}^{d}(\omega_1,\omega_2;\eta_{\varphi}) = -\frac{1}{2}k^{2(n_1+n_2)-d}\tilde{\partial}_t \int_0^\infty \mathrm{d}x\, x^{\frac{d}{2}-1}[P_{\varphi,k}(x) + \omega_1 k^2]^{-n_1}[P_{\varphi,k}(x) + \omega_2 k^2]^{-n_2}, \tag{B.4}$$

$$l_{n_1,n_2}^{(\mathrm{FB})d}(\omega_1,\omega_2;\eta_{\psi},\eta_{\varphi}) = -\frac{1}{2}k^{2(n_1+n_2)-d}\tilde{\partial}_t \int_0^\infty \mathrm{d}x\, x^{\frac{d}{2}-1}[P_{\psi,k}(x) + \omega_1 k^2]^{-n_1}[P_{\varphi,k}(x) + \omega_2 k^2]^{-n_2}, \tag{B.5}$$

$$m_{2,2}^{d}(\omega_1,\omega_2;\eta_{\varphi}) = -\frac{1}{2}k^{6-d}\tilde{\partial}_t \int_0^\infty \mathrm{d}x\, x^{\frac{d}{2}}\left[\partial_x \frac{1}{P_{\varphi,k}(x) + \omega_1 k^2}\right]\left[\partial_x \frac{1}{P_{\varphi,k}(x) + \omega_2 k^2}\right], \tag{B.6}$$

$$m_4^{(\mathrm{F})d}(\omega;\eta_{\psi}) = -\frac{1}{2}k^{4-d}\tilde{\partial}_t \int_0^\infty \mathrm{d}x\, x^{\frac{d}{2}+1}\left[\partial_x \frac{1 + r_{\psi,k}(x)}{P_{\psi,k}(x) + \omega k^2}\right]^2, \tag{B.7}$$

$$m_{1,2}^{(\mathrm{FB})d}(\omega_1,\omega_2;\eta_{\psi},\eta_{\varphi}) = \frac{1}{2}k^{4-d}\tilde{\partial}_t \int_0^\infty \mathrm{d}x\, x^{\frac{d}{2}} \frac{1 + r_{\psi,k}(x)}{P_{\psi,k}(x) + \omega_1 k^2}\partial_x \frac{1}{P_{\varphi,k}(x) + \omega_2 k^2}, \tag{B.8}$$

where we have denoted $l_n^{(\mathrm{B})d}(\omega;\eta_{\varphi}) := l_n^d(\omega;\eta_{\varphi})$ and

$$P_{\psi,k} := x[1 + r_{\psi,k}(x)]^2 \quad \text{and} \quad P_{\varphi,k} := x[1 + r_{\varphi,k}(x)] \tag{B.9}$$

for a shorter notation. The integers n have to be chosen $n > 0$. We emphasize that we have only listed those threshold functions which play a role in our investigations. In the integrals, we have used the substitution $p^2 \mapsto x$,

$$\int \frac{\mathrm{d}^d p}{(2\pi)^d} = 4v_d \int \mathrm{d}p\, p^{d-1} = 2v_d \int \mathrm{d}x\, x^{\frac{d}{2}-1}, \tag{B.10}$$

where $v_d := 1/[2^{d+1}\pi^{d/2}\Gamma(d/2)]$. The derivative operator $\tilde{\partial}_t$ is defined in the way

$$\begin{aligned}\tilde{\partial}_t :=& \sum_{\Phi=\psi,\varphi} \frac{\partial_t(Z_{\Phi,k}r_{\Phi,k})}{Z_{\Phi,k}}\frac{\partial}{\partial r_{\Phi,k}} \\ =& \frac{\partial_t(Z_{\psi,k}r_{\psi,k})}{Z_{\psi,k}}\frac{2P_{\psi,k}}{1 + r_{\psi,k}}\frac{\partial}{\partial P_{\psi,k}} + \frac{\partial_t R_{\varphi,k}}{Z_{\varphi,k}}\frac{\partial}{\partial P_{\varphi,k}}\end{aligned} \tag{B.11}$$

[1]The organisation of this chapter is close to appendix B of [27]

and only acts on the regulator's k-dependency. For the linear regulator the one-loop integrals can be evaluated analytically. We obtain

$$l_n^d(\omega;\eta_\varphi) = \frac{2}{d}\left(1-\frac{\eta_\varphi}{d+2}\right)\frac{n}{(1+\omega)^{n+1}}, \tag{B.12}$$

$$l_n^{(\mathrm{F})d}(\omega;\eta_\psi) = \frac{2}{d}\left(1-\frac{\eta_\psi}{d+1}\right)\frac{n}{(1+\omega)^{n+1}}, \tag{B.13}$$

$$l_{n_1,n_2}^d(\omega_1,\omega_2;\eta_\varphi) = \frac{2}{d}\left(1-\frac{\eta_\varphi}{d+2}\right)\left(\frac{n_1}{1+\omega_1}+\frac{n_2}{1+\omega_2}\right)\frac{1}{(1+\omega_1)^{n_1}(1+\omega_2)^{n_2}}, \tag{B.14}$$

$$l_{n_1,n_2}^{(\mathrm{FB})d}(\omega_1,\omega_2;\eta_\psi,\eta_\varphi) = \frac{2}{d}\left[\left(1-\frac{\eta_\psi}{d+1}\right)\frac{n_1}{1+\omega_1}+\left(1-\frac{\eta_\varphi}{d+2}\right)\frac{n_2}{1+\omega_2}\right]\frac{1}{(1+\omega_1)^{n_1}(1+\omega_2)^{n_2}}, \tag{B.15}$$

$$m_{2,2}^d(\omega_1,\omega_2;\eta_\varphi) = \frac{1}{(1+\omega_1)^2(1+\omega_2)^2}, \tag{B.16}$$

$$m_4^{(\mathrm{F})d}(\omega;\eta_\psi) = \frac{1}{(1+\omega)^4}+\frac{1-\eta_\psi}{d-2}\frac{1}{(1+\omega)^3}-\left(\frac{1-\eta_\psi}{2d-4}+\frac{1}{4}\right)\frac{1}{(1+\omega)^2}, \tag{B.17}$$

$$m_{1,2}^{(\mathrm{FB})d}(\omega_1,\omega_2;\eta_\psi,\eta_\varphi) = \left(1-\frac{\eta_\varphi}{d+1}\right)\frac{1}{(1+\omega_1)(1+\omega_2)^2}. \tag{B.18}$$

Danksagung

Auf den letzten Seiten möchte ich ein Wort des Dankes an all diejenigen richten, die mich während oder bei der Erstellung der vorliegenden Arbeit unterstützt haben. Zunächst gilt ein großer Dank Professor Gies und Dr. Lukas Janssen, die mir das Thema der Arbeit vorgeschlagen haben und nie müde wurden, meine vielen Fragen während der Einarbeitung zu beantworten. Auch haben mich beide bei der Lösungsfindung der in der Bearbeitung dieses Themas auftretenden Probleme stets unterstützt. Dabei bedanke ich mich insbesondere bei Professor Gies, der auch in der Elternzeit von Lukas Janssen immer Zeit für mich hatte und zum Schluss für eine gelungene Aufschrift aller Ergebnisse, diese Arbeit Korrektur gelesen hat.

In diesem Zusammenhang möchte ich mich weiterhin bei Nico Seegert, Friedrich Gehring, Christian Vitense und Alexander Blinne bedanken, die der Arbeit zum letzten Feinschliff verholfen haben. Zum Schluss, geht ein besonderer Dank an meine Familie, die mir während der Zeit manchmal beschwerlich kleiner Fortschritte eine große Stütze war.

Eigenständigkeitserklärung

Ich erkläre hiermit, dass ich die vorliegende Arbeit selbstständig verfasst und keine anderen als die angegebenen Quellen und Hilfsmittel verwendet habe. Die eingereichte Arbeit ist nicht anderweitig als Prüfungsleistung verwendet worden oder als Veröffentlichung erschienen. Seitens des Verfassers bestehen keine Einwände, die Arbeit für die öffentliche Nutzung der Thüringer Universitäts- und Landesbibliothek zur Verfügung zu stellen.

Jena, den